Titre: Title:	Extending neutron activation analysis to materials with high concentrations of neutron absorbing elements
Auteur: Author:	Cornelia Chilian
Date:	2008
Type:	Mémoire ou thèse / Dissertation or Thesis
Référence: Citation:	Chilian, C. (2008). Extending neutron activation analysis to materials with high concentrations of neutron absorbing elements [Ph.D. thesis, École Polytechnique de Montréal]. PolyPublie. https://publications.polymtl.ca/8124/

UNIVERSITÉ DE MONTRÉAL

EXTENDING NEUTRON ACTIVATION ANALYSIS TO MATERIALS WITH HIGH CONCENTRATIONS OF NEUTRON ABSORBING ELEMENTS

CORNELIA CHILIAN
DÉPARTEMENT DE GÉNIE PHYSIQUE
ÉCOLE POLYTECHNIQUE DE MONTRÉAL

THÈSE PRÉSENTÉE EN VUE DE L'OBTENTION DU DIPLÔME DE
PHILOSOPHIAE DOCTOR
(GÉNIE NUCLÉAIRE)
AVRIL 2008

Your file Votre référence
ISBN: 978-0-494-41744-7
Our file Notre référence
ISBN: 978-0-494-41744-7

UNIVERSITÉ DE MONTRÉAL

ÉCOLE POLYTECHNIQUE DE MONTRÉAL

Cette thèse intitulée:

EXTENDING NEUTRON ACTIVATION ANALYSIS TO MATERIALS WITH HIGH CONCENTRATIONS OF NEUTRON ABSORBING ELEMENTS

présentée par: CHILIAN Cornelia
en vue de l'obtention du diplôme de: Philosophiae Doctor
a été dûment acceptée par le jury d'examen constitué de:

M. MARLEAU Guy, Ph. D., président
M. KENNEDY Gregory, Ph D., membre et directeur de recherche
M. ZIKOVSKY Lubomir, Ph. D., membre et codirecteur de recherche
M. HÉBERT Alain, D. Ing., membre
M. JONKMANS Guy, Ph. D., membre

Dedication

In the memory of my parents, Ion and Venera Turtoi

Acknowledgements

Foremost, I would like to thank my Research Director, Dr. Greg Kennedy, for giving me the opportunity to work on such an interesting research project. Dr. Greg Kennedy saw the potential of this project from the very beginning, and his expertise, scientific rigor, and enthusiasm inspired me and helped me to make it a success.

I would like to thank Mr. Jean St-Pierre, for generously sharing with me his vast and diversified knowledge and laboratory techniques in activation analysis.

I would also like to thank my second Research Director, Dr. Lubomir Zikovsky; both his advice and pertinent remarks had great value for me.

I am grateful for the stimulating academic atmosphere of the Nuclear Engineering Institute of Ecole Polytechnique Montreal; among them, I would like to thank the members of my thesis and qualifying committees, Prof. Alain Hébert and Prof. Guy Marleau, for all their guidance and recommendations in this project.

I would like to thank my colleagues and friends, Nihan Onder, Monchai Assawaroongruengchot, Karthikeyan Ramamoorthy, Florina-Elena Truica-Marasescu, Rodica Matei, Anca and Viorel Poenariu, Aurora and Ionut Dranga, Ovidiu-Mihai Popescu, for their support, for their encouragements and friendship.

I would like to express my gratitude for the constant support, understanding and love that I received from my brother Valeriu-Cornel Turtoi during the past years.

Finally, I would especially like to thank my husband, Toma-Mircea Chilian, for his love, for supporting me throughout this entire process and for our daughter, Victoria-Ioana, who has provided me with that extra bit of inspiration when I really needed it.

Résumé

L'objectif de cette étude a été d'investiguer la correction de l'autoprotection de résonance pour les neutrons épithermiques pour tous les nuclides utilisés dans l'Analyse par Activation Neutronique (AAN). Des études récentes suggèrent que les facteurs d'autoprotection thermiques et épithermiques peuvent être exprimés par une fonction analytique, un sigmoïde. En appliquant cette fonction en AAN pour des matériaux purs, la variable du sigmoïde a été exprimée comme le produit d'un facteur nucléaire, d'un facteur géométrique pour des échantillons cylindriques et de la quantité de l'élément chimique présent dans l'échantillon. Cette nouvelle approche dans l'AAN a conduit à une méthode nouvelle pour la correction de l'effet des neutrons thermiques et épithermiques sur l'autoprotection dans n'importe quel échantillon cylindrique irradié dans n'importe quel réacteur. Ainsi, tous les avantages de l'AAN, soient la précision sans préparation préliminaire de l'échantillon, la reproductibilité ainsi que la possibilité de la paramétriser et de l'appliquer à un travail de routine, sont maintenant disponibles pour des matériaux contenant des quantités significatives d'éléments chimiques avec grandes sections efficaces d'absorption pour les neutrons thermiques et épithermiques.

Cette étude a démarré par une vérification de la théorie et par la mesure des facteurs nucléaires caractérisant l'autoprotection thermique et de résonance pour des échantillons de 1 mL contenant les halogènes Cl, Br et I. Ces échantillons ont été irradiés dans un spectre de neutrons mixte, thermique et épithermique. Pour des échantillons contenant un seul élément, les deux facteurs de l'autoprotection, thermiques et de résonance, ont été

bien estimés par des fonctions sigmoïdes. Ces expériences préliminaires ont indiqué que, pour corriger l'autoprotection par des neutrons thermiques, le sigmoïde utilise un seul paramètre, m_{th}, qui peut être calculé pour tout élément à partir des dimensions de l'échantillon, la somme pondérée des sections efficaces d'absorption thermique des éléments présents dans l'échantillon, σ_{abs}, et une constante $k_{th,.}$ caractéristique du site d'irradiation. Au contraire, pour corriger l'autoprotection de résonance, le paramètre m_{ep}, aussi fonction de la géométrie et de la composition de l'échantillon, des conditions d'irradiation et des caractéristiques nucléaires de l'élément, doit être mesuré expérimentalement pour chaque nuclide activé.

Etant donné que les tests préliminaires ont montré qu'une autoprotection de résonance atteignant 30% peut être corrigée avec une précision d'environ 1%, exception faite des cas impliquant l'autoprotection de résonance mutuelle d'un élément sur un autre élément, l'étude a été poussée vers l'étape suivante, soit la vérification de deux autres aspects. Premièrement, la dépendance des paramètres m_{th} et m_{ep} sur les propriétés du site d'irradiation a été évaluée pour trois sites d'irradiation différents du réacteur SLOWPOKE, ce qui a permis de conclure que l'autoprotection thermique et l'autoprotection de résonance varient de moins de 10% d'un site à l'autre. Deuxièmement, la variation des paramètres de l'autoprotection, m_{th} et m_{ep}, avec les dimensions de l'échantillon cylindrique, variant en $r(r+h)$, a été testée pour des rapports h/r de 0.02 à 6.00, et cette variation a été confirmée même dans des champs neutroniques légèrement non-isotropes. Ces résultats ont permis de séparer du paramètre de l'autoprotection m_{ep} la quantité de l'élément et le facteur géométrique. Le facteur

nucléaire restant, surnommé section efficace d'absorption épithermique, $\sigma_{abs,ep}$, est estimé comme étant le produit de caractéristiques nucléaires composites du nuclide activé. Ce paramètre nucléaire empirique, similaire à la section efficace d'absorption thermique, permettra d'évaluer l'autoprotection de résonance pour n'importe quelle géométrie cylindrique et n'importe quel site d'irradiation.

Parmi les 76 nuclides utilisés dans l'analyse par activation neutronique, 38 ont un rapport de l'intégrale de résonance sur la section efficace d'absorption thermique, Q_0, plus grand que 10, valeur qui révèle une activation par des neutrons épithermiques plus importante que l'activation par des neutrons thermiques. De ces 38, l'étude a expérimentalement analysé 13 réactions nucléaires: $^{79}Br(n,\gamma)^{80}Br$, $^{81}Br(n,\gamma)^{82}Br$, $^{96}Zr(n,\gamma)^{97}Zr$, $^{114}Cd(n,\gamma)^{115}Cd$, $^{127}I(n,\gamma)^{128}I$, $^{115}In(n,\gamma)^{116m}In$, $^{121}Sb(n,\gamma)^{122}Sb$, $^{123}Sb(n,\gamma)^{124}Sb$, $^{133}Cs(n,\gamma)^{134}Cs$, $^{152}Sm(n,\gamma)^{153}Sm$, $^{186}W(n,\gamma)^{187}W$, $^{197}Au(n,\gamma)^{198}Au$ et $^{238}U(n,\gamma)^{239}U$.

Pour les 13 cas étudiés, le facteur d'autoprotection de résonance, G_{ep}, a été obtenu par soustraction du facteur d'autoprotection effectif expérimental, G_{eff}, le facteur d'autoprotection thermique, G_{th}, calculé avec la formulation sigmoïde. En utilisant la méthode des moindres carrés, une fonction sigmoïde a été utilisée pour estimer les G_{ep} expérimentaux exprimés comme fonction de la masse de l'élément présent dans l'échantillon. Cette approximation a généré le $\sigma_{abs,ep}$ pour chaque nuclide activé. De plus, pour tous les nuclides utilisés couramment dans l'analyse par activation neutronique, $\sigma_{abs,ep}$, a été calculé par la formule de Salgado et al. qui utilise les valeurs de sections efficaces totales aux pics des résonances. La comparaison des valeurs calculées de $\sigma_{abs,ep}$

avec celles mesurées expérimentalement indique des différences allant jusqu'à 20%. Ceci montre l'avantage de déterminer expérimentalement les valeurs de $\sigma_{abs,ep}$.

Finalement, à partir de $\sigma_{abs,ep}$ calculés ou mesurés expérimentalement, pour tous les 76 nuclides utilisés couramment dans l'AAN, un programme utilisant une feuille de calcul Excel a été créé. Ce programme corrige itérativement l'autoprotection neutronique dans les concentrations mesurées par analyse par activation. L'utilisateur fournit les paramètres f et α du spectre neutronique, la masse et les dimensions de l'échantillon ainsi que les concentrations mesurées. Dans un cas typique avec 10% d'autoprotection thermique et 30% d'autoprotection de résonance, les concentrations corrigées ont une incertitude variant de 2% à 3%.

Mots-clés: Analyse par Activation Neutronique Instrumentale, facteur d'autoprotection thermique, facteur d'autoprotection de résonance.

Abstract

The purpose of this study was to investigate epithermal neutron self-shielding for all nuclides used in Neutron Activation Analysis, NAA. Recent studies suggested that both thermal and epithermal self-shielding factors could be expressed by a unique sigmoid function. Applying this function to NAA for pure materials, the sigmoid variable was expressed as product of a nuclear factor, a geometrical factor for cylindrical samples, and the amount of the element present in the sample. This new approach in NAA led to an easily usable method to correct both thermal and epithermal self-shielding for any cylindrical sample and any reactor irradiation site. Thus, all advantages of NAA, such as accuracy without sample preparation, reproducibility, and applicability to routine work by parameterization, are now available for materials containing large amounts of elements with high absorption cross sections for thermal and epithermal neutrons.

The study started with testing the theory and measuring the nuclear factors characterizing thermal and epithermal self-shielding for 1 mL cylindrical samples containing the halogens Cl, Br and I irradiated in a mixed thermal and epithermal neutron spectrum. For mono-element samples, both thermal and epithermal experimental self-shielding factors were well fitted by sigmoid functions. As a result, to correct thermal neutron self-shielding, the sigmoid uses a single parameter, m_{th}, which can be directly calculated for any element from the sample size, the weighted sum of the thermal absorption cross-sections, σ_{abs}, of the elements in the sample and a constant k_{th} characteristic of the irradiation site. However, to correct epithermal self-shielding, the parameter m_{ep}, a

function of sample geometry and composition, irradiation conditions and nuclear characteristics, needs to be measured for each activated nuclide.

Since the preliminary tests were positive and showed that self-shielding, as high as 30%, could be corrected with an accuracy of about 1%, except in cases with significant epithermal shielding of one element by another, we pursued the study with the verification of two additional aspects. First, the dependency of the self-shielding parameters m_{th} and m_{ep} on the properties of the irradiation site was evaluated using three different irradiation sites of a SLOWPOKE reactor, and it was concluded that the amount of both thermal and epithermal self-shielding varied by less than 10% from one site to another. Second, the variation of the self-shielding parameters, m_{th} and m_{ep}, with the size of the cylinder, as $r(r+h)$, was tested for h/r ratios from 0.02 to 6.0, and this geometry dependence was confirmed even in slightly non-isotropic neutron fields. These results allowed separating from the m_{ep} parameter the amount of chemical element and the sample geometrical factor. Therefore, the remaining nuclear factor, considered as a product of nuclide composite nuclear characteristics and irradiation site characteristics, led to the introduction of a so-called epithermal neutron absorption cross-sections, $\sigma_{abs,ep}$. This new nuclear parameter will allow the calculation of the epithermal self-shielding for all cylindrical samples activated in all types of irradiation sites.

Among the 76 nuclides used in neutron activation analysis, epithermal neutron absorption cross-sections were experimentally measured for 13 (n,γ) reactions: $^{79}Br(n,\gamma)^{80}Br$, $^{81}Br(n,\gamma)^{82}Br$, $^{96}Zr(n,\gamma)^{97}Zr$, $^{114}Cd(n,\gamma)^{115}Cd$, $^{127}I(n,\gamma)^{128}I$, $^{115}In(n,\gamma)^{116m}In$, $^{121}Sb(n,\gamma)^{122}Sb$,

$^{123}Sb(n,\gamma)^{124}Sb$, $^{133}Cs(n,\gamma)^{134}Cs$, $^{152}Sm(n,\gamma)^{153}Sm$, $^{186}W(n,\gamma)^{187}W$, $^{197}Au(n,\gamma)^{198}Au$ and $^{238}U(n,\gamma)^{239}U$. These nuclides were selected from the 38 nuclides having a resonance integral to thermal absorption cross section ratio, Q_0, higher than 10, corresponding to a high importance of activation by epithermal neutrons relative to thermal activation.

For the 13 cases studied, the epithermal self-shielding factor, G_{ep}, was obtained from the experimental effective self-shielding factor, G_{eff}, by extracting the thermal neutron self-shielding factor, calculated with the sigmoid formulation. A least-squares fit of the experimental G_{ep} values as a function of the mass of element yielded $\sigma_{abs,ep}$ for each activated nuclide. In addition, for all nuclides commonly used in neutron activation analysis, $\sigma_{abs,ep}$ was calculated with the Martinho, Salgado and Gonçalves sigmoid formulation, which uses the total cross-section values at the peaks of the resonances. A comparison of the calculated $\sigma_{abs,ep}$ with the 13 measured values reveals that the calculated values are accurate to about 20%.

Finally, for all 76 nuclides commonly used in NAA, a spreadsheet program was written to use experimental or calculated $\sigma_{abs,ep}$ nuclear parameters to perform iterative self-shielding corrections of concentrations measured by neutron activation analysis. The user provides the parameters f and α of the neutron spectrum, the sample mass and dimensions, and the measured concentrations. In a typical case with 10% thermal self-shielding and 30% epithermal self-shielding, the corrected concentrations had uncertainties varying from 2% to 3%.

Keywords: Instrumental Neutron Activation Analysis, epithermal, thermal, self-shielding factors

Condensé en français

La majorité des laboratoires d'Analyse par Activation Neutronique (AAN) ont concentré leurs efforts vers l'amélioration de la sensibilité de la méthode dans le but d'obtenir une analyse pertinente même pour les éléments à très faibles concentrations. Pourtant, à très faible concentration, il y a maintenant d'autres méthodes d'analyse chimique aussi performantes. À l'opposé, pour l'analyse des substances solides ayant de fortes concentrations, souvent, la seule méthode possible est l'AAN. Toutefois, dans certains cas de concentrations élevées, l'activité produite par activation neutronique n'est plus une fonction linéaire de la concentration de l'élément à déterminer. Cette non-linéarité est générée par l'autoprotection des atomes qui sont activés.

L'objectif principal de ce projet a été de caractériser l'autoprotection des résonances pour les éléments qui ont une section efficace élevée pour l'absorption des neutrons épithermiques, afin d'étendre la méthode d'analyse par activation aux échantillons qui contiennent ce type d'éléments. Pour atteindre l'objectif de cette étude, la réalisation du présent projet de recherche s'est appuyée sur une démarche de recherche de type expérimental, c'est-à-dire avec un contrôle des variables, le point de départ étant les équations de Salgado et al. proposées pour le calcul des facteurs d'autoprotection contre les neutrons thermiques et de résonance. Ces équations ont été adaptées aux besoins de l'analyse par activation neutronique. Ainsi, de nouveaux paramètres ont été définis pour les courbes décrites par ces équations, courbes qui épousent très bien les données expérimentales. À partir des données expérimentales, on a proposé de nouvelles

équations capables de décrire l'autoprotection dans le cas des échantillons qui contiennent des éléments fortement absorbants pour les neutrons épithermiques.

La première hypothèse qui appuie cette étude est : pour chaque élément qui absorbe aux énergies des neutrons épithermiques, l'autoprotection de résonance est décrite par une fonction sigmoïde de type : $G_{ep} = 0{,}94 / (1 + (m / m_{ep})^{0{,}82}) + 0{,}06$. Dans l'analyse des échantillons qui contiennent plusieurs éléments absorbant des neutrons épithermiques, le point de départ est la deuxième hypothèse : chaque nuclide se protège lui-même sans être affecté par la présence des autres nuclides parce que les résonances d'absorption sont situées à des énergies différentes.

L'analyse par activation neutronique est une méthode d'analyse chimique très puissante, rapide et d'une grande sensibilité qui permet d'identifier et de quantifier chaque élément indépendamment de sa forme chimique ou de son emplacement physique dans l'échantillon. Le principe de l'AAN est l'irradiation d'une substance avec les neutrons, provoquant des réactions nucléaires. Par ce processus, les noyaux atomiques de l'échantillon sont activés. L'activité de chaque élément est mesurée en détectant les rayons γ émis par le nuclide activé. Cette radioactivité est spécifique aux éléments contenus dans l'échantillon, ce qui permet de déterminer sa composition chimique.

La méthode k_0, largement utilisée dans l'AAN pour les réacteurs de grandes dimensions, a été standardisée pour les petits réacteurs, avec un flux stable, comme le SLOWPOKE. Dans le laboratoire d'activation neutronique de l'École Polytechnique de Montréal, les études menées par Kennedy et St-Pierre ont permis d'établir avec une grande précision

les paramètres f et α des spectres de neutrons et les paramètres k_0 et Q_0 des réactions de capture neutronique. De plus, ils ont investigué les effets des conditions d'irradiation et des caractéristiques de l'échantillon sur l'activité de l'échantillon. Ces effets sont induits par des substances modératrices présentes dans l'échantillon, par les variations de température du caloporteur de réacteur SLOWPOKE, par l'anisotropie du flux neutronique dans les sites d'irradiation, ainsi que par la géométrie de détection étroitement reliée à celle de l'échantillon. Toutes ces études combinées avec l'outil puissant qu'est la méthode d'analyse k_0, ont permis d'oser franchir une nouvelle étape dans l'AAN : le calcul et la correction de l'autoprotection neutronique thermique et épithermique.

L'autoprotection est l'absorption de neutrons par les couches successives d'un échantillon, ce qui implique que l'intérieur de l'échantillon subit un flux neutronique plus petit que l'extérieur. C'est un phénomène complexe car les probabilités d'absorption varient avec l'énergie des neutrons. Pour simplifier, la réduction du flux neutronique dans l'échantillon est caractérisée par le facteur d'autoprotection effectif G_{eff}, défini comme étant le rapport : A/A_0, où A est l'activité de l'échantillon réel avec autoprotection et A_0 est l'activité du même échantillon dans le cas idéal sans autoprotection. Cette réduction du flux est fonction de l'énergie des neutrons. Dans cette étude, A et A_0 ont été exprimés en utilisant la convention de Hoghdahl. Dans le calcul du flux thermique φ_{th} et du flux épithermique φ_{ep}, on suppose que, dans la région thermique, la densité neutronique a une distribution de type Maxwell-Boltzmann et que le flux épithermique en fonction de l'énergie a une variation de type $1/E^{1+\alpha}$. Dans le cas de l'irradiation dans le réflecteur du

réacteur SLOWPOKE de l'École Polytechnique de Montréal, α = -0.051. Pour les neutrons thermiques, la section efficace de capture neutronique a une variation de type $1/E^{1/2}$, et pour la région épithermique, on utilise les formules Breit-Wigner pour représenter la variation de la section efficace de capture neutronique aux résonances. Le flux neutronique est composé de neutrons thermiques, intermédiaires épithermiques et rapides. Conséquemment, l'autoprotection est la somme des deux effets : l'autoprotection contre les neutrons thermiques, G_{th}, et l'autoprotection contre les neutrons épithermiques, G_{ep}, l'activation avec neutrons rapides étant négligeable comparativement aux deux premières contributions. Ensuite, on peut écrire pour G_{eff} la formule suivante : $G_{eff} = (G_{th} + G_{ep}Q_0/f) /(1 + Q_0/f)$, avec $f = \varphi_{th}/\varphi_{ep}$ et $Q_0 = I_0/\sigma_{th}$ où I_0 est l'intégrale de résonance et σ_{th} la section efficace de capture neutronique à 2200m/s.

Le premier effet, l'autoprotection contre les neutrons thermiques, peut se calculer à l'aide des équations bien connues. Pour les échantillons contenant un seul élément qui capture des neutrons, la variation du facteur d'autoprotection thermique, G_{th}, avec la concentration et la géométrie de l'échantillon est assez bien connue ; la section efficace d'absorption pour les neutrons thermiques varie lentement avec l'énergie, en général comme $E^{-1/2}$ et, conséquemment, le facteur d'autoprotection thermique pour tous les éléments peut être exprimé par la même fonction de la quantité de l'élément et de la section efficace d'absorption pour les neutrons thermiques à 2200 m/s, σ_{abs}. De plus, pour les échantillons cylindriques, G_{th} varie avec les dimensions de l'échantillon selon le facteur $rh/(r+h)$, où r est le rayon et h est la hauteur de l'échantillon.

Contrairement à l'absorption thermique, le calcul du G_{ep} en fonction de la concentration de l'élément et de la géométrie de l'échantillon est complexe puisque la section efficace d'absorption pour les neutrons de résonance en fonction de l'énergie est différente d'un nuclide à l'autre. Les diverses méthodes numériques utilisées pour évaluer l'autoprotection de résonance ne sont pas pratiques pour l'activation neutronique et difficiles à appliquer dans les analyses de routine dans lesquelles la composition et les concentrations des éléments absorbants ne sont pas connues d'avance.

La série récente de publications de Salgado et al. sur l'autoprotection de résonance et, plus tard, sur l'autoprotection due aux neutrons thermiques dans le calcul des réacteurs nucléaires, suggère la possibilité de quantifier G_{ep} et G_{th}, en les exprimant sous la forme de fonctions sigmoïdes des masses des éléments présentes dans l'échantillon. Conséquemment, on a pu appliquer cette découverte en AAN et on a développé une méthode de correction de l'autoprotection neutronique pour des échantillons cylindriques de composition *a priori* inconnue, irradiés dans un flux mixte de neutrons thermiques et épithermiques. Le facteur d'autoprotection pour les neutrons thermiques dépend de tous les nuclides présents dans l'échantillon et il a la même valeur pour chacun de ces nuclides. Contrairement à l'autoprotection thermique, le facteur d'autoprotection épithermique pour un nuclide est influencé par la présence des autres éléments dans l'échantillon, seulement quand ces éléments absorberont des neutrons aux énergies d'une résonance qui chevauche la résonance d'activation du nuclide considéré.

À partir des données expérimentales, cette étude a premièrement vérifié que les prémices théoriques suggérées s'appliquent dans le cas de l'analyse par activation neutronique. Des échantillons cylindriques de 1 ml contenant différentes quantités de l'élément ont été irradiés dans le site intérieur du réacteur SLOWPOKE de l'École Polytechnique dans un flux de neutrons thermiques de 5,59 x $10^{11}cm^{-2}s^{-1}$. L'activité des nuclides activés de chaque échantillon a été mesurée en comptant les rayons gamma à une distance de 10 cm d'un détecteur de germanium. Pour chaque comptage, avant d'acquérir le spectre, on a attendu le temps de décroissance nécessaire pour que l'analyseur ait un temps mort de moins de 20%. Les activités ont été calculées en utilisant la surface du pic caractéristique du nuclide et corrigées pour le temps de décroissance et la variation du flux neutronique due aux effets modérateurs associés à la composition de l'échantillon et pour les effets liés aux changements de température du caloporteur.

Dans les expériences préliminaires, pour vérifier l'expression de l'autoprotection thermique, on a préparé des échantillons cylindriques qui contiennent différentes quantités de chlore. Le chlore a une grande section efficace d'absorption pour les neutrons thermiques, 33,5 b, et la réaction $^{37}Cl(n,\gamma)^{38}Cl$ a un bas rapport de l'intégrale de résonance sur la section efficace d'activation thermique, Q_0 = 0.85. Même si le flux neutronique n'est pas bien thermalisé dans ce site d'irradiation, à cause de la valeur réduite du Q_0, 96% de l'activité de ^{38}Cl est produite par les neutrons thermiques et la contribution à l'activité des neutrons de résonance a pu être considérée comme étant constante à 4%. En utilisant la méthode des moindres carrés, les données expérimentales ont été estimées avec la fonction sigmoïde. Ceci a permis de vérifier la formule de G_{th}

avec une erreur de 2% comparable aux incertitudes expérimentales. Pour corriger l'autoprotection thermique, les équations utilisent un seul paramètre, m_{th}, pouvant être calculé pour chaque élément à partir de la dimension de l'échantillon, de la section efficace d'absorption neutronique de l'élément à 2200 m/s, σ_{abs}, et une constante reliée aux conditions d'irradiation, k_{th}, déterminée ici comme étant 0,81. Dans le reste de l'étude, pour calculer G_{th}, la formule sigmoïde a été utilisée tout en négligeant le facteur relié à la diffusion. Ce facteur est d'habitude très proche de l'unité, surtout pour les éléments avec une très grande section efficace d'absorption pour les neutrons thermiques.

Comme précédemment pour le facteur d'autoprotection thermique, la formulation sigmoïde pour le facteur d'autoprotection de résonance, G_{ep}, a été vérifiée pour les réactions (n,γ) des ^{127}I, ^{79}Br et ^{81}Br. Ces réactions ont des valeurs de Q_0 de 31.9, 14.4 et 23.8, respectivement. Ainsi, avec f = 18.0 et en l'absence d'autoprotection, 63.6%, 44.0% et 56.5% des activités de ^{128}I, ^{80}Br and ^{82}Br sont produites par des neutrons ayant des énergies correspondant à la région des résonances. Des échantillons de 1 ml de ces solutions ont été scellés dans des capsules de polyéthylène puis irradiés et comptés de la même manière que pour le chlore. Les activités spécifiques des radionuclides mesurées ont été comparées avec leurs G_{eff} calculés avec les formules sigmoïdes de G_{ep} et G_{th}. Ceci a permis de vérifier l'expression théorique proposée pour G_{ep}. De plus, séparer la masse de l'élément et le facteur géométrique $rh/(r+h)$ a conduit à l'identification du facteur nucléaire caractérisant l'activation par des neutrons de résonance.

Après la validation de l'expression de G_{ep}, pour vérifier la deuxième hypothèse, des mesures ont été effectuées avec des mélanges d'éléments qui présentent le phénomène de l'autoprotection de résonance. Premièrement, les masses de chlore et d'iode mesurées dans un échantillon concentré, corrigées pour l'autoprotection par une procédure itérative, et comparées avec les masses réelles, ont indiqué une différence entre les valeurs calculées et les valeurs réelles de +1% pour le chlore et −1,6% pour l'iode, respectivement. Ce calcul itératif conduit rapidement à une valeur convergente en prouvant la validité de la méthode pour la correction de l'autoprotection pour des échantillons contenant des mélanges d'absorbeurs de neutrons thermiques et de résonance. Deuxièmement, un échantillon de 1 ml de poudre, avec des concentrations élevées de Br et d'I, a été irradié et compté, et les concentrations mesurées en comptant l'activité de ^{80}Br, ^{82}Br et ^{128}I ont été corrigées pour l'autoprotection. Pour déterminer les vraies concentrations de Br et I, l'échantillon a été dissout dans l'eau et 1 ml de cette solution diluée, équivalant à une autoprotection négligeable, a été analysée. Pour les échantillons concentrés en poudre, les masses finales corrigées pour l'autoprotection ont été déterminées par une procédure itérative dans laquelle G_{eff} a été calculé à chaque étape en utilisant les paramètres déterminés antérieurement. La comparaison de ces valeurs avec les valeurs réelles des masses utilisées dans la préparation de l'échantillon a montré une différence pouvant aller jusqu'à 6% entre les deux. Cette différence est expliquée par l'autoprotection mutuelle entre les résonances d'absorption neutronique de Br et I, ce qui suggère une limitation de la méthode pour les échantillons contenant plusieurs éléments en fortes concentrations qui absorbent des neutrons de résonance.

Les fonctions sigmoïdes proposées par Salgado et al. pour calculer les facteurs d'autoprotection neutronique thermique et de résonance ont été déterminées pour des échantillons cylindriques d'un seul élément n'ayant qu'un seul nuclide avec quelques résonances isolées, échantillons irradiés dans un flux neutronique isotrope. Ces suppositions sont loin des conditions expérimentales réelles de l'activation neutronique. Conséquemment, la deuxième étape de l'étude avait pour but de valider la formulation sigmoïde des facteurs d'autoprotection thermique et de résonance pour les conditions d'irradiation spécifiques du SLOWPOKE. Ceci implique la présence d'un flux neutronique anisotrope, des sites d'irradiation entourés de différents matériaux réflecteurs, et des échantillons ayant différentes géométries. La dépendance de G_{th} en fonction de la géométrie de l'échantillon a été vérifiée en utilisant la réaction $^{37}Cl(n,\gamma)^{38}Cl$ et des échantillons cylindriques de rayon de 5.0 mm et de 7.2 mm. Les données expérimentales ont été estimées par la courbe théorique avec une erreur variant de 2% jusqu'à 5%, ce qui montre une bonne concordance entre la théorie et l'expérience.

Ensuite, la dépendance de G_{ep} en fonction des dimensions de l'échantillon a été vérifiée avec des disques de zirconium, $^{96}Zr(n,\gamma)^{97}Zr$, de rayon de 3.0 mm, 5.0 mm et 7.0 mm. De plus, des mélanges d'oxyde de zirconium avec oxyde d'aluminium dans des échantillons de 1 ml ont été ajoutés aux données expérimentales. L'approximation des données expérimentales avec la courbe sigmoïde, avec une erreur de moins de 5%, prouve que G_{ep} varie avec les dimensions de l'échantillon comme $rh/(r+h)$. Les expressions analytiques de G_{ep} et G_{th} ont été vérifiées aussi dans trois sites différents du réacteur SLOWPOKE, un site intérieur situé dans le réflecteur de béryllium et deux sites extérieurs situés dans

l'eau. Pour G_{ep} aussi bien que pour G_{th}, les résultats expérimentaux indiquent que les facteurs d'autoprotection varient de moins de 10% d'un site à l'autre, même si l'anisotropie du flux neutronique est plus prononcée dans les sites extérieurs et même si l'importance des neutrons réfléchis est différente d'un site à l'autre.

Après la quantification de l'autoprotection de résonance, il a été possible de séparer du $G_{ep,}$ le paramètre nucléaire caractérisant l'activation par neutrons épithermiques, nommé section efficace d'absorption neutronique épithermique, $\sigma_{abs,ep}$. Ce nouveau paramètre nucléaire est indépendant de la masse et de la géométrie de l'échantillon, ainsi que des conditions d'irradiation.

La dernière étape de l'étude a identifié tous les éléments chimiques qui peuvent présenter des sections efficaces macroscopiques élevées pour l'autoprotection de résonance. Parmi les 76 nuclides importants en AAN, 38 nuclides possèdent un $Q_0 > 10$, et, avec le spectre neutronique du réacteur SLOWPOKE, plus de 35% de leur activité est produite par des neutrons épithermiques. Dans cette étude, des nuclides avec un $Q_0 > 10$, 13 ont été expérimentalement analysés à l'aide des réactions nucléaires: $^{79}Br(n,\gamma)^{80}Br$, $^{81}Br(n,\gamma)^{82}Br$, $^{96}Zr(n,\gamma)^{97}Zr$, $^{114}Cd(n,\gamma)^{115}Cd$, $^{127}I(n,\gamma)^{128}I$, $^{115}In(n,\gamma)^{116m}In$, $^{121}Sb(n,\gamma)^{122}Sb$, $^{123}Sb(n,\gamma)^{124}Sb$, $^{133}Cs(n,\gamma)^{134}Cs$, $^{152}Sm(n,\gamma)^{153}Sm$, $^{186}W(n,\gamma)^{187}W$, $^{197}Au(n,\gamma)^{198}Au$ et $^{238}U(n,\gamma)^{239}U$.

Pour chacun des 13 nuclides étudiés expérimentalement, des échantillons ayant la même géométrie de 1 ml de volume, mais contenant des quantités contrôlées de l'élément considéré, ont été préparés. Pour ces échantillons, l'autoprotection de résonance en

fonction de la masse a été mesurée par activation neutronique. L'activation des échantillons a été réalisée en utilisant le site d'irradiation intérieur du réacteur SLOWPOKE, site où la composante épithermique du flux neutronique est plus importante, f = 18,0. Les activités induites par irradiation ont été mesurées par spectrométrie gamma avec les installations du laboratoire d'activation neutronique de l'École Polytechnique de Montréal. La partie de l'activité induite thermiquement a été corrigée en utilisant la formulation sigmoïde déjà vérifiée pour le facteur d'autoprotection thermique, G_{th}. En séparant de G_{ep} la masse de l'élément et le facteur géométrique, les paramètres $\sigma_{abs,ep}$ ont été établis pour chaque réaction nucléaire.

Pour certains nuclides étudiés, comme ^{127}I, on remarque une différence de l'ordre de 20% entre les valeurs expérimentales et théoriques de $\sigma_{abs,ep}$, différence qui peut s'expliquer par l'emploi de l'équation théorique proposée pour les nuclides ayant quelques résonances isolées, ce qui n'est pas le cas de l'iode. Même pour les nuclides de la catégorie « noyaux avec quelques résonances isolées », on observe des différences allant jusqu'à 50% entre les valeurs expérimentales et théoriques. En plus de l'incertitude expérimentale, de l'ordre de 10%, cette différence peut résulter de l'anisotropie du flux expérimental, comparativement au flux théorique (considéré isotrope). Elle pourrait aussi être due aux limites de la formule ou aux imprécisions des données nucléaires utilisées dans le calcul théorique.

Finalement, en utilisant les résultats antérieurs, on a développé une méthode itérative qui permet de corriger l'autoprotection thermique et de résonance pour tout échantillon

cylindrique et toutes conditions d'irradiations. À l'aide d'une feuille de calcul, cette méthode évalue les G_{th}, G_{ep} et G_{eff} pour les 76 nuclides utilisés en activation neutronique. Elle utilise les sections efficaces thermiques d'absorption neutronique de l'élément, σ_{abs} trouvées dans le Tableau des Éléments; pour les 13 nuclides étudiés ici, la méthode utilise les $\sigma_{abs,ep}$ mesurés, et pour les 63 autres nuclides, les $\sigma_{abs,ep}$ calculés; la méthode suppose que ces dernières valeurs ont une incertitude de 20%. Puisqu'une expression analytique est utilisée, les incertitudes des concentrations corrigées peuvent être calculées à partir des incertitudes de tous les paramètres par propagation des erreurs. En supposant des mesures précises de concentrations, les incertitudes des concentrations corrigées dépendront des incertitudes des G_{eff}, qui sont de moins de 3% pour une incertitude de 20% en $\sigma_{abs,ep}$. Finalement, cette façon de corriger l'autoprotection pour un échantillon irradié dans un flux neutronique mixte est préférable aux calculs numériques (Monte-Carlo), inapplicables dans l'analyse par activation neutronique de routine, car la composition de l'échantillon n'est pas connue d'avance.

Le seul point faible de la méthode est le cas où plusieurs éléments sont activés par des neutrons épithermiques dans un échantillon qui contient un élément fortement absorbant de neutrons épithermiques: il est alors nécessaire de connaître l'autoprotection de cet élément sur les résonances des nuclides appartenant aux autres éléments présents dans l'échantillon. Dans un tel cas, il faut effectuer de nombreuses mesures expérimentales pour chaque paire de nuclides ou des calculs Monte-Carlo, suivis d'approximations par moindres carrés pour établir les paramètres d'autoprotection de résonance mutuelle.

L'avènement des nouveaux matériaux ayant de fortes concentrations en éléments exotiques, comme les convertisseurs catalytiques ou les piles à combustible, contenant platine, ruthénium, rhodium, impose le développement d'une nouvelle méthode d'analyse d'une grande précision et non destructive. Le modèle développé dans cette étude apporte la correction due à l'autoprotection des résonances aux énergies des neutrons épithermiques. Conséquemment, la nouvelle méthode développée permet d'analyser toute substance, sans préparation ni dilution de l'échantillon, tout en conservant son état physique initial. Le modèle est utilisable dans tous les réacteurs nucléaires, pour tous les spectres neutroniques et pour toute taille d'échantillon cylindrique.

Table of Contents

List of Tables

List of Figures

List of Appendices

List of Symbols and Abbreviations

b - barn (10^{-24} cm^2);

const. - constant related to the monitor used in EPAA;

f - thermal to epithermal flux ratio, $f = \varphi_{th}/\varphi_{ep}$;

g - statistical weighting factor: $g = (2J+1)/2(2I+1)$;

h - sample height (cm);

$k_{0,\,Au}(a)$ - experimentally determined k_0 factor of analyte a versus a monitor, usually *Au*;

k_{ep} - dimensionless epithermal self-shielding constant related to the geometry of the sample and to the irradiation site;

k_{th} - dimensionless thermal self-shielding constant related to the geometry of the sample and to the irradiation site;

m - amount of the element (g);

m_{ep} - amount of the element that causes 50% epithermal neutron self-shielding for a given sized cylinder (g);

m_{th} - amount of the element that causes 50% thermal neutron self-shielding for a given sized cylinder (g);

r - sample radius (cm);

t - typical dimension of the sample; for cylindrical geometry, $t=r\cdot h/(r+h)$ (cm);

t_c - counting time (s);

t_d - decay time (s);

t_i - irradiation time (s);

w - mass of the monitor element (g);

w_i - resonance i weighting factor, $w_i = (\Gamma_{\gamma,i} \cdot g \cdot \Gamma_{n,i})/(E_{res,i}^2 \cdot \Gamma_i)$

z - dimensionless self-shielding variable;

z_0 - parameter of the self-shielding factor sigmoid function;

A - measured sample activity (Bq);

A_0 - activity of the sample without self-shielding (Bq);

AAN - Analyse par Activation Neutronique;

A_{sp} - the specific count rate (counts/g);

Au - coirradiated neutron fluence rate monitor, usually gold;

$B_{a,EPAA}$ - sensitivity factor for the analyte a, $B_{a,EPAA}$ = const. $k_{0,Au}(a)\ \varepsilon_{p,a,EPAA}\ (1+ Q_0(\alpha)/f)$;

C - counting factor; $=(1- \exp(-\lambda t_c))/\lambda$;

CANDU - "Canada Deuterium Uranium" reactor;

C_T - correction for neutron flux changes caused by reactor temperature variations;

C_M - correction for neutron flux moderating effects in the sample;

D - decay factor; $= \exp(-\lambda t_d)$;

E - neutron energy (eV);

EPAA - Ecole Polytechnique Activation Analysis software;

EPOXY - organic resin;

E_{res} - energy at the resonance peak (eV);

G_{eff} - effective neutron self-shielding factor;

G_{ep} - epithermal neutron self-shielding factor;

G_{th} - thermal neutron self-shielding factor;

K - normalizing constant;

I - the target nucleus spin;

I_0 - resonance integral (b);

INAA - Instrumental Analyse par Activation Neutronique;

J - resonance state spin momentum;

JANIS - Java based nuclear display program (JANIS 3.0);

L - diffusion length (cm)

M - fraction related to the volume and the type of the moderator present in the sample;

M_{at} - atomic weight;

N - number of atoms of the target nuclide;

NAA - Neutron Activation Analysis;

N_{Av} - Avogadro's number;

NIST - National Institute for Standards and Technology;

N_p - measured net peak area (counts);

$Q_0(\alpha)$ - ratio of resonance integral to 2200 m/s cross section, equal to $I_0(\alpha)/\sigma_{th}$;

S - saturation factor; $=1- \exp(-\lambda t_i)$;

SLOWPOKE - "Safe Low Power Critical Experiment" reactor;

T - temperature indicated at the reactor operating console (^0C);

W - sample mass (g);

Z - atomic number;

α - parameter describing $1/E^{1+\alpha}$ epithermal neutron flux distribution;

ε_p - full-energy peak detection efficiency (%);

$\varepsilon_{p,a}$ - experimental full energy peak detection efficiency (%);

$\varepsilon_{p,a,EPAA}$ - EPAA default full-energy peak detection efficiency (%);

φ_{ep} - average unperturbed epithermal neutron flux inside the sample (cm^{-2} s^{-1});

φ_{th} - average unperturbed thermal neutron flux inside the sample(cm^{-2} s^{-1});

λ - decay constant (s^{-1});

ρ_a - concentration of analyte a (μg/g);

σ_{abs} - thermal neutron absorption cross section of the element (b);

$\sigma_{abs,ep}$ - experimental epithermal neutron absorption cross-section (b);

$\sigma_{abs,ep,Salgado}$ - calculated epithermal neutron absorption cross-section (b);

σ_{th} - (n, γ) cross-section at 2200 m/s (b);

σ_{tot} (E_{res}) - resonance peak value of the total neutron cross section (b);

θ - isotopic abundance;

$\Sigma(E_{res})$ - value of the total macroscopic neutron cross section at the resonace peak (cm^{-1});

Σ_{abs} - macroscopic thermal neutron absorption cross section (cm^{-1});

Γ - total resonance width (eV);

Γ_γ - radiative resonance width (eV);

Γ_n - neutron resonance width (eV).

Chapter 1 Introduction

1.1. Research context

Because of the complexity of the epithermal self-shielding corrections particular to each nuclide, in the past, few studies [Abrashkin 1984, Blaauw et al. 2003, De Corte 1987, Kenna and Van Domelen 1966, Scherbakov and Harada 2002, Reynolds and Mullins 1963, Tomuro and Tomura 2002] tried to address this problem for some particular sample geometries or compositions. In NAA, to avoid correcting epithermal neutron self-shielding, the general practice is to dilute the sample or to use chemical separations to isolate the nuclide of interest [De Corte 1987, De Soete et al. 1973, Király et al. 2003, Kučera and Zeisler, 2004]. However, in some instances, preserving the sample integrity is a requirement. So having a universal correction formula for epithermal neutron self-shielding in NAA alleviates the need for complex, time consuming, and expensive sample preparation, and introduces the possibility of routine analysis for all types of sample matrices.

When irradiating a sample in a well-thermalized neutron spectrum, thermal neutron self-shielding can be accurately corrected because it has been well understood for many years [Blaauw 1996, Crane and Doerner 1963, De Soete et al. 1973, Fleming 1982, Gilat and Gurfinkel 1963, Shakir and Jervis 2001, Tzika and Stamatelos 2004]. However, with the poorly thermalized neutron spectra common at many research reactors, accurate corrections are difficult because of the complexity of resonance neutron self-shielding.

The task is especially difficult for the analysis of materials with high concentrations of heavy elements, which often have relatively high resonance cross-sections.

Recently, a series of studies [Goncalves[b] et al. 2001, Martinho et al. 2003, Salgado[c] et al. 2004] of epithermal neutron self-shielding in reactor physics, propose an empirical correction formula for several different epithermal neutron absorbers in different types of geometries: slabs, wires and spheres, and irradiated in an ideal homogeneous epithermal neutron flux with a neutron spectrum varying with neutron energy as 1/E. The same authors extended this empirical approach to cylindrical geometries, formulation used further in this study [Goncalves et al. 2004, Martinho et al. 2004]. Adapting this discovery to instrumental neutron activation analysis led to a totally new neutron self-shielding correction method, which has now been implemented for routine sample analysis in the Activation Analysis Laboratory of Ecole Polytechnique Montreal.

At the Ecole Polytechnique Montreal Activation Analysis Laboratory, several previous studies investigated the effects of neutron flux anisotropy in the reactor irradiation sites, changes in coolant temperature and the amount of moderating hydrogenous material present in the sample [St-Pierre and Kennedy 1999, St-Pierre and Kennedy 2004]. In addition, another study resulted in a detector efficiency parameterization model [Kennedy and St-Pierre 1997] that was introduced later in the laboratory neutron activation analysis software EPAA [EPAA 2.2, User's Manual]. All these studies provided a solid base for an accurate epithermal neutron self-shielding factor determination, which allowed us to

develop this study's new method to correct thermal and epithermal neutron self-shielding in activation analysis.

Chapter 2 of this thesis presents an overview of the literature and introduces some of the basic notions regarding the instrumental neutron activation analysis equations, thermal and epithermal neutron self-shielding, and the k_0 method and its fundamental equations. In Chapter 3, the SLOWPOKE reactor and its irradiation facilities are briefly described. In the same chapter, the characteristics of the experimental set-up, sample preparation and gamma ray detection techniques are presented. The end of Chapter 3 identifies and quantifies the sources of uncertainty in instrumental neutron activation analysis. The experimental results are then presented and discussed in Chapters 4, 5 and 6. The first set of experiments is introduced in Chapter 4, where the validity of the neutron self-shielding correction formula is studied and the accuracy of the proposed correction method is tested in two extreme cases: concentrated samples containing a mixture of strong thermal and epithermal neutron absorbers, and a mixture of strong epithermal neutron absorbers. Chapter 5 describes the second set of experiments, were the dependence of the thermal and epithermal neutron self-shielding factors on sample size and irradiation conditions is systematically investigated. Completing the first two steps of the study allow us to conceive an iterative method to correct neutron self-shielding for samples of unknown composition. Chapter 6 introduces this method by reporting the methods for calculating or experimentally determining all the necessary parameters. The differences among the experimental and calculated parameters are discussed, and the method uncertainties are discussed and evaluated. In the final chapter conclusions derived from this work are

presented and some new directions for future research are suggested. The core of this doctoral thesis is presented in the form of research articles in international journals with a peer-review system. Accordingly, the three chapters, 4,5 and 6, are such articles, two published, one in press. In appendices, we present the calculation of the epithermal absorption cross section and the neutron self-shielding correction method spreadsheet to which the author of this thesis has been an important contributor and co-author.

1.2. Objectives

The work presented in this thesis represents a completely new approach to correcting epithermal self-shielding in neutron activation analysis. The main objective followed throughout this work is to characterize the epithermal neutron self-shielding for nuclides having an important absorption cross section for epithermal neutrons, which will result in extending instrumental neutron activation analysis to samples containing this type of nuclides.

In order to achieve our main goal, we have identified several specific objectives: adapting the reactor physics equations of Martinho, Salgado and Gonçalves for calculating the thermal and epithermal self-shielding factors in activation analysis; selecting judiciously the best experimental approach for measuring these factors; experimentally validating the theoretical equations for cylindrical mono-element samples irradiated in a slightly non-isotropic neutron flux; identifying the nuclear parameters that characterize epithermal self-shielding; developing a new method to correct neutron self-shielding in activation

analysis; checking the applicability of this method for concentrated mixtures of epithermal and thermal neutron absorbers.

These objectives required the following steps:

1. Choosing suitable chemical elements having nuclides with various resonance patterns and epithermal absorption cross sections, elements in a chemical form that can be easily diluted in order to investigate the variation of epithermal self-shielding factor with sample mass, and elements in a chemical form that will lead to significant neutron self-shielding, more than 30%, for 1 mL samples. In addition, the selection criteria for these elements included radiation safety aspects related to the manipulation of the samples, type of waste resulting after irradiation, and half-lives of the nuclides activated, short lived nuclides being preferred.

2. Quantitatively estimating neutron flux variations caused by the amount of moderating materials present in the samples, and by the temperature variations of the reactor coolant. The latter values allow us to apply the necessary corrections of the neutron flux, corrections that led to an accurate measurement of the activity and indirectly to an accurate measurement of the effective self-shielding factor.

3. For each selected element, preparing a set of 1 mL cylindrical samples of different concentrations, irradiating and detecting them in identical conditions. As a result, the effective self-shielding factors were plotted as a function of the mass of

element present in sample, and these values were fitted by the least squares method with the proposed sigmoid formulas.

4. Measuring or calculating the nuclear parameters that characterize the self-shielding and implementing these values in the spreadsheet that uses the iterative self-shielding correction method for all nuclides commonly used in neutron activation analysis.

For the first time in the activation analysis field, a practical expression has been proposed to correct both thermal and epithermal neutron self-shielding in neutron activation analysis with cylindrical samples for all types of sample compositions and dimensions, and for all types of irradiation conditions. Based on this expression, a spreadsheet was developed and implemented in routine activation analysis that calculates the thermal and epithermal neutron self-shielding for any nuclide in a cylindrical sample irradiated in a reactor neutron spectrum. Element concentrations measured by neutron activation analysis are corrected for self-shielding with typical accuracy of 2%.

Chapter 2 Epithermal Self-Shielding in NAA

This chapter is divided into four main sections. In the first part the NAA equations are briefly presented. The second introduces this study's approach in calculating the thermal self-shielding factor. The new calculation of the epithermal self-shielding factor by a sigmoid formula is introduced in the third section, and the limitations of this formulation are highlighted. Finally, the NAA k_0 method equations and the Neutron Activation Analysis Laboratory of Ecole Polytechnique Montreal implementation of the k_0 method are also presented.

2.1. Instrumental Neutron Activation Analysis

In a typical neutron spectrum, the neutron activity of a nuclide, A, induced in a sample by radiative neutron capture is usually expressed as the sum of the contributions from thermal and epithermal neutrons, that in the Høgdahl convention take the following form:

$$A = N\ (G_{th}\,\sigma_{th}\,\varphi_{th} + G_{ep} I_0 \varphi_{ep})\left(1 - e^{-\lambda t_i}\right) \qquad (2.1)$$

where:

N - number of atoms of the target nuclide;

σ_{th} - (n, γ) cross-section at 2200 m/s;

I_0 - resonance integral measured in barn;

φ_{th}, φ_{ep} - average unperturbed thermal and epithermal fluxes inside the sample;

G_{th}, G_{ep} - thermal and epithermal self-shielding factors;

λ - decay constant of the considered nuclide;

t_i - irradiation time of the sample.

The thermal self-shielding factor is the same for all nuclides and it depends on the amounts of all elements in the sample absorbing thermal neutrons. The epithermal self-shielding factor for a given nuclide will be influenced by other elements in the sample only if these elements absorb neutrons at resonance energies overlapping with the resonances that activate the nuclide in question.

To calculate σ_{th}, I_0, φ_{th} and φ_{ep}, we used the characteristics of $\sigma(E)$ and $\varphi(E)$:

1. In the thermal region, between 0.00 eV and 0.55 eV, $\sigma(E)$ has a $1/E^{1/2}$ dependence and $\varphi_{th}(E)$ can be described by a Maxwell-Boltzmann distribution;

2. In the epithermal region, between 0.55 eV and 100 keV, $\sigma(E)$ presents several resonances, all described by Breit-Wigner equation, and also the $1/E^{1/2}$ tail, and $\varphi_{ep}(E)$ is a $1/E$ function.

In actual reactor irradiation sites, we have a $1/E^{1+\alpha}$ dependence, where α is a measure of the deviation of the epithermal fluence rate distribution from the $1/E$ shape and is an irradiation site characteristic considered independent of neutron energy. So I_0 in Eq. 2.1 will be replaced by $I_0(\alpha)$ defined as:

$$I_0(\alpha) = \int_{0.55eV}^{\infty} \sigma(E) dE / E^{1+\alpha} \qquad (2.2)$$

Since $\sigma(E)$ becomes very small in the MeV-region, the contribution of the fast neutrons to the (n, γ) reaction rate can be neglected, also because in most NAA irradiation conditions the fast neutron flux component is relatively small.

If we express the activity in Eq. 2.1 in terms of the amount, m, of the element in the sample, we obtain:

$$A = \frac{m N_{Av} \theta}{M_{at}} \sigma_{th} \varphi_{th} (G_{th} + G_{ep} Q_0(\alpha)/f)\left(1 - e^{-\lambda t_i}\right) \qquad (2.3)$$

where:

$Q_0(\alpha)$ - is equal to $I_0(\alpha)/\sigma_{th}$;

f - thermal to epithermal flux ratio, equal to $\varphi_{th}/\varphi_{ep}$;

θ - isotopic abundance of the element isotope that produces the studied (n, γ) reaction;

N_{Av} - Avogadro's number;

M_{at} - atomic weight;

λ - decay constant of the considered nuclide;

t_i - irradiation time.

In neutron activation analysis, to determine the amount of the element in the sample, we compare its activity with that of a standard, which usually has negligible self-shielding. Thus, we need to know the activity the sample would have produced if the self-shielding had been negligible. This is obtained by dividing the sample-measured activity by its effective self-shielding factor, G_{eff}. The sample effective self-shielding factor is defined

as the ratio between the reaction rate per atom in the real sample and reaction rate per atom in a similar and infinitely diluted sample. Using this definition, we can determine theoretically the effective self-shielding factor by dividing the activity of Eq. 2.3 by the activity calculated when G_{th} =1 and G_{ep} =1. Thus, G_{eff} is given by:

$$G_{eff} = \frac{G_{th} + G_{ep}\, Q_0(\alpha)/f}{1+Q_0(\alpha)/f} \qquad (2.4)$$

The variation of G_{th} with the sample geometry and the concentration of the neutron-absorbing element is relatively well understood and, since the cross section for activation by thermal neutrons is a slowly varying function of neutron energy, usually $1/E^{1/2}$, the thermal neutron self-shielding factor for any element can be expressed by the same function of the amount of the element and the element thermal neutron absorption cross-section σ_{abs}.

The determination of G_{ep} as a function of element concentration and sample geometry has always been a difficult task because the variation of absorption cross-section with neutron energy, over the range of the resonances is very different for each nuclide. The numerical methods employed to calculate epithermal neutron self-shielding are impractical for routine NAA work, and impossible to use in the usual case when the concentration of the absorbing element is not known in advance.

All these fundamentals of neutron activation analysis are well-described in the classic text book "Neutron Activation Analysis" [de Soete et al. 1973].

2.2. Thermal Self-Shielding

In relation to G_{th}, several studies have been carried out to determine this factor for different elements in various geometries. In all of these studies, the thermal self-shielding factor was expressed as functions of a variable z. For example, in a given geometry and for elements with a high absorption cross-section compared to the scattering cross-section, Shakir et al. [2001] propose the expression: $z=t\cdot\Sigma_{abs}$, were t represented the characteristic dimension of the sample. If the scattering cross-section is non-negligible, Tzika et al. [2004] propose another formula: $z=t/L$, where L is the diffusion length. Also, all the collisions can be considered as absorbing collisions and, consequently, in the calculation of the self-shielding factor one may use the total macroscopic cross-section instead of the macroscopic absorption cross-section [Gilat and Gurfinkel 1963]. In these papers, the function G_{th} takes different forms: from simple, like an exponential, to complex, like combinations of Bessel and modified Bessel, in the case of cylindrical geometry, for example.

A recent paper of Gonçalves et al. [2005] proposes a universal sigmoid function for thermal neutron self-shielding. Rewriting their expression for G_{th} as a function of the amount of the element in the sample gives:

$$G_{th} = \frac{1.00}{1+ \left(m/m_{th} \right)^{0.964}} \qquad (2.5)$$

where:

m_{th} - amount of the element that causes 50% thermal neutron self-shielding for a given sized cylinder.

The work of Gonçalves et al. [2005] suggests that m_{th} varies with the radius and height of the cylinder as $r(r+h)$. In the publications of Gonçalves et al. we usually see the geometrical factor $rh/(r+h)$. The reason for this different geometrical factor is that in their work they express the self-shielding as a function of the concentration of the element, while in the present work we express it as a function of the mass of the element; thus, the difference between the two approaches is the volume of the sample, which is proportional to r^2h. If neutron scattering in the sample is considered, m_{th} can be estimated from the thermal neutron total and absorption cross-section as follows:

$$\frac{1}{m_{th}} = \frac{k_{th} N_{Av} \sigma_{abs}}{r(r+h) M_{at}} \left(\sigma / \sigma_{abs}\right)^{0.15} \qquad (2.6)$$

where:

k_{th} - dimensionless constant related to the geometry of the sample and to the irradiation site;

σ_{abs}, σ - thermal absorption cross section and the total cross section of the element.

If neutron scattering in the sample is neglected, for a sample containing several elements that absorb thermal neutrons, G_{th} can be calculated by replacing $z = m/m_{th}$ in Eq. 2.6 by the sum of the contributions of all the elements:

$$z = \frac{k_{th} N_{Av}}{r(r+h)} \sum_i \frac{m_i \sigma_{abs,i}}{M_{at,i}} \qquad (2.7)$$

The value of G_{th} thus calculated applies to the thermal neutron activation of all nuclides in the sample.

2.3. Epithermal Self-Shielding for Mono-Element Samples

Until recently, the only way to estimate reliably the epithermal neutron self-shielding has been to perform numerical calculations, such as Monte-Carlo, modelling the shape and density of the object irradiated in an isotropic 1/E neutron spectrum and using tabulated cross-sections. In a few specific cases, an analytical expression was developed, writing G_{ep} as a function of a dimensionless parameter $z = t \cdot \Sigma(E_{res})(\Gamma_\gamma/\Gamma)$, where t is the typical dimension of the sample (for a cylindrical geometry $t=r \cdot h/(r+h)$) and $\Sigma(E_{res})(\Gamma_\gamma/\Gamma)$ is the linear absorption coefficient at the resonance energy E_{res} [Scherbakov and Harada 2002]. In the literature [Abrashkin 1984, Blaauw et al. 2003, De Corte 1987, Kenna and Van Domelen 1966, Scherbakov and Harada 2002, Reynolds and Mullins 1963, Tomuro and Tomura 2002], the G_{ep} function, always described by the same variable z, takes different forms from one paper to another, from one geometry to another, from one nuclide to another.

However, for mono-nuclide samples, nuclides having only one important isolated resonance at the beginning of the epithermal region, and irradiated in an ideal *1/E* epithermal flux, homogeneous and isotropic, in their most recent papers, Martinho and al. [2003] claimed that G_{ep} can be expressed by a universal function, a sigmoid, with only one nuclide-dependent parameter. The G_{ep} calculated with this function agreed with

Monte Carlo calculations for foils, wires and spheres, within 5%. Figure 2.1 give an example of a mono-isotopic element, ^{197}Au, having only one important isolated resonance at the beginning of the epithermal region.

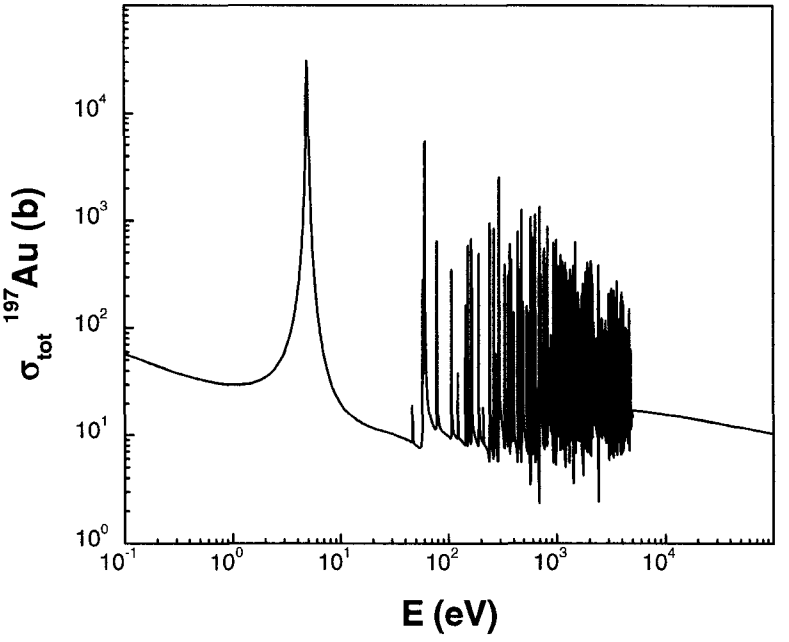

Figure 2.1 Epithermal region of the ^{197}Au total cross section

The same authors [Gonçalves et al. 2004, Martinho et al. 2004] extended their sigmoid function to cylindrical samples of a pure mono-nuclide sample irradiated in an isotropic epithermal neutron field. To adapt their expression to neutron activation analysis, we rewrite it as a function of the amount m of the element in a cylindrical sample of fixed size:

$$G_{ep} = \frac{0.94}{1 + (m/m_{ep})^{0.82}} + 0.06 \qquad (2.8)$$

According to the Martinho et al. 2004, for a homogeneous sample, containing only one mono-isotopic element, and irradiated in an isotropic neutron flux, where the epithermal absorption cross-section of the element has only one isolated resonance, m_{ep} has the following expression:

$$\frac{1}{m_{ep}} = \frac{0.195\ \theta\ N_{Av}\ \sigma_{tot}(E_{res})}{r(r+h)M_{at}}\ (\Gamma_\gamma/\Gamma)^{0.5} \tag{2.9}$$

where:

$\sigma_{tot}(E_{res})$ - peak value of the total cross section;

Γ_γ, Γ - radiative and total resonance width.

In the case of a nuclide having a few isolated resonances, Salgado[c] et al. [2004] propose a formula similar to Eq. 2.9. For n resonances at the beginning of the epithermal region, m_{ep} became:

$$\frac{1}{m_{ep}} = \frac{0.195\ \theta\ N_{Av}}{r(r+h)M_{at}}\ \frac{\sum_{i=1}^{n} w_i \sigma_{tot,i}(E_{res,i})(\Gamma_{\gamma,i}/\Gamma_i)^{0.5}}{\sum_{i=1}^{n} w_i} \tag{2.10}$$

where:

w_i - weighting factor defined by the following formula:

$$w_i = \frac{\Gamma_{\gamma,i}}{E_{res,i}^2}\frac{g\cdot\Gamma_{n,i}}{\Gamma_i} \tag{2.11}$$

with g being a statistical weighting factor: $g = (2J+1)/2(2I+1)$, J is the resonance state spin, I is the target nucleus spin, and $\Gamma_{n,i}$ is scattering resonance width. With the weighting factors defined in this way, the weight w_i is the fraction of the resonance integral due to resonance i.

Eqs. 2.9 and 2.10 may not be applicable in practical activation analysis conditions since the neutron flux is non-isotropic, and in the epithermal region varies as $1/E^{1+\alpha}$. Also, the samples contain more than one element, each element having one or more isotopes. In addition, the activated isotope could have more than few isolated resonances at the beginning of the epithermal region, as is the case of complex total cross section of ^{238}U, illustrated in the Figure 2.2.

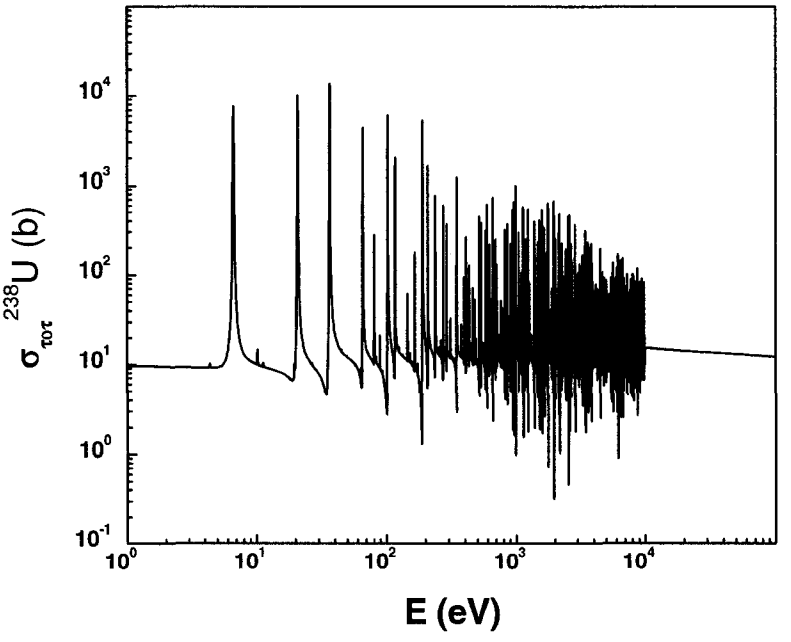

Figure 2.2 Epithermal region of the ^{238}U total cross section

Consequently, from Martinho, Salgado and Gonçalves studies, we conserved only the main idea: the epithermal self-shielding factor can be described by a sigmoid function that depends on the amount of the studied element in the sample and on a parameter m_{ep}, Eq. 2.8. The parameter m_{ep} contains the geometrical and nuclear factors, and can be thought of as the amount of the element that causes about 50% epithermal neutron self-shielding for a given sized cylinder. From Eqs 2.9 and 2.10 it can be seen that m_{ep} varies with the radius and height of the cylinder as $r(r+h)$.

In this study, the epithermal neutron self-shielding factor is given by [Chilian[b] et al. 2006]:

$$G_{ep} = \frac{0.94}{1+\left(\frac{m N_{Av} k_{ep} \sigma_{abs,ep}}{r(r+h) M_{at}}\right)^{0.82}} + 0.06 \qquad (2.12)$$

k_{ep} - epithermal self-shielding constant

$\sigma_{abs,ep}$ - epithermal neutron absorption cross-section

The epithermal self-shielding constant, k_{ep}, depends of the characteristics of the reactor irradiation site. The epithermal neutron absorption cross-section, $\sigma_{abs,ep}$, by definition, includes the absorption of neutrons by the resonances of all isotopes of the element which may overlap with the resonances of the nuclide being activated. Considering the complexity of the nuclide resonance pattern of the absorption cross section, and the practical irradiation conditions, $\sigma_{abs,ep}$, was experimentally measured for several nuclides.

Eq. 2.12 ignores the possible shielding by other elements in the sample; this should usually be negligible if the resonances of nuclides from different elements will not overlap. At contrary, the mutual epithermal self-shielding became significant if the sample contains very high concentrations of certain elements with nuclides having resonances that overlap. Figure 2.3 shows the case of ^{127}I, ^{79}Br, which present a resonance overlapping between two important resonances of ^{127}I and the first two resonances of ^{79}Br.

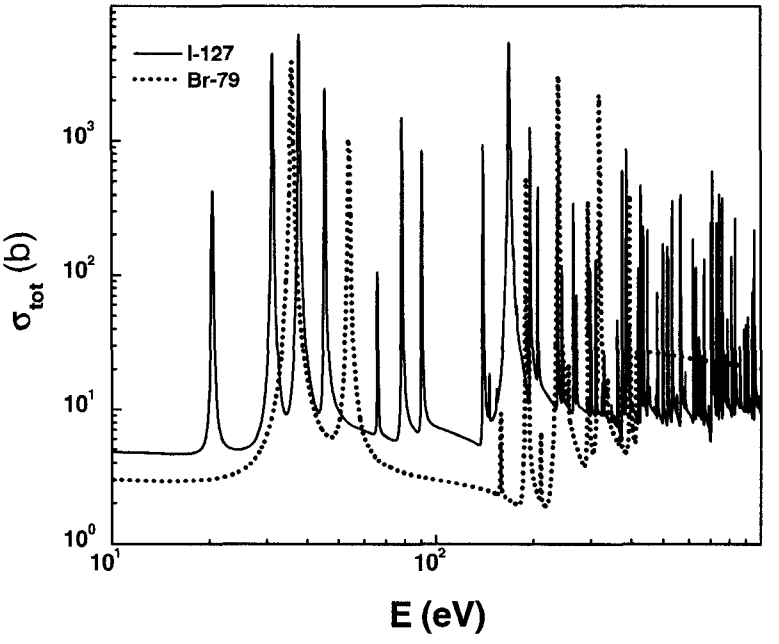

Figure 2.3 Total cross section resonance overlapping for ^{127}I and ^{79}Br

Values of $\sigma_{abs,ep}$ were also calculated by a formula derived from Eqs 2.10 for capture reactions with several isolated resonances at the beginning of the resonance region:

$$\sigma_{abs,ep,Salgado} = 0.195\ \theta\ \frac{\sum_{i=1}^{n} w_i \left(\sigma_{tot,i}(E_{res,i}) \sqrt{\frac{\Gamma_{\gamma,i}}{\Gamma_i}} \right)}{\sum_{i=1}^{n} w_i} \qquad (2.13)$$

An example of $\sigma_{abs,ep}$ calculation is given at the end of this thesis, in Appendix A.

2.4. NAA k_0-method and its fundamental equations

In order to experimentally determine the concentration of the analyte a in the sample, in this study we use the NAA k_0-standardization [De Corte 1987]. According to this method, the concentration of an element in the sample is obtained as:

$$\rho_a(\mu g / g) = \left(\frac{N_p}{SDCW} \right)_a \frac{1}{A_{sp,Au}} \frac{1}{k_{0,Au}(a)} \frac{G_{th,Au} f + G_{ep,Au} Q_{0,Au}(\alpha)}{G_{th,a} f + G_{ep,a} Q_{0,a}(\alpha)} \frac{\varepsilon_{p,Au}}{\varepsilon_{p,a}} 10^6 \qquad (2.14)$$

where:

ρ_a - concentration of analyte a;

Au - coirradiated neutron fluence rate monitor, usually gold;

N_p - measured net peak area, corrected for pulse losses (dead time, random coincidence (pulse pile-up));

t_c - counting time;

S - saturation factor; =1- exp(-λt_i);

D - decay factor; = exp(-λt_d);

C - counting factor; =(1- exp(-λt_c))/ λ, correcting for decay during counting;

W - sample mass (g);

A_{sp} - the specific count rate; = $(N_p)/SDCw$, with w the mass of the monitor element (g);

$k_{0,Au}(a)$ - experimentally determined k_0 factor of analyte a versus a monitor Au, defined as:

$$k_{0,Au}(a) = \frac{M_{Au}\theta_a\sigma_{th,a}\gamma_a}{M_a\theta_{Au}\sigma_{th,Au}\gamma_{Au}} \qquad (2.15)$$

- with M the atomic mass, θ the isotopic abundance, and γ the absolute gamma intensity;

ε_p - full-energy peak detection efficiency, including true coincidence effect.

In Eqs. 2.14 and 2.15 the co-irradiated monitor is the gold comparator (^{197}Au(n, γ)^{198}Au; E_γ = 411.8 keV), versus which the k_0 factors are expressed in the published tabulations [De Corte and Simonits 2003]. However, by making the necessary transformations, we can replace the gold comparator with any other monitor. Note that, with the SLOWPOKE reactor, the co-irradiated monitor does not need to be irradiated each time because the neutron flux is reproducible.

Based on the k_0-standardization equations, in order to calculate the concentration of a given element in a sample to be analyzed, at SLOWPOKE laboratory of Ecole Polytechnique of Montreal, a homemade Java program EPAA (Ecole Polytechnique Activation Analysis) was developed [EPAA 2.2, User's Manual]. To simplify the form of the Eq. 2.14, a sensitivity factor $B_{a,EPAA}$ is introduced and we obtained:

$$\rho_{a,EPAA}(\mu g/g) = \frac{N_p}{B_{a,EPAA}\ \varphi_{th}} \frac{1}{SDCW} \tag{2.16}$$

where φ_{th} is the value of the flux indicated at the rector console and the sensitivity factor is taken from the EPAA library built by considering samples without self-shielding ($G_{th,a}$ and $G_{ep,a}$ are equal to one). In this library, for analyte a, the sensitivity factor has the following form:

$$B_{a,EPAA} = const.\ k_{0,Au}(a)\ \varepsilon_{p,a,EPAA}\ \left(1 + Q_{0,a}(\alpha)/f\right) \tag{2.17}$$

with the *const.* related to the monitor used in EPAA to build the library of experimentally determined sensitivity factors and $\varepsilon_{p,a,EPAA}$ calculated in the EPAA program as indicated in Section 3.4.

Any neutron flux variations in the reactor, caused by the presence of moderating substances in the sample or temperature variations in the reactor, will modify B_a and φ_{th} in Eq. 2.16. In addition, the detector efficiency $\varepsilon_{p,a}$ for some samples having special geometry or special composition can differ from the value used in the EPAA program. So, to obtain the most accurate concentration for analyte a in a sample with self-shielding

($G_{th,a}$ and $G_{ep,a}$ are smaller than one), the necessary corrections related to those effects must be introduced. Thus, we obtained the following expression:

$$\rho_{a,weighing} = \rho_{a,EPAA} \frac{\varepsilon_{p.a.EPAA}\left(1+Q_0(\alpha)/f\ \right)}{\varepsilon_{p,a}\left(G_{th,a}+G_{ep,a}\,Q_0(\alpha)/\left(f\ C_T C_M\right)\right)\ C_T C_M} \qquad (2.18)$$

where C_T is the correction for reactor temperature variations and C_M is the correction for flux moderating effects in the sample. Those corrections will be discussed in more detail in the Sections 3.1.3, 3.1.4, and 3.4 of this thesis.

With the real concentration of the analyte a obtained by weighing the chemical substances used in sample preparation, and by replacing $(1 + Q_0(\alpha)/f)$ with $(1 + Q_0(\alpha)/f\ C_T C_M)$ in Eq. 2.18, we can extract the G_{eff} as is defined in Eq. 2.4: ($G_{eff,a} = (G_{th,a} + G_{ep,a}Q_0(\alpha)/f\ C_T C_M)/(\ 1 + Q_0(\alpha)/f\ C_T C_M\ )$; in the real sample the neutron flux being corrected for the temperature and moderating effects) and we obtain:

$$G_{eff,a} = \frac{\rho_{a.EPAA}}{\rho_{a,weighing}} \frac{\varepsilon_{p,a.EPAA}}{\varepsilon_{p,a}\ C_T C_M} \qquad (2.19)$$

To experimentally determine G_{eff} for the analyzed samples, the following work will use Eq. 2.19 with the appropriate C_T and C_M corrections.

Chapter 3 Experimental Methodology

The Ecole Polytechnique SLOWPOKE reactor and its irradiation facilities are descried in the beginning of this chapter. In the following sections, the sample preparation, the gamma detection system, detection efficiency calculation techniques, and the sources of uncertainties in NAA are presented.

3.1. SLOWPOKE Reactor and its Irradiation Facilities

SLOWPOKE, an acronym for Safe Low Power Critical Experiment, is a 20 kW pool type reactor designed and produced by Atomic Energy Canada Limited as a neutron source for activation analysis and the production of short-lived isotopes. The core of the reactor contains 198 low enriched uranium (20%) fuel elements based on the Zircaloy-4 clad UO_2 CANDU fuel element, but with a smaller diameter (5.25 mm) [El Hajjaji 1999, Townes and Hilborn 1985]. The general design specifications for the SLOWPOKE reactor are introduced in Table 3.1.

Table 3.1 SLOWPOKE Design Specifications

Pool Diameter	2.5 m
Pool depth	6.1 m
Container Diameter	0.6 m
Container Height	5.3 m
Core Diameter	22.0 cm
Core Height	22.0 cm
Maximum Fission Power	20.0 kW

Fig. 3.1 presents the core of the SLOWPOKE reactor with the five inner irradiation sites in the annular beryllium reflector that surrounds the fuel and up to five outer irradiation sites in the surrounding water [Townes and Hilborn 1985]. Irradiation capsules are transferred to and from the reactor using a pneumatic system that extends from the loading station to the irradiation sites.

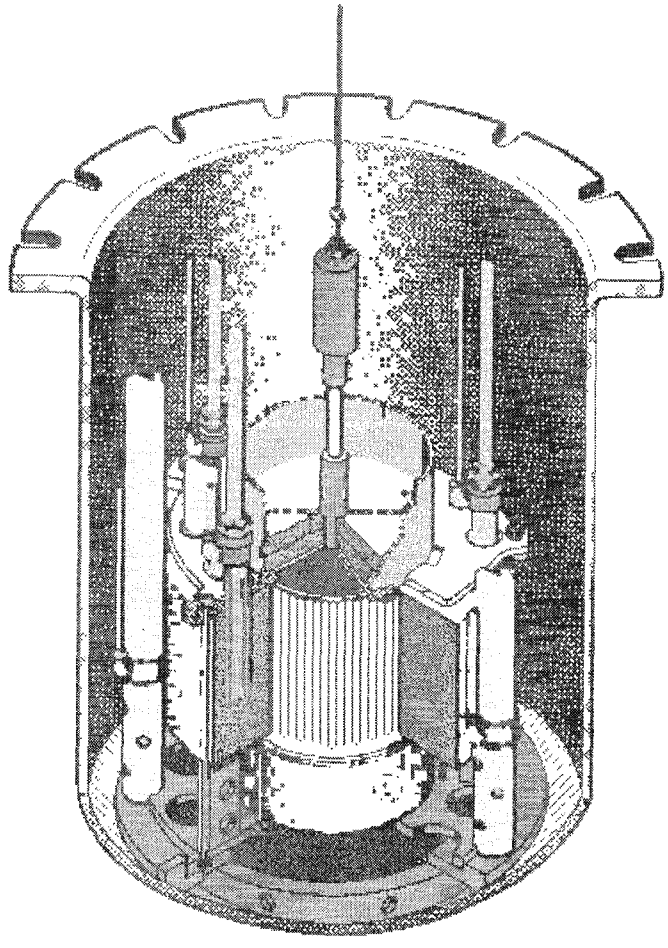

Figure 3.1 SLOWPOKE Critical Assembly

Having negative fuel temperature coefficient and negative coolant temperature and void coefficients, the core of the reactor is designed so that the most severe reactivity transients are safely limited. The reactor has a single motor-driven cadmium control rod that moves along the central axis of the core through a hole in the top reflector. The total worth of the control rod is 5.1 mk.

In this third chapter, the characteristics of the Ecole Polytechnique SLOWPOKE reactor irradiation sites are presented together with the variation of neutron flux with the reactor temperature and with the amount of moderator in the irradiation vial.

3.1.1. Characteristics of the irradiation sites

The SLOWPOKE reactor is a small research reactor for which the neutron flux in a given irradiation site is reproducible to within 1% [Kennedy and St-Pierre 2003]. For NAA, using k_0-standardization, the sensitivity constants (counts per microgram) are measured once for each element and used for subsequent analyzes over a long period of time.

In this study the control console flux setting was $5*10^{11}/cm^2/s$ which corresponds to a reactor power of 10 kW. The samples were irradiated in the inner irradiation site no.1 and in the outer sites no. 6 and 8. Table 3.2 gives some characteristics of these SLOWPOKE irradiation sites.

Table 3.2 Characteristics of the SLOWPOKE irradiation sites

Irradiation Site No.	Reflector Material	Inner Diam. (cm)	Outer Diam. (cm)	Radius from Core Axis (cm)	f	α
1 - inner	beryllium	1.58	2.56	15	18.0	-0.051
6 - outer	water	2.90	3.54	25	48.6	+0.016
8 - outer	water	1.58	2.22	25	52.7	+0.018

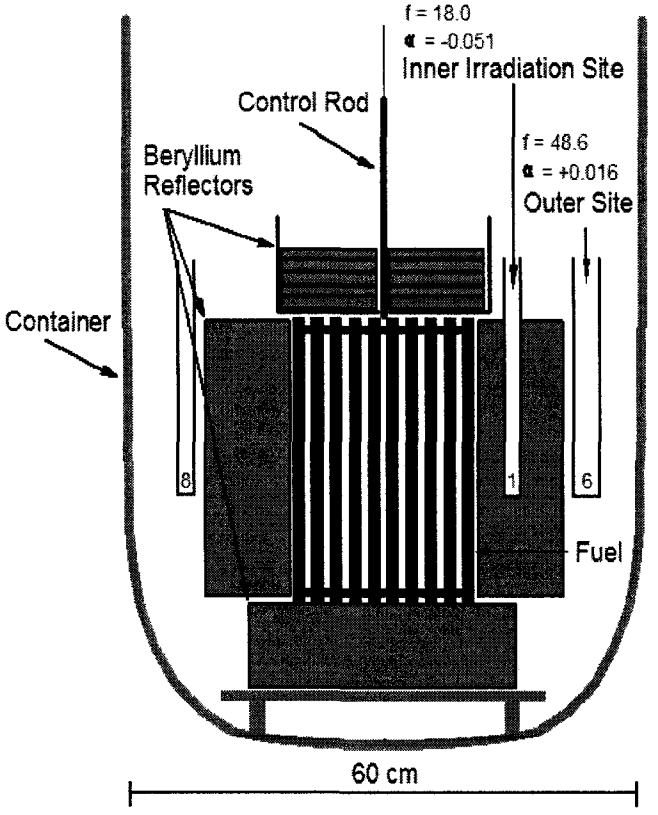

Figure 3.2 SLOWPOKE reactor core with irradiation sites

Fig. 3.2 presents schematically the irradiation sites with their location in the reactor [St-Pierre and Kennedy 1999]. Because the outer irradiations sites no. 6 and 8 are situated at the same radial distance from the core, the values of f and α are almost identical.

3.1.2. Flux Anisotropy

In the SLOWPOKE reactor both inner and outer irradiation sites are relatively close to the reactor core and are situated in beryllium or water reflectors. In these conditions, the thermal and epithermal fluxes are nearly isotropic; they become increasingly anisotropic with an increase in the radial distance from the core.

Using grids of Cr and Zr wires, St-Pierre and Kennedy [2004] measured the flux gradients in the inner and outer irradiation sites of the Ecole Polytechnique SLOWPOKE reactor. Fig. 3.3 presents these gradients.

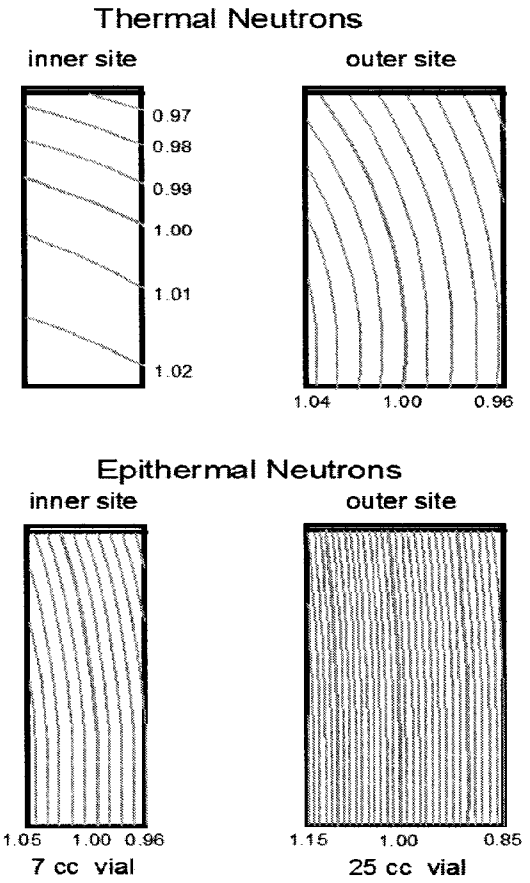

Figure 3.3 Thermal and epithermal flux gradients across the vial in the inner and outer irradiations sites

Because the inner sites were purposely placed at the radius of maximum thermal flux in the annular beryllium reflector, in these sites the horizontal gradient of the thermal flux is less than 1% across the 14 mm diameter of the vial. Over the height of the vial the thermal flux decreases by only 5%. These very small gradients are indicative of a very isotropic thermal neutron flux. For the outer site, the thermal flux gradient was found to be 5% across the 14 mm diameter of a 7 cc vial, and about 2% over the height of the vial [St-Pierre and Kennedy 2004].

In the inner and outer sites, over the height of the vials, the variation of the epithermal flux is small. However, the horizontal epithermal flux gradients are larger than the horizontal thermal flux gradients. Across the 14 mm diameter of the vial in the radial direction, for the inner site, the epithermal gradient was found to be 9% and, for the outer site, 17% [St-Pierre and Kennedy 2004]. This indicates that the epithermal flux is less isotropic than the thermal flux.

3.1.3. Flux Changes Caused by Temperature Variations

In the SLOWPOKE reactor a variation of the temperature changes the properties of the moderator causing a variation of the neutron flux. In addition, the reactor is designed to automatically adjust the position of the control rod in order to maintain a constant $^{113}Cd(n, \gamma)$ reaction rate in the cadmium flux detector, reaction rate that corresponds to the thermal neutron flux value chosen by the operator at the reactor console.

For most elements, in the thermal region, the activation cross section varies as $1/v$, where v is the neutron velocity. However, up to 0.5 eV neutron energy, the cross section for the $^{113}Cd(n, \gamma)$ reaction is fairly independent of neutron velocity. Consequently, for a constant $^{113}Cd(n, \gamma)$ reaction rate, as the temperature increases, the reaction rate for the activated elements decreases. This is seen as an apparent decrease in the neutron flux.

The thermal neutron flux measured as a function of the reactor temperature using a *1/v* flux monitor indicates a decrease of thermal neutron flux by about 0.2% per degree Celsius. For the epithermal and fast fluxes no significant variation was observed [St-Pierre and Kennedy 1999]. The variation of neutron flux with the temperature imposes a correction in the formula used for calculating G_{eff}, Eq. 2.4, as follows:

$$G_{eff} = \frac{G_{th} + G_{ep}\, Q_0(\alpha)/f\; C_T}{1+Q_0(\alpha)/f\; C_T} \tag{3.1}$$

where:

$$C_T = 1 - \frac{\left(T(^0C) - 45^0C\right)\cdot 0.2}{100} \tag{3.2}$$

and $T(^0C)$ is the temperature indicated at the reactor operating console, value that represents the temperature of the reactor coolant obtained from a thermocouple that measures the temperature of the water leaving the core.

To be able to compare experimental results obtained from different sets of samples irradiated at different reactor temperatures, we arbitrarily choose the reference

temperature of 45^0C and we use this value in all the flux corrections related to the temperature variation.

3.1.4. Flux Changes in Hydrogenous Samples

By using samples of different sizes, containing different types of moderating materials: water, polyethylene and SiO_2, and irradiated in the inner and outer irradiation sites of the SLOWPOKE reactor, the variation of the neutron flux with sample size was studied by St-Pierre and Kennedy [2004]. None of the materials used contained elements with high absorption cross section. The samples of silica or carbon were found to have a negligible effect and the results for polyethylene and water are similar. The experimental data indicate that the effect is zero for zero sample volume and tends toward a maximum as the samples increase in size.

In the inner site of the SLOWPOKE reactor the flux is poorly thermalized, the thermal-to-epithermal ratio being 18.0 and the thermal-to-fast neutron flux ratio being 4.0 [Kennedy et al. 2000]. In outer site 6 the thermal-to-epithermal ratio is 48.6 and the thermal-to-fast neutron flux ratio is 15.8 [Kennedy et al. 2000]. For fast neutrons, the hydrogen reduces the average flux.

The amount of hydrogen in the inner site has no effect on the epithermal neutron flux because it produces as many epithermal neutrons as it removes. On the contrary, in the outer site, there are relatively few fast neutrons to moderate; thus, the removal of epithermal neutrons dominates [St-Pierre and Kennedy 2004].

For the thermal neutrons in the inner site there are fewer absorptions by hydrogen, which makes dominant the thermalization of the epithermal neutrons and the thermal neutron flux increases with the sample size. In the outer site, for thermal neutrons, adding moderator has no effect because absorption by hydrogen in the sample equals production by thermalization.

In the present work, in order to obtain homogeneous samples having different concentrations of the studied element, water solution samples, powdered sugar mixtures or metallic oxides fixed in organic resin were prepared. All diluting materials used in this study, water, sugar and organic resin, are hydrogenous substances that will modify the neutron flux inside the irradiated sample. So the effect of the neutron flux moderation and absorption on the average neutron flux in the sample must be considered and Eq.3.1 becomes:

$$G_{eff} = \frac{G_{th} + G_{ep}\, Q_0(\alpha)/f\; C_T C_M}{1 + Q_0(\alpha)/f\; C_T C_M} \tag{3.3}$$

where:

$$C_M = 1 + M \tag{3.4}$$

and M is a fraction related to the volume and the type of the moderator present in the sample. For water and sugar moderators, the values of M were determined considering the results obtained by St-Pierre and Kennedy [2004]. Beside water and sugar, another diluting substance, organic resin, was used to prepare homogeneous metallic oxide samples having different concentrations. For this type of moderator M was

experimentally determined by comparing the activity of Zr monitors immersed in the same 6 mL volume of air, water, sugar or organic resin and irradiated in the same conditions. Table 3.3 shows the values of M used in this study for different volumes of water, sugar and resin moderator present in the sample for the inner and outer irradiation sites.

Table 3.3 M values for different volumes of water, sugar and resin moderator in the inner and outer irradiation sites

		Water		Sugar		Organic Raisin	
Vol (cm^3)	r (cm)	M_{in}	M_{out}	M_{in}	M_{out}	M_{in}	M_{out}
1.0	0.5	0.030	-0.020	0.030	-0.020	0.030	-0.015
3.0	0.7	0.060	-0.040	0.055	-0.030	0.050	-0.015
4.4	0.7	0.070	-0.060	0.060	-0.030	0.055	-0.030
6.0	0.7	0.075	-0.070	0.060	-0.050	0.055	-0.030

Using the activation analysis technique, in the composition of the organic resin we detected the following elements: Si (1090 ± 83 μg/g), Sn (97 ± 4 μg/g), Ba (14.9 ± 0.7 μg/g), Br (15.6 ± 0.5 μg/g), and traces of Na, Cl, Al and Mn (less than 10 μg/g).

3.2. Sample Preparation

The chemical substances used in this study were: water solutions of KBr, $Cd(NO_3)_2$:$4H_2O$, $InCl_3$, KI, $CsNO_3$, Sm_2O_3, $NaAuCl_4$:$2H_2O$, $UO_2(C_2H_3O_2)$:$2H_2O$; HCl solutions of K(SbO)C4H4O6; solid mixtures of WO_2 powder and K(SbO)C4H4O6 powder; and Zr metal discs.

38 nuclides were identified to have a resonance integral to thermal absorption cross section ratio, Q_0, higher than 10, corresponding to a high importance of activation by epithermal neutrons relative to thermal activation. Among these 38 nuclides, we preferred the ones present in highly soluble chemical substances, which allow preparation of homogeneous, small volume samples of a wide range of concentrations. In addition, to reduce the irradiation time and decay time, and also to minimize the radioactive waste generated by activation, relatively short half-life activation resulting radionuclides (10 minutes to 3 days, with an exception: 60.2 days for ^{124}Sb) were selected.

For each selected nuclide and it's chemical element, the epithermal neutron self-shielding was studied by preparing, irradiating and counting a set of 1 mL cylindrical standards, with r = 5.0 mm and h = 12.7 mm, containing different masses of the element. To vary the element concentration in the sample, water, sugar or organic resin were employed as diluting materials. For solid mixtures, during the irradiation and the counting, the powder sample geometry was conserved by using a wooden plug.

To study the thermal neutron self-shielding factor, it's dependence on the amount of the element present in the sample, on the sample size and on the irradiation site, several

sample sets were prepared by mixing NH_4Cl powder with powdered sugar and pressed into 10 mm or 14.4 mm diameter polyethylene irradiation vials. The height of the cylindrical sample was maintained at 12.7 mm or 30.7 mm with a wooden plug, to give volumes of 1 mL or 3 mL. Both sets were completed with more dilute samples, prepared by dissolving NH_4Cl in water and sealing 1 mL or 3 mL of solution in polyethylene vials.

The dependence of the epithermal self-shielding factor on sample size and on irradiation site was studied by using various stacks of Zr metal disks with three different diameters, 6 mm, 10 mm and 14 mm. The stacks of disks, with heights varying between 0.127 mm and 12.7 mm, In addition to the Zr disks, measurements were also done with several 1 mL powder samples of different concentrations, up to 2.12 g Zr, obtained by mixing ZrO_2 powder with Al_2O_3 powder. The powder samples, sealed in polyethylene vials of 10 mm diameter, six 4.4 mL samples, with diameter 14 mm and different Zr concentrations, were prepared by using different materials: zirconium plate, zirconium oxide powder, zirconium metal powder, zirconium nitrate, zirconium sulfate and zirconium nitrate diluted in organic resin.

3.3. Gamma Detection Chain

In this work, an intrinsic germanium detector (p-type) with efficiency of 14.6% relative to a 76 mm × 76 mm NaI(Tl) detector was used together with a model that parameterises the detector efficiency.

The detector characteristics are introduced in the Table 3.4.

Table 3.4 Intrinsic germanium detector (p-type) with efficiency of 14.6 % relative to a 76 mm × 76 mm NaI(Tl) detector characteristics

Resolution (keV, FWHM)	Peak/ Compton	Diameter (mm)	Length (mm)	Active Area Window (cm^2)	Distance from Window (mm)
1.75 (1.33 Mev)	44.9:1	45	40	15.9	3

The following section of chapter 4 will discuss the applicability of the detector efficiency model for our experimental conditions: samples having different cylindrical geometries, different compositions and densities, which may contain activated isotopes with γlines at low energies.

3.4. Detection Efficiency

Detection efficiency is defined as the observed counts per unit of time divided by the absolute gamma-ray emission rate, and depends on the following:

1. Intrinsic efficiency of the detector (probability that the gamma ray is totally absorbed in the detector crystal)

2. Distance of source from the detector (for distances large relative to the detector, this goes as $1/r^2$, were r is the distance between the center of mass of the sample and the detector effective center). To first order, this is pure

geometry, although as the sample approaches the detector, edge effects can become significant.

3. Gamma-ray absorption in the sample. The higher the gamma energy-ray energy, the smaller this effect is. Transmission decreases exponentially with absorber thickness and the half thickness depends strongly on the energy and less strongly on the density of the sample.

In this work, to calculate the detector efficiency, we used the parameterisation of detector efficiency for the standardization of NAA with stable low flux reactors, developed by Kennedy and St-Pierre [1996]. The improved relative method uses standards activated once and the sensitivity factors determined are used for all subsequent analyses with the same counting geometry. This method is extended to any other counting geometry by parameterising the detection efficiency, taking into account γ-ray energy, sample-detector distance, sample size and γ-ray coincidence summing effects. The low activity produced in low flux reactors requires close counting geometries that imposes more precaution to be taken in order to reach accuracies of a few percent.

The method employs the concept of effective interaction depth (EID), [Tian et al. 1993, Tian and Ni 1994]. At a point on the axis far from detector, the absolute efficiency as a function of γ-ray energy is measured. At several energies, the efficiency as a function of distance along the axis is then measured. Coincidence summing is calculated using information from the decay schemes and total efficiencies are determined using measured peak-to-total ratios.

Working with the point sources, a model was developed that calculates efficiencies as a function of position of point sources on the detector axis [Kennedy and St-Pierre 1997]. For NAA samples, which may have a volume of several mL, the source position was taken as the geometrical centre of the sample. In the development of this model a very important part was the accurate calculation of the relative efficiencies because the model will be used to calculate sensitivity factors for a given geometry from those measured on another detector.

This technique for estimating detection efficiencies was validated for this study specific experimental and detection conditions. Because samples of different densities, compositions and geometries were used, a particular attention was given to the sample gamma absorption correction term in the detection efficiency calculation.

To estimate gamma self-absorption in the sample, the mass attenuation coefficients were used [De Soete et al. 1973]. For each element the mass attenuation coefficient was expressed as a second order polynomial function of energy. The polynomial function coefficients were determined by fitting the existing data. For the composite materials (like homogeneous mixtures of iron oxide with sugar samples), the total mass attenuation coefficient can be obtained by summing the products of the mass attenuation coefficient and the fraction of the composing elements. For missing Z values in the mass attenuation coefficients tables, interpolation was made.

The parameterisation of detector efficiency method was experimentally verified for two types of standards in the same geometry as the samples prepared in this study: one set of

metallic zirconium samples having a density of 6.49 g/cm^3 and various geometries and one set of iron oxide and sugar mixture samples having the same geometry but various iron concentrations. These standards were irradiated in the inner site of SLOWPOKE reactor and were counted at 10 cm from the HPGe detector. It was found that the method works well for the considered counting geometries and the analyzed small cylindrical homogeneous samples (1 ml to 7 mL samples with 0.5 cm to 0.7 cm radius). The standard uncertainty in relative detection efficiency for the actual 1 mL geometry was estimated to be 2% or less.

3.5. NAA sources of uncertainties

According to the individual steps of activation analysis, several sources of uncertainties are identified in NAA [Smodiš and Bučar 2006].

In the first source of uncertainties, sample preparation, the most important contribution is the precision of the balance, ± 0.05 mg for the four digit balance and 0.5 mg for the three digit balance. Because the samples of hygroscopic substances were prepared in a glove box in an argon atmosphere with negative pressure applied, the moisture determination introduced negligible uncertainties. The uncertainties associated with the variation of the isotopic abundance are considered negligible since all the substances used in this study were bought from NIST certified suppliers. Also, the impurities of the irradiation vials or diluting materials: epoxy organic resin, water and sugar, are considered sources of negligible uncertainties.

In the second source of uncertainties, irradiation conditions, the irradiation geometry component related to the neutron flux gradient (usually very low) was minimized by irradiating a set of samples in the same irradiation site and in the same geometry. For relatively long irradiation times, above 10 min, the timing uncertainties are negligible. For short irradiation times, when possible, the samples of a given set all had the same irradiation time, which minimizes the related uncertainty. It should be mentioned that the short irradiation times, up to 10 min, were corrected for the transit time of the sample through the pneumatic system [Kassakov 2007]. Uncertainties due to nuclear interferences and neutron spectrum variation are considered negligible.

The third step, detection by gamma spectrometry, has multiple sources of uncertainties. In this study, the uncertainty due to counting statistics is less than 0.5% considering that usually peaks of at least 50,000 counts were acquired. The counting dead time was always under 20%, so the related uncertainties are less than 1%. Since the standardization was performed in the same geometry, true coincidence uncertainty is negligible. Decay timing, counting time, gamma interferences and background corrections are considered negligible sources of uncertainties. The last detection sources of uncertainties, gamma self-absorption, counting geometry and intrinsic detector efficiency are included in the detection efficiency parameterisation, and result in less than 2% uncertainty.

The last source of uncertainty in activation analysis is the k_0 method of standardization and its factors, k_0, Q_0, f and α. Among these factors the main components in the

uncertainty budget are k_0 and Q_0, and their uncertainties are tabulated [De Corte and Simonits 2003].

In this study, the combined uncertainty (one standard deviation) of the experimental G_{ep} is calculated according to the law of propagation of uncertainties, and the uncertainty in $\sigma_{abs,ep}$ results from fitting these experimental G_{ep} with the theoretical curve by the least squares method.

Chapter 4 First Article: Extending NAA to Materials with High Concentrations of Neutron Absorbing Elements*

C. Chilian, M. Kassakov, J. St-Pierre and G. Kennedy

Ecole Polytechnique, P.O.Box 6079, Downtown, Montreal, Quebec, H3C 3A7, Canada

Abstract

The recently discovered universal functions for thermal and epithermal neutron self-shielding were adapted to NAA of cylindrical samples, expressing the magnitude as the product of a nuclear factor, a geometrical factor and the amount of the neutron absorbing element. The theory was tested and the nuclear factors were measured for 1 mL samples containing the halogens Cl, Br and I. Tests on samples containing these elements at a priori unknown concentrations, irradiated in a mixed thermal and epithermal neutron spectrum, showed that self-shielding as high as 30% could be corrected with an accuracy of about 1%, except in cases with significant epithermal shielding of one element by another.

---

* Journal of Radioanalytical and Nuclear Chemistry, Vol.270, No.2 (2006) 417-423

4.1. Introduction

The most important advantage of neutron activation analysis over other methods of chemical analysis is its ability to give accurate average concentrations of many elements in bulk solids with no sample preparation. For samples with high concentrations of neutron absorbing elements and significant neutron self-shielding, it is possible to obtain accurate results when irradiating in a well-thermalized neutron spectrum, because thermal neutron self-shielding has been well understood for many years and can be accurately corrected. However, with the poorly thermalized neutron spectra common at many research reactors, accurate corrections are difficult because of the complexity of resonance neutron self-shielding. The task is especially difficult for the analysis of materials with high concentrations of heavy elements, which often have relatively high resonance cross-sections. In this work, a recent discovery in the field of resonance neutron self-shielding is exploited to develop a self-shielding correction method for cylindrical samples, of a priori unknown composition, irradiated in a mixed thermal and epithermal neutron spectrum.

4.2. Theory

For irradiations in a typical reactor neutron spectrum, the activity of a nuclide produced by neutron capture is usually expressed as the sum of the contributions from thermal and epithermal neutrons:

$$A = N\,(G_{th}\,\sigma_{th}\,\varphi_{th} + G_{ep} I_0 \varphi_{ep})\left(1 - e^{-\lambda t_i}\right) \qquad (4.1)$$

where N is the number of atoms of the target nuclide, σ_{th} the thermal neutron activation cross-section, I_0 is the resonance integral, φ_{th} and φ_{ep} the unperturbed thermal and epithermal fluxes averaged over the volume of the sample. In practice, the latter may be measured by simultaneously irradiating flux monitors near the absorbing sample, taking in account flux gradients and the fact that the absorbing sample may perturb the nearby fluxes outside the samples. For short irradiations, assuming the unperturbed fluxes are constant with the time, they may be measured by irradiating flux monitors before or after the absorbing sample at the same position. G_{th} and G_{ep} are the thermal and epithermal self-shielding factors. They depend on sample geometry and they are unity for sufficiently dilute samples. The thermal self-shielding factor depends on the amounts of all elements in the sample that absorb thermal neutrons. The epithermal self-shielding factor will be influenced by other elements in the sample only if these elements absorb neutrons at resonance energies overlapping with the resonances that activate the nuclide in question.

If we express the activity in Eq. 4.1 in terms of the amount, m, of the element in the sample, it becomes:

$$A = \frac{m N_{Av} \theta}{M_{at}} \sigma_{th} \varphi_{th} (G_{th} + G_{ep} Q_0 / f) \left(1 - e^{-\lambda t_i}\right) \qquad (4.2)$$

where $Q_0 = I_0/\sigma_0$ and $f = \varphi_{th}/\varphi_{ep}$. In neutron activation analysis, to determine the amount of the element in a sample, we compare its activity with that of a standard, which usually has little enough of the element that self-shielding is negligible. Thus, we need to know

the activity the sample would have produced had self-shielding been negligible. This is obtained by dividing the sample's measured activity by its effective self-shielding factor, G_{eff}. This effective self-shielding factor is determined theoretically by dividing the activity of Eq. 4.2 by the activity calculated with $G_{th} = 1$ and $G_{ep} = 1$. Thus, G_{eff} is given by:

$$G_{eff} = \frac{G_{th} + G_{ep} Q_0 / f}{1 + Q_0 / f} \tag{4.3}$$

The variation of G_{th} with sample geometry and the concentration of the neutron-absorbing element is relatively well understood. For cylindrical samples of a given concentration, irradiated in an isotropic neutron field, the variation of G_{th} with sample size depends on the factor $rh/(r+h)$, where r is the radius and h the height [Gilat and Gurfinkel 1963]. Since the cross-section for activation by thermal neutrons is a slowly varying function of neutron energy, usually $E^{-1/2}$, the thermal neutron self-shielding factor for any element can be expressed by the same simple function of the amount of the element and the element's thermal neutron absorption cross-section σ_{abs}.

On the other hand, the determination of G_{ep} as a function of element concentration and sample geometry has always been a difficult task because the variation of absorption cross-section with neutron energy, over the range of the resonances, is very different for each nuclide. Reactor physicists usually calculate epithermal neutron self-shielding by the Monte Carlo method, using a model of the object being activated and absorption and scattering cross-sections as a function of neutron energy. This is impractical for routine

NAA work, and impossible in the usual case where the concentration of the absorbing element is not known in advance. However, in a recent paper, Martinho et al. [2003] claimed that G_{ep} can be expressed by a universal function, a sigmoid, with only one nuclide-dependent parameter. The G_{ep} calculated with this function agreed with experimental data and Monte Carlo calculations for foils, wires and spheres, within 5%.

The same authors [Gonçalves et al. 2004] recently extended their sigmoid function to cylindrical samples of a pure element irradiated in an isotropic epithermal neutron field:

$$G_{ep} = \frac{0.94}{1+(z/z_0)^{0.82}} + 0.06 \qquad (4.4)$$

with $z_0 = 2.70$ and $z = 1.65\ rh/(r+h)\ \Sigma_{tot}(E_{res})\ (\Gamma_\gamma/\Gamma)^{1/2}$, where r and h are the radius and height of the cylinder and, in the case of a single dominant resonance, $\Sigma_{tot}(E_{res})$ is the total macroscopic cross-section at the resonance peak and Γ_γ and Γ are the radiative and total resonance widths.

To adapt their expression to neutron activation analysis, we rewrite it as a function of the amount of the element in a cylindrical sample of fixed size:

$$G_{ep} = \frac{0.94}{1+(m/m_{ep})^{0.82}} + 0.06 \qquad (4.5)$$

The parameter m_{ep} contains the geometrical and nuclear factors, and can be thought of as the amount of the element that causes about 50% epithermal neutron self-shielding for a

given sized cylinder. Comparing Eqs 4.4 and 4.5, m_{ep} varies with the radius and height of the cylinder as $r(r+h)$.

Another recent paper of Gonçalves et al. [2005] proposes a similar universal sigmoid function for thermal neutron self-shielding. Rewriting their expression for G_{th} as a function of the amount of the element in the sample gives:

$$G_{th} = \frac{1.00}{1 + (m/m_{th})^{0.964}} \tag{4.6}$$

The parameter m_{th} is the amount of the element that causes 50% thermal neutron self-shielding for a given sized cylinder. The work of Gonçalves et al. [2003, 2004] suggests that m_{th} varies with the radius and height of the cylinder as $r(r+h)$ and, if neutron scattering in the sample is neglected, it can be estimated from the thermal neutron absorption cross-section as follows:

$$\frac{1}{m_{th}} = \frac{k N_{Av} \sigma_{abs}}{r(r+h) M_{at}} \tag{4.7}$$

where N_{Av} is Avogadro's number, M_{at} the atomic mass and k a universal constant.

For a sample containing several elements that absorb thermal neutrons, G_{th} can be calculated by replacing m/m_{th} in Eq. 4.6 by the sum of the contributions of all the elements. The value of G_{th} thus calculated applies to the thermal neutron activation of all nuclides in the sample. In a mixed thermal-epithermal neutron spectrum, the effective self-shielding factor for a nuclide, j, in a cylindrical sample containing an amount m_j of that element and amounts m_i of other elements is then given by:

$$G_{eff\,j} = \frac{f}{f + Q_{0\,j}} \frac{1.00}{1 + (\sum_i m_i / m_{thi})^{0.964}} + \frac{Q_{0\,j}}{f + Q_{0\,j}} \left(\frac{0.94}{1 + (m_j / m_{ep\,j})^{0.82}} + 0.06 \right) \quad (4.8)$$

This assumes negligible epithermal self-shielding on nuclide *j* by the other elements. The values of $m_{th\,i}$ can be determined from Eq. 4.7. The value of $m_{ep\,j}$ needs to be measured for the nuclide in question.

4.3. Experimental

4.3.1. Confirming the theory

To verify the expression for the thermal neutron self-shielding factor, Eq. 4.6 and first part of Eq. 4.8, cylindrical samples were prepared containing various amounts of chlorine. Chlorine has a high thermal neutron absorption cross-section, 33.5 b, and the $^{37}Cl(n,\gamma)\,^{38}Cl$ reaction has a low ratio of resonance integral to thermal neutron activation cross-section, Q_0 = 0.69. Up to 1.6 g of $MgCl_2$ powder was mixed with powdered sugar and pressed into a 10 mm diameter polyethylene irradiation vial. The height of the cylindrical sample was maintained at 12.7 mm with a wooden plug. The samples thus had a volume of 1 mL. More dilute samples were prepared by dissolving $MgCl_2$ in water and sealing 1 mL of solution in the polyethylene vials. The samples were irradiated for 60 s in the inner irradiation site of the Ecole Polytechnique SLOWPOKE reactor at a thermal neutron flux of 5.59 x 10^{11} $cm^{-2}s^{-1}$. The neutron spectrum of this irradiation site is poorly thermalized [Kennedy and St-Pierre, 2003], f = 17.9 and shape parameter α = -0.042, but, because of the low Q_0 value, 96% of the ^{38}Cl activity is produced by thermal neutrons.

Another series of measurements was performed by irradiating 1 mL samples of NaCl, mixed with powdered sugar, in the outer irradiation site of the SLOWPOKE reactor. This outer site has $f = 51.1$ and thus 98 % of the ^{38}Cl activity is produced by thermal neutrons.

For each sample, the ^{38}Cl activity was measured by counting the gamma-rays 10 cm from a germanium detector. In each case the ^{38}Cl activity was allowed to decay until the analyzer dead-time was below 20% before acquiring the spectrum. The activities were calculated from the areas of the 1642 keV peak and corrected for decay time. In the absence of self-shielding, the measured activities would be proportional to the mass of chlorine in the samples. These activities were divided by the known mass of chlorine to determine the specific activity, which would be constant in the absence of self-shielding. The specific activities are thus proportional to G_{eff}. For the two series of measurements, using the inner and outer irradiation sites, the relative G_{eff} were then compared to those calculated by Eq. 4.8 as a function of the mass of chlorine.

Iodine and bromine were irradiated in the inner irradiation site of the reactor to study epithermal neutron self-shielding, using the $^{127}I(n,\gamma)^{128}I$, $^{79}Br(n,\gamma)^{80}Br$ and $^{81}Br(n,\gamma)^{82}Br$ reactions. These reactions have $Q_0(\alpha)$ values of 31.9, 14.4 and 23.8, respectively [Kennedy and St-Pierre 2003, Van Lierde et al. 1999, De Corte et al. 1989]. Thus, with f = 17.9 and in the absence of self-shielding, 63.6%, 44.0% and 56.5% of the ^{128}I, ^{80}Br and ^{82}Br activities, respectively, are produced by epithermal neutrons. Solutions with iodine concentrations up to 300 g/L or bromine concentrations up to 400 g/L were made by dissolving NH_4I or NH_4Br in water. Samples of these solutions, of volume 1 mL, were

sealed in polyethylene vials and irradiated and counted in the same way as the chlorine samples. The ^{128}I, ^{80}Br and ^{82}Br specific activities, measured using their 443 keV, 617 keV and 554 keV gamma-rays, respectively, were then compared to their G_{eff} calculated by Eq. 4.8.

4.3.2. Tests on samples of unknown composition

The above measurements allowed the determination of the parameter m_{th} of Eq. 4.6 for ^{38}Cl, and m_{ep} of Eq. 4.5 for ^{128}I, ^{80}Br and ^{82}Br. Measurements were then carried out to demonstrate the use of these parameters to correct self-shielding in highly absorbing samples of these elements with a priori unknown concentrations. A concentrated solution of $MgCl_2$ and NH_4I was dried to produce a fine powder with high concentrations of Cl and I. This powder was pressed into an irradiation vial and retained with a wooden plug to produce a 1 mL sample. It was irradiated and counted, and the measured concentrations were corrected for self-shielding. To determine the real Cl and I concentrations, the sample was re-dissolved in water and 1 mL of this dilute solution (with negligible self-shielding) was analyzed.

To test the method on a sample containing two elements that absorb epithermal neutrons, a concentrated solution of NH_4Br and NH_4I was dried to produce a fine powder with high concentrations of Br and I. A 1 mL sample of this powder was irradiated and counted, and the concentrations measured using ^{80}Br, ^{82}Br and ^{128}I were corrected for self-

shielding. To determine the real Br and I concentrations, the sample was re-dissolved in water and 1 mL of the dilute solution (with negligible self-shielding) was analyzed.

4.4. Results and discussion

4.4.1. Confirmation of the theory

The measured relative specific activities of the chlorine samples, prepared with $MgCl_2$ and irradiated in the inner irradiation site, are shown in Fig. 4.1. Also shown is the function KG_{eff}, with G_{eff} calculated by Eq. 4.8, which was fitted to the data using least-squares. The two fitted parameters were the normalizing constant K and the thermal neutron self-shielding parameter m_{th}. After the fit, the data and the fitted function were renormalized by dividing by K; they thus now represent G_{eff}. The second term of Eq. 4.8, describing epithermal neutron self-shielding, was not fitted to the data; it is only 4.4% of the total and it should be fairly constant because the chlorine isotopes have low cross-sections for the absorption of epithermal neutrons. It was therefore kept fixed at 0.044. As can be seen, the curve fits the data well, which confirms the use of the exponent 0.964 in the first term of Eq. 4.8. The fit gave a value of 1.94±0.06 g for the m_{th} of chlorine for a 1 mL cylindrical sample with r = 0.5 cm and h = 1.27 cm. Using these values in Eq. 4.7, one obtains k = 0.81±0.03. The small contribution of Mg to the thermal neutron self-shielding, about 0.1% of the total, was ignored.

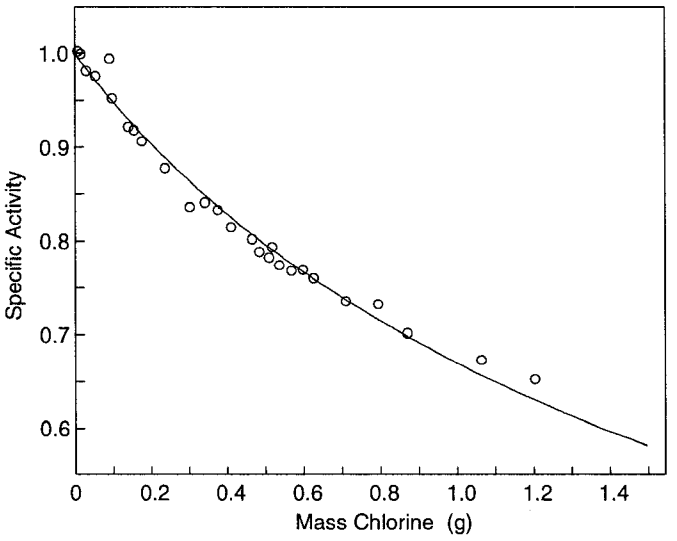

Figure 4.1 Measured relative specific activities of ^{38}Cl and the fitted self-shielding expression

The data obtained by irradiating NaCl in the outer irradiation site yielded a similar curve (not shown). After applying a 1.6% correction for the self-shielding due to Na, the fit to these data gave 1.88±0.13 g for the m_{th} of chlorine for a 1 mL cylindrical sample and k = 0.84±0.06. The weighted mean of this measurement and the above measurement with $MgCl_2$ is k = 0.82±0.03.

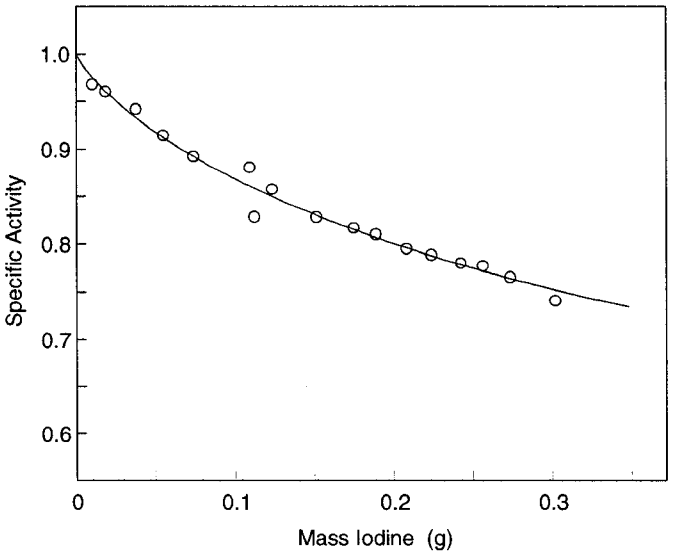

Figure 4.2 Measured relative specific activities of ^{128}I and the fitted self-shielding expression

The measured relative specific activities of the iodine samples are shown in Fig. 4.2, along with the fitted function KG_{eff}, with G_{eff} calculated by Eq. 4.8. The two fitted parameters were the normalizing constant K and the epithermal self-shielding parameter m_{ep}. After the fit, the data and the fitted function were renormalized by dividing by K, so that they now represent G_{eff}. The first term of Eq. 4.8 was not fitted to the data since thermal neutron self-shielding is not significant: using $k = 0.82$ and $\sigma_{abs} = 6.2$ b for I and $\sigma_{abs} = 1.9$ b for N, this first term was calculated to vary from 0.364 for the lowest iodine concentration to 0.353 for the highest concentration; it was therefore kept fixed at those values. The goodness of the fit confirms the use of the exponent 0.82 in the second term of Eq. 4.8. The fit gave a value of $m_{ep} = 0.48 \pm 0.03$ g for iodine in a 1 mL cylindrical sample.

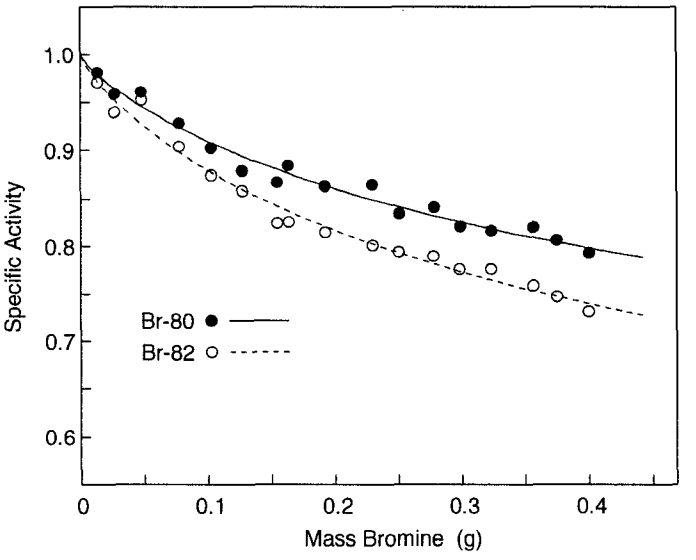

Figure 4.3 Measured relative specific activities of ^{80}Br and ^{82}Br and the fitted self-shielding expressions

The measured relative specific activities for ^{80}Br and ^{82}Br are shown in Fig. 4.3, along with the fitted functions KG_{eff}. As for iodine, the two fitted parameters were the normalizing constant K and the epithermal self-shielding parameter m_{ep}. Again, the first term of Eq. 4.8 was not fitted: with σ_{abs} = 6.8 b for Br and σ_{abs} = 1.9 b for N, this first term was estimated to vary from 0.560 to 0.534 for ^{80}Br and from 0.435 to 0.414 for ^{82}Br, and it was kept fixed at those values. The fits gave m_{ep} = 0.50±0.04 g for ^{80}Br and m_{ep} = 0.46±0.03 g for ^{82}Br.

A comparison of the curve of Fig. 4.1 with those of Figs 4.2 and 4.3 illustrates the difference between thermal neutron self-shielding and epithermal neutron self-shielding. In fact, there is only a slight difference between the curves. Thermal neutron self-

shielding, with the exponent 0.964, is a slowly varying function of the mass of the element. The epithermal self-shielding curves, with the exponent 0.82, decrease quickly at first and then more slowly. All three cases of epithermal self-shielding can be explained the same way: a few milligrams of the nuclide absorb the neutrons at the energies of the peaks of the resonances, and then much larger amounts are needed to absorb the neutrons at the energies of the wings of the resonances and between the resonances. At first it seems surprising that three nuclides with widely differing resonance patterns, i.e. number of resonances, resonance energies, resonance widths and maximum resonance cross-sections, would have exactly the same shaped curves of G_{ep} vs. mass. As Salgado et al. discovered [Martinho et al. 2003, Salgado et al. 2004], the different resonance patterns have no effect; the dominant effect is the fact that the main resonances have roughly similar shapes in the three cases, causing the curves of G_{ep} vs. mass to be the same. The extreme difference between the slowly varying cross-sections at thermal energies ($E^{-1/2}$) and the wildly varying cross-sections at epithermal energies (resonances) only has the effect of changing the exponent from 0.964 for G_{th} to 0.82 for G_{ep}; the differences in the patterns of the resonances for different nuclides have no effect on the exponent. From one nuclide to another, only the parameter m_{ep} changes as a function of resonance peak cross-section, resonance width, atomic mass and isotopic abundance.

4.4.2. Results for two unknown samples

The results of the analysis of the concentrated 1 mL powder sample containing chlorine and iodine are shown in Table 4.1. The true amounts, determined from the analysis of the sample diluted in water, are given in the second last line of the table. For the concentrated powder sample, the final amounts, corrected for self-shielding, were determined by an iterative procedure. The original amounts, the uncorrected NAA measurement results, were used to calculate G_{eff} for Cl and I, using Eq. 4.8 with the measured parameters given above. The original amounts were then divided by these G_{eff} to obtain the amounts of the first iteration. The procedure continued for six iterations, each time dividing the original amounts by the G_{eff} calculated from the masses obtained in the previous iteration. The amounts converged to the final values, 0.5994 g Cl and 0.1431 g I, which differed from the true values by +1.3% and -0.7%, respectively. It is not surprising that the agreement is within about 1% of the true values, because the powder sample containing Cl and I is fairly similar to the $MgCl_2$ powders and the NH_4I solutions used to develop the model. This does confirm that the epithermal self-shielding for iodine is similar whether it is in solution or as a homogeneous compressed powder.

Table 4.1 Chlorine and Iodine concentrations measured in a concentrated sample and corrected for self-shielding, compared to the true amounts determined after diluting the sample

	Chlorine		Iodine	
	G_{eff}	Amount, mg	G_{eff}	Amount, mg
Uncorrected measurement	1.000	458.6	1.000	107.1
1st iteration	0.8078	567.7	0.7914	135.3
2nd iteration	0.7743	592.3	0.7575	141.4
3rd iteration	0.7671	597.8	0.7506	142.7
4th iteration	0.7655	599.1	0.7491	143.0
5th iteration	0.7652	599.3	0.7488	143.0
6th iteration	0.7651	599.4	0.7487	143.1
True amount		591.8		144.1
Corrected-true		+1.3%		-0.7%

The results of the analysis of the concentrated powder sample containing bromine and iodine are shown in Table 4.2. The true amounts, determined from the analysis of the sample diluted in water, are given in the second last line of the table. For the concentrated powder sample, the final amounts, corrected for self-shielding, were determined by the iterative procedure, where the G_{eff} at each step were calculated using Eq. 4.8 with the measured parameters given above. The amounts converged to the final values, 0.2838 g I and 0.6381 g Br (^{80}Br) and 0.7032 g Br (^{82}Br), which differed from the true values by -

6.1%, -2.8% and +6.5%, respectively. For the concentrated powder sample, G_{th} was 0.962 while the G_{ep} were 0.629, 0.485 and 0.451 for ^{128}I, ^{80}Br and ^{82}Br, respectively.

Table 4.2 Iodine and Bromine concentrations measured in a concentrated sample and corrected for self-shielding, compared to the true amounts determined after diluting the sample

	Iodine		Bromine (^{80}Br)		Bromine (^{82}Br)	
	G_{eff}	Amount, mg	G_{eff}	Amount, mg	G_{eff}	Amount, mg
Uncorrected measurement	1.000	213.0	1.000	479.7	1.000	472.3
1st iteration	0.7864	270.8	0.7809	614.3	0.7198	656.1
2nd iteration	0.7565	281.6	0.7557	634.8	0.6801	694.5
3rd iteration	0.7516	283.4	0.7523	637.6	0.6732	701.6
4th iteration	0.7508	283.7	0.7518	638.0	0.6719	702.9
5th iteration	0.7506	283.8	0.7518	638.1	0.6717	703.1
6th iteration	0.7506	283.8	0.7518	638.1	0.6717	703.2
True amount		302.1		656.2		660.4
Corrected-true		-6.1%		-2.8%		+6.5%

The results for ^{80}Br and ^{82}Br are reasonable considering the sample contained almost 0.7 g Br, which is well beyond the range of the calibration measurements shown in Figure

4.3. The low result for iodine, -6.1%, must be due to some other cause, because the sample contained about 0.3 g I, which is within the range of the calibration measurements shown in Figure 4.2. It suggests a limitation of the method for samples containing several elements activated by epithermal neutrons. An examination of the neutron capture cross-sections [Janis 3.0, http://www.nea.fr/janis/] for ^{127}I, ^{79}Br and ^{81}Br indicates that there is no overlap between the ^{81}Br resonances and the other two, but there is overlap between the ^{127}I and ^{79}Br resonances. A close look at this overlap suggests that the largest effect would be the shielding of the main ^{127}I resonance by the wider main ^{79}Br resonance, an effect not included in our epithermal neutron self-shielding model and which may explain the low ^{128}I result in Table 4.2.

4.5. Conclusions

The method developed here can be used to correct neutron self-shielding in cylindrical samples, using the measured concentrations of the neutron absorbing elements to determine G_{th} and G_{ep} by iteration. To correct thermal neutron self-shielding, the equations use a single parameter, m_{th}, which can be calculated for any element from the sample size, the absorption cross-section and the constant k, measured here to be 0.82. To correct epithermal self-shielding, the parameter m_{ep}, measured here for ^{80}Br, ^{82}Br and ^{128}I, needs to be measured for each nuclide. Since the expressions for self-shielding are slowly varying functions of the amounts of the elements and the other parameters, the correction factors should be more accurate than the parameters used to calculate them. For example,

at a level of 30% self-shielding, an uncertainty of 4% in m_{th} and m_{ep} will cause an uncertainty of 1% in the self-shielding corrected NAA result.

The correction for thermal neutron self-shielding should be accurate for samples that contain several strongly absorbing elements because the effects of several elements are combined in a straightforward manner, but, for epithermal self-shielding, the same cannot be said because the theory developed here takes into account only the shielding of the resonances of a nuclide caused by the nuclide itself and other isotopes of the same element. If one wishes to determine several elements activated by epithermal neutrons, in a sample containing one element that strongly absorbs epithermal neutrons, one would need to know the shielding of the strongly absorbing element on the resonances of the nuclides of the other elements. This would require a large number of calibration measurements, one measurement per element-nuclide pair, or Monte Carlo calculations.

4.6. Acknowledgement

The authors would like to thank Dr. Isabel Gonçalves of Instituto Technologico e Nuclear, Sacavem, Portugal for useful discussions and for sharing results before publication.

4.7. References

DE CORTE, F., SIMONITS, A., DE WISPELAERE, A., 1989. Comparative Study of Measured and Critically Evaluated Resonance Integral to Thermal Cross Section Ratios, III. . *Journal of Radioanalytical and Nuclear Chemistry.* 133: 1, 131-151

GILAT, J., GURFINKEL, Y., 1963. Self-Shielding in Activation Analysis. *Nucleonics.* 21 :8. 143-144.

GONÇALVES, I.F., MARTINHO, E., SALGADO, J., 2004. Extension to cylindrical samples of the universal curve of resonance neutron self-shielding factors. *Nuclear Instruments and Methods in Physics Research, Section B.* 213, 186-188.

GONÇALVES, I.F., MARTINHO, E., SALGADO, J., 2005. Thermal Neutron Self-Shielding in Foils, A Universal Curve. *Proc. IAEA Int. Conf. On Research Reactors,* Santiago, Chile, 2003. IAEA, Vienna 375.

JANIS 3.0, http://www.nea.fr/janis/

KENNEDY, G., ST-PIERRE, J. 2003. Is the k_0 Method Accurate for Elements with High Q_0 Values?. *Journal of Radioanalytical and Nuclear Chemistry.* 257:3, 475-480.

MARTINHO, E., GONÇALVES, I.F., SALGADO, J. 2003. Universal curve of epithermal neutron resonance self-shielding factors in foils, wires and spheres. *Applied Radiation and Isotopes.* 58:3. 371-375.

SALGADO, J., MARTINHO, E., GONÇALVES, I.F., 2004. The calculation of neutron self-shielding factors of a group of isolated resonances. *Journal of Radioanalytical and Nuclear Chemistry.* 260:2, 317-320.

VAN LIERDE, S., DE CORTE, F., BOSSUS, D., VAN SLUIJS, R., POMME, S., 1999. Determination of k0 and Related Nuclear Data to be Used in KAYZERO-NAA at DSM research. *Nuclear and Instruments and Methods in Physics Research A.* 422, 874-879.

Chapter 5 Second Article: Dependence of Thermal and Epithermal Neutron Self-Shielding on Sample Size and Irradiation Site*

C. Chilian, J. St-Pierre and G. Kennedy

Ecole Polytechnique, P.O.Box 6079, Downtown, Montreal, Quebec, H3C 3A7, Canada

Abstract

Analytical expressions recently developed for calculating thermal and epithermal neutron self-shielding for cylindrical samples used in neutron activation analysis were verified using three different irradiation sites of a SLOWPOKE reactor. The amount of self-shielding varied by less than 10% from one site to another. The self-shielding parameters varied with the size of the cylinder as $r(r+h)$, for h/r ratios from 0.02 to 6.0, even in slightly non-isotropic neutron fields. A practical expression, based on the parameters of the neutron spectrum and the well-known thermal neutron absorption cross-section and the newly defined epithermal neutron absorption cross-section, is proposed for calculating the self-shielding in cylindrical samples.

Keywords: Neutron activation analysis, epithermal, thermal, self-shielding factors

---

*Nuclear Instruments and Methods in Physics Research A 564 (2006) 629-635

5.1. Introduction

The k_0 standardization method, widely used for multi-element neutron activation analysis (NAA) with large research reactors, was adapted for small reactors like SLOWPOKE with highly stable neutron fluxes [Kennedy et al. 2000]. Regardless of the reactor type, for large samples and for samples with high concentrations of neutron absorbing elements, the equation used in k_0 neutron activation requires the knowledge of thermal and epithermal self-shielding factors. Recent studies [Martinho et al. 2003, Gonçalves et al. 2005, Gonçalves et al. 2004] indicate that both self-shielding factors, G_{th} and G_{ep}, can be expressed by a sigmoid function with a parameter depending on the nuclide and the geometry and the composition of the sample. The sigmoid function was established for mono-element objects irradiated in an isotropic neutron field, conditions not applicable in the real NAA situation. Thus, in a previous paper [Chilian[a] et al. 2006], we developed an experimental method to determine the epithermal self-shielding as a function of the amount of the element present in the sample, and the experimental parameter of the thermal and epithermal sigmoid self-shielding functions was determined.

In our previous work [Chilian[a] et al. 2006], measurements were done only for 1 mL cylindrical samples irradiated in the inner irradiation site of the SLOWPOKE reactor where the thermal neutron field is very nearly isotropic. In the present work, we verify experimentally the validity of the theoretical sample geometry dependence of the expressions for thermal and epithermal self-shielding. We also verify whether the magnitude of the self-shielding varies with the size of the irradiation site and the surrounding neutron reflecting materials.

5.2. Theory

5.2.1. General

In a typical reactor neutron spectrum, the activity A of a given nuclide produced by the (n,γ) reaction upon irradiating a sample containing an amount m of the element is given by

$$A = \frac{m N_{Av} \theta}{M_{at}} \sigma_{th} \varphi_{th} (G_{th} + G_{ep} Q_0 / f)\left(1 - e^{-\lambda t_i}\right) \qquad (5.1)$$

where N_{Av} is Avogadro's number, θ is the isotopic abundance, M_{at} is the atomic mass, σ_{th} is the thermal neutron cross section, $Q_0 = I_0/\sigma_{th}$, the ratio of the resonance integral to 2200 ms^{-1} cross section, $f = \varphi_{th}/\varphi_{ep}$, φ_{th} and φ_{ep} are the average unperturbed thermal and epithermal fluxes, λ is the decay constant and t_i is the irradiation time. In practice, the unperturbed thermal and epithermal fluxes may be measured by simultaneously irradiating flux monitors near the absorbing sample, taking into account flux gradients and the fact that the absorbing sample may perturb the nearby fluxes outside the sample. For short irradiations, assuming that the unperturbed thermal and epithermal fluxes are constant with time, they may be measured by irradiating flux monitors before or after the absorbing sample at the same position. G_{th} and G_{ep} are the thermal and epithermal self-shielding factors for the given (n, γ) reaction. These definitions of φ_{th}, φ_{ep}, G_{th} and G_{ep} are consistent with those used in Monte-Carlo simulations [Martinho et al. 2003, Gonçalves et al. 2005, Gonçalves et al. 2004] were φ_{th} and φ_{ep} are found by simulating a sample of infinite dilution. G_{th} and G_{ep} depend on sample geometry and they are equal to

unity for sufficiently dilute samples. The thermal self-shielding factor depends on the amounts of all elements in the sample that absorb thermal neutrons. The epithermal self-shielding factor will be influenced by nuclides other than the nuclide being activated (isotopes of the same element or isotopes of the different elements present in the sample), only if these nuclides absorb neutrons at resonance energies that overlap with the resonances that activate the nuclide in question.

The sample activity that would have been produced if self-shielding had been negligible is obtained by dividing the sample's measured activity by its effective self-shielding factor, G_{eff}. This factor is defined as the ratio between the reaction rate per atom in the real sample and in a similar and indefinitely diluted sample. Using this definition, the effective self-shielding factor is obtained by dividing the activity of Eq. 5.1 with the activity calculated with the same equation when $G_{th} = 1$ and $G_{ep} = 1$. Thus, G_{eff} is given by

$$G_{eff} = \frac{G_{th} + G_{ep} Q_0 / f}{1 + Q_0 / f} \tag{5.2}$$

Experimentally, G_{eff} is proportional to the specific activity of the nuclide in the irradiated sample, which may be obtained from the area of the detected peak divided by the element concentration in the sample and by the detection efficiency and corrected for the decay time. The proportionality factor between G_{eff} and the specific activity is found by irradiating sufficiently dilute samples.

5.2.2. Thermal Self-Shielding

For almost all nuclides, the thermal cross section of radiative capture is a slowly varying function of neutron energy, proportional to $E^{-1/2}$. Hence, the thermal neutron self-shielding factor for any nuclide can be expressed by the same function of the amount of the element and the element's thermal neutron absorption cross-section σ_{abs}. In the literature [Tzika and Stamatelos 2004, Gilat and Gurfinkel 1963] we find different forms for this function but, in all of them, the thermal self-shielding factor dependence on the sample geometry is the same. In the particular case of cylindrical samples of a given concentration, it varies with sample size according to the factor $rh/(r+h)$, where r is the radius and h is the height. If the self-shielding is expressed as a function of the total amount of the element m, then, for a given m, as the sample size increases, the sample is diluted and the self-shielding decreases. It then varies with the size of the cylinder according to the factor $1/r(r+h)$.

This study will use results from a recent paper of Martinho et al. [Gonçalves et al. 2004] that propose a universal sigmoid function for thermal neutron self-shielding. Simplifying and rewriting their expression for G_{th} as a function of the amount of the element in the sample of a given geometry [Chilian[a] et al. 2006], one obtains

$$G_{th} = \frac{1.00}{1 + (m/m_{th})^{0.964}} \tag{5.3}$$

where m is the amount of the element. For cylindrical samples, the parameter m_{th} varies with the radius and height of the cylinder as $r(r+h)$ and can be estimated from the thermal neutron absorption cross-section as follows

$$\frac{1}{m_{th}} = \frac{k_{th} N_{Av} \sigma_{abs}}{r(r+h) M_{at}} \left(\sigma_{tot}/\sigma_{abs}\right)^{0.15} \qquad (5.4)$$

where σ_{tot} is the element total thermal neutron cross-section (scattering plus absorption) and k_{th} is a parameter which may depend on the irradiation site, but is independent of the nuclide and the sample composition. In Eq. 5.4, the factor involving neutron scattering is usually close to unity and can be neglected, especially for elements with high absorption cross-sections.

5.2.3. Epithermal Self-Shielding

The estimation of G_{ep} as a function of element concentration and sample geometry has always been a difficult task because each nuclide has a different and sometimes complex resonance pattern; in nuclear reactor studies it is usually done by the Monte-Carlo method. Such calculations are time consuming and impractical for routine NAA where the concentration of the absorbing element is not known in advance; indeed that is the aim of the analysis. The most common approach has been to avoid the problem by diluting the samples or by irradiating in a neutron spectrum with a very small epithermal component. Thus, the question of a practical solution to the problem of epithermal self-shielding in neutron activation analysis has not been investigated systematically.

Recently, Salgado et al. [Martinho et al. 2003, Salgado et al. 2004] claimed that, for nuclides having one resonance or a few isolated resonances, G_{ep} could be expressed by the same universal function, a sigmoid, with only one nuclide-dependant parameter. The same authors [Gonçalves et al. 2004] extend their theory for cylindrical samples by introducing a sigmoid expression for G_{ep} that fits the data generated by a Monte-Carlo calculation for a pure element sample irradiated in an isotropic neutron flux. The nuclides quantified by epithermal neutron activation analysis often have more than a few isolated resonances and, also, the real neutron flux is non-isotropic. In addition, their expression, with all parameters derived from theory, fits the data with an insufficient precision (within 5% to 10%) for practical purposes in activation analysis. Thus, from this theory we take only the main idea: the epithermal self-shielding can be expressed by a universal sigmoid function. To adapt their expression to neutron activation analysis, we rewrite it as function of the amount m of the element in a cylindrical sample:

$$G_{ep} = \frac{0.94}{1 + (m/m_{ep})^{0.82}} + 0.06 \qquad (5.5)$$

The parameter m_{ep} can be thought of as the amount of the element that causes about 50% epithermal neutron self-shielding for a given sized cylinder. The m_{ep} varies with the radius and height of the cylinder as $r(r+h)$ and can be estimated from the width and position of the resonances, the cross-section at the peak of each resonance, and also includes the mutual self-shielding generated by the isotopes of the given element, other than the isotope that produces the studied (n,γ) reaction. Here, we express all this nuclear dependence by a single nuclear parameter, $\sigma_{abs,ep}$, which we call the epithermal neutron

absorption cross-section. We can now write an expression for m_{ep} similar to the one for the thermal self-shielding parameter:

$$\frac{1}{m_{ep}} = \frac{N_{Av}}{r(r+h)M_{at}} k_{ep}\,\sigma_{abs,ep} \qquad (5.6)$$

where k_{ep} is a parameter that depends on the properties of the actual irradiation site, such as the shape of the neutron spectrum and the surrounding reflecting materials. Since neither k_{ep} nor $\sigma_{abs,ep}$ are known *a priori*, we will need to assign a value to k_{ep} for one irradiation site and then we can determine $\sigma_{abs,ep}$ for each nuclide experimentally and also k_{ep} for other irradiation sites. Note that, analogous to the elemental thermal neutron absorption cross-section σ_{abs}, $\sigma_{abs,ep}$ includes the effect of epithermal neutron absorption of all isotopes of the element on the nuclide being activated.

5.3. Experimental Methodology

5.3.1. Dependence of the Thermal Neutron Self-Shielding on Sample Geometry and Irradiation Site

To verify the $r(r+h)$ variation of m_{th} with the geometry of the sample, Eq. 5.4, two sets of cylindrical samples were prepared containing various amounts of chlorine. The first set consists of 1 mL samples with r = 5.0 mm and h = 12.7 mm that contained up to 1.0 g chlorine. The second set is represented by six 3 mL samples, r = 7.2 mm and h = 30.7 mm, containing up to 2.2 g chlorine. Chlorine has a high thermal neutron absorption cross-section, 33.5 b, and the $^{37}Cl(n,\gamma)^{38}Cl$ reaction has a low ratio of resonance integral

to thermal neutron activation cross-section, Q_0 = 0.59. The samples were prepared by mixing NH_4Cl powder with powdered sugar and pressed into 10 mm or 14.4 mm diameter polyethylene irradiation vials. The height of the cylindrical sample was maintained at 12.7 mm or 30.7 mm with a wooden plug, to give volumes of 1 mL or 3 mL. Both sets were completed with more dilute samples, prepared by dissolving NH_4Cl in water and sealing 1 mL or 3 mL of solution in polyethylene vials.

The samples were irradiated for 60 s in the inner irradiation site in the beryllium reflector of the Ecole Polytechnique SLOWPOKE reactor, site no.1, at a thermal neutron flux of 5.59 x $10^{11}cm^{-2}s^{-1}$. Despite the poorly thermalized neutron spectrum of this irradiation site, f = 18.0 and shape parameter α = -0.051, 96% of the ^{38}Cl activity is produced by thermal neutrons due to the low Q_0 value.

In order to investigate the dependence of the thermal self-shielding on the irradiation site, six 3 mL NH_4Cl samples having the same geometry (r = 7.2 mm, h = 30.7 mm) but different chlorine concentration, were prepared and irradiated for 60 s first in the no.1 beryllium reflector inner irradiation site, tube diameter = 31 mm, then one day later in an outer irradiation site, site no.6, tube diameter = 38 mm and, finally, after another day, irradiated again in another outer irradiation site, no. 8, tube diameter = 22 mm. Sites no.6 and no.8 are situated in water and have a thermal neutron flux of 2.71 x $10^{11}cm^{-2}s^{-1}$; it is known to be more non-isotropic than the neutron flux of site no.1. In the outer sites the neutron spectrum is well thermalized, f = 48.6, and the ^{38}Cl activity produced by epithermal neutrons can be neglected.

For each chlorine sample, the ^{38}Cl activity was measured by counting the gamma rays 10 cm from a germanium detector. Before acquiring the spectrum, in each case the ^{38}Cl activity was allowed to decay until the analyzer dead time was below 20%. The activities were calculated from the areas of the 1642 keV peak and corrected for decay time. To determine the specific activity, these activities were divided by the known amounts of chlorine in the sample. The specific activities are thus proportional to G_{eff}. They are normalized to G_{eff} using the dilute samples which are known to have $G_{eff} = 1$. Then, using Eq. 5.2 with $G_{ep} = 1$, the epithermal part was subtracted to obtain the experimental G_{th}. A least-squares fit of the data as a function of the mass of chlorine, using Eq. 5.3, gives the parameter m_{th}, which includes the dependence on $r(r+h)$ and k_{th}, as given by Eq. 5.4.

5.3.2. Dependence of epithermal neutron self-shielding on sample geometry and irradiation site

To check the $r(r+h)$ dependence of epithermal self-shielding on sample geometry, measurements were done with various stacks of Zr metal disks with three different diameters, 6 mm, 10 mm and 14 mm. The stacks of disks, with heights varying between 0.127 mm and 12.7 mm, were irradiated in polyethylene vials in the inner irradiation site of the SLOWPOKE reactor, for times varying between 5 minutes and 2 hours, depending of the total mass of Zr. Metallic disks are easy to manipulate and, in this irradiation site, the $^{96}Zr(n,\gamma)^{97}Zr$ reaction has $Q_0(\alpha) = 338.5$ indicating negligible activation by thermal neutrons. In addition to the Zr disks, measurements were also done with several 1 mL powder samples of different concentrations, up to 2.12 g Zr, obtained by mixing ZrO_2

powder with Al_2O_3 powder. The powder samples, sealed in polyethylene vials of 10 mm diameter, were irradiated between 10 min and 125 min in the same irradiation site.

To study the variation of epithermal neutron self-shielding with the irradiation site, six 4.4 mL samples, with diameter 14 mm and different Zr concentrations, were prepared by using different materials: zirconium plate, zirconium oxide powder, zirconium metal powder, zirconium nitrate, zirconium sulfate and zirconium nitrate diluted in organic resin, and irradiated in inner irradiation site no.1 between 5 min and 1 h. One week later, the samples were irradiated again in outer irradiation site no.6 and, after another week, in outer irradiation site no.8. In the outer sites the $^{96}Zr(n,\gamma)^{97}Zr$ reaction has a $Q_0(\alpha)$ = 229.2.

All the Zr samples, powders, cylinders or stacks of disks, were counted 10 cm from the germanium detector to determine the ^{97}Zr specific activity using the 742 keV gamma-ray. The photopeak count rates were converted to specific activities using detector efficiencies calculated by an empirical method [Kennedy and St-Pierre 1997], which takes into account sample-detector distance, sample geometry and gamma-ray attenuation in the sample. The measured specific activities were normalized to give G_{eff}. Then, using Eq. 5.2 with G_{th}= 1, the thermal part was subtracted to obtain the experimental G_{ep}. For each case the G_{ep} were fitted with an expression given by Eq. 5.5 that includes the $r(r+h)$ dependence and the product $k_{ep}\sigma_{abs,ep}$.

5.4. Results

5.4.1. Dependence of Thermal Neutron Self-Shielding on Sample Geometry

To illustrate the dependence of thermal neutron self-shielding on the geometry of the sample, the measured G_{th} of the 1 mL and 3 mL chlorine samples, prepared with NH_4Cl and irradiated in the inner reactor site no.1, are shown in Fig. 5.1. The experimental chlorine thermal self-shielding factors, G_{th}, obtained from Eq. 5.2 with $G_{ep} \cong 1$, were fitted by the expression of Eq. 5.3 with m_{th} calculated by Eq. 5.4. The fit give $k_{th} = 0.872 \pm 0.035$ for the inner irradiation site. For both geometries, all the experimental data can be described, within 2–5%, by a unique curve obtained from Eq. 5.3 with the geometrical dependence of Eq. 5.4.

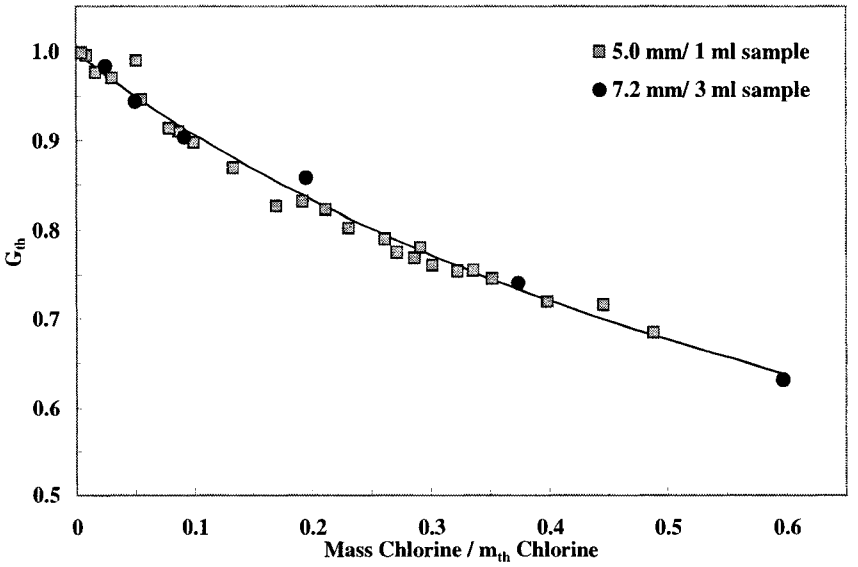

Figure 5.1 The measured G_{th} of $^{37}Cl(n,\gamma)^{38}Cl$ for cylindrical samples of radii 5.0 mm and 7.2 mm and the fitted self-shielding curve

These results confirm the $r(r+h)$ geometrical dependence of the thermal self-shielding parameter, m_{th}, and allow the use of this form for further calculations of the thermal self-shielding factor for activated samples containing highly absorbing elements.

5.4.2. Dependence of epithermal neutron self-shielding on sample geometry

In Fig. 5.2 are shown the G_{ep} measured with the stacks of disks and the powder samples. To determine G_{ep}, it was necessary to subtract the thermal neutron contribution to the measured G_{eff} using Eq. 5.2. For the powder samples, the first thermal term in Eq. 5.2 was calculated with Eq. 5.3 and Eq. 5.4 with k_{th} =0.87 and σ_{abs} = 6.6 b for zirconium and σ_{abs} = 0.2 b for aluminium. The term $G_{th}/(1+Q_0/f)$ is small and it was estimated to vary from 0.060 for the lowest zirconium concentration to 0.054 for the highest concentration.

The curve fitted to the data was calculated with Eq. 5.5 using the zirconium m_{ep} calculated with Eq. 5.6 and containing the $r(r+h)$ dependence. The least-squares fit yielded the parameter $k_{ep}\sigma_{abs,ep}$ = 10.4 ± 0.4 b for the relative epithermal neutron absorption cross-section for $^{96}Zr(n,\gamma)^{97}Zr$ in the inner irradiation site no. 1.

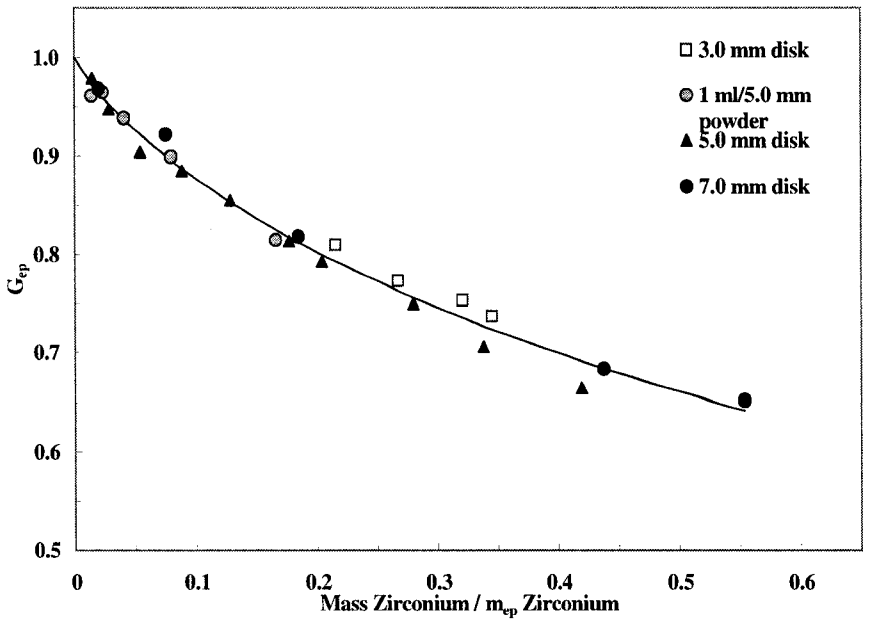

Figure 5.2 The measured G_{ep} of $^{96}Zr(n,\gamma)^{97}Zr$ for 3.0 mm, 5.0 mm and 7.0 mm radius cylindrical samples and the fitted self-shielding curve

Despite of differences between the Zr samples: powder samples with the same volume and same geometry but different concentrations and stacks of disks with diameters 6 mm, 10 mm or 14 mm and different heights, Fig. 5.2 indicates a good agreement (maximum 5% difference) between the experimental data and the calculated curve. There is no significant deviation from the curve, which confirms that the epithermal self-shielding parameter, m_{ep}, varies with the size of the cylinder as $r(r+h)$ for ratios h/r varying from 0.02 to 6.0. This result validates Eqs. 5.5 and 5.6 for the calculation of epithermal self-shielding factors for cylindrical samples, containing more than 0.05 g zirconium, irradiated in a real irradiation site with non-isotropic epithermal neutron flux. It was not

possible to verify the accuracy of Eq. 5.6 for the smallest samples, the thin disks, because the epithermal self-shielding effect with zirconium is of the same order of magnitude as the experimental uncertainty.

5.4.3. Variation of thermal neutron self-shielding with irradiation site

To show the variation of thermal self-shielding with the irradiation site, Fig. 5.3 presents the experimental G_{th} of $^{37}Cl(n,\gamma)^{38}Cl$ for the inner irradiation site no.1 and for outer irradiation sites no.6 and no.8 as a function of the mass of chlorine in the sample. All samples had volume 3 mL. To determine G_{th}, the measured G_{eff} were corrected for the epithermal contribution (maximum 4.4%) as before. To find the k_{th} characteristic of each irradiation site, the experimental data were fitted using Eq. 5.3 with m_{th} calculated as in Eq. 5.4. The fitted k_{th} values for each site are presented in the Table 1. The value of k_{th} determined for site no.1 is essentially equal to that of site no.8, while that of site no.6 is about 8% lower. This 8% difference is not significant, considering the experimental uncertainties.

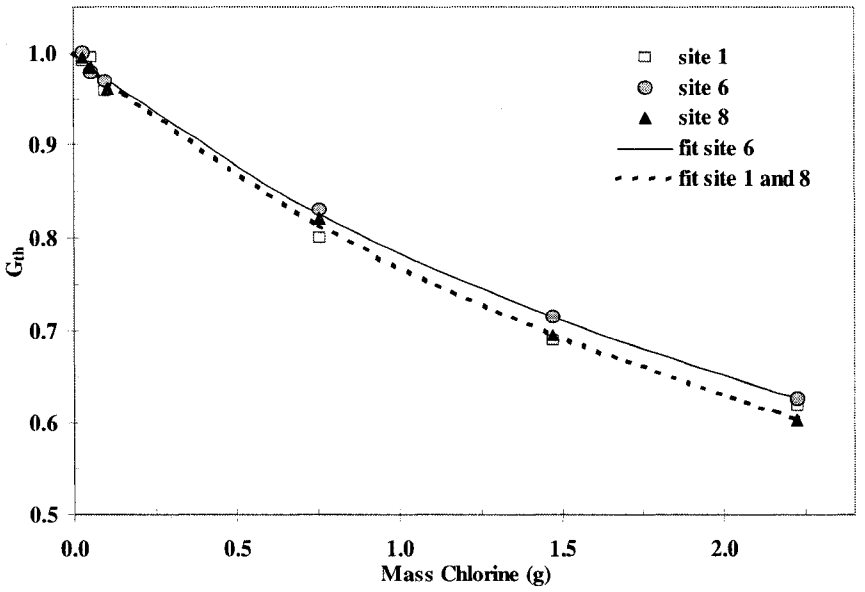

Figure 5.3 The measured G_{th} of $^{37}Cl(n,\gamma)^{38}Cl$ for inner site no.1 and for outer sites no.6 and no.8, along with the fitted expressions for G_{th}

Some physical details of the irradiation sites are also given in Table 5.1. A study of St-Pierre and Kennedy [2004] found a larger thermal flux gradient in sites no.6 and no.8 than in site no.1, indicating that the flux is less isotropic in sites no.6 and no.8 than in site no.1. Since the self-shielding is the same in site no.1 and site no.8, the anisotropy does not seem to have had an influence. The small difference in self-shielding between sites no.6 and no.8 may be due to the differences in the diameters of the irradiation tubes. In site no.6, a neutron passing through the sample would have to travel a larger distance before being reflected back into the sample, which might reduce the self-shielding slightly.

Table 5.1 Properties of the irradiation sites and fitted values of the thermal self-shielding parameter, k_{th}, and the epithermal self-shielding parameter, k_{ep}, for each site

Site no.	Reflector	Tube diam.(mm)	Dist.core-site (mm)	k_{th}	$\sigma_{abs,ep}$ ^{96}Zr (b)	k_{ep}
1	beryllium	31	42	0.94 ±0.08	10.3 ±0.8	1
6	water	38	125	0.86 ±0.07	10.3	0.93 ±0.08
8	water	22	125	0.94 ±0.08	10.3	0.93 ±0.07

5.4.4. Variation of epithermal neutron self-shielding with irradiation site

Fig. 5.4 presents the experimental epithermal self-shielding factors of ^{96}Zr for inner irradiation site no. 1 and outer sites no. 6 and 8 and the corresponding fitted curves calculated with Eq. 5.5, and m_{ep} calculated with Eq. 5.6. For site no.1, the value of k_{ep}, defined here for the first time, is set equal to unity. The fit then gave a value of 10.3 ± 0.8b for $\sigma_{abs,ep}$, the epithermal neutron absorption cross-section of ^{96}Zr. With $\sigma_{abs,ep}$ fixed at that value, the fits gave values of k_{ep} of 0.93 ± 0.08 and 0.93 ± 0.07, for sites no.6 and no.8, respectively, as shown in Table 1. The 7% difference between k_{ep} of site no.1 and k_{ep} of sites no.6 and 8 indicates that the epithermal self-shielding may be more important in the inner site in the beryllium reflector than in the outer sites in the water reflector, although the difference is not significant when considering the corresponding uncertainties.

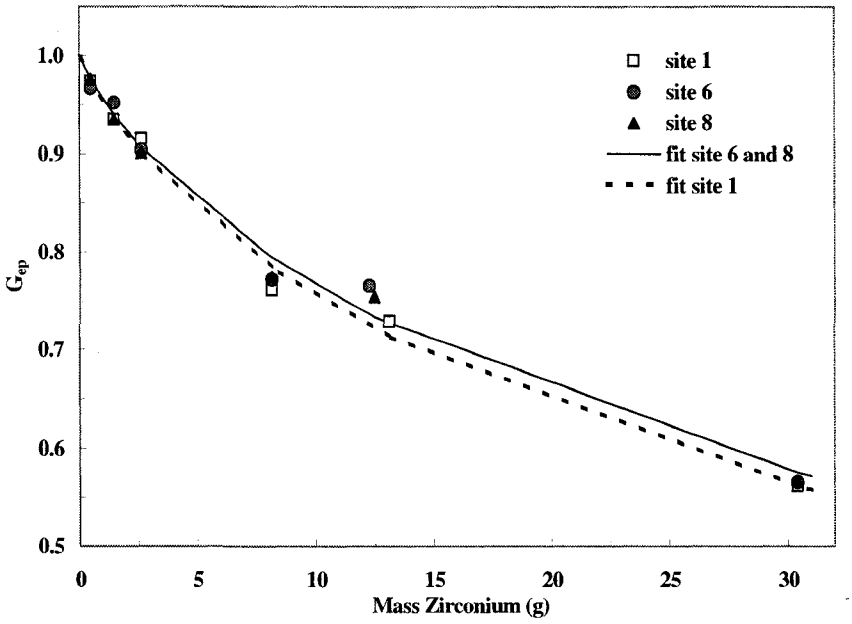

Figure 5.4 The measured G_{ep} of $^{96}Zr(n,\gamma)^{97}Zr$ for inner site no.1 and for outer sites no.6 and no.8, along with the fitted self-shielding expressions

Table 5.1 indicates less than 10% differences between the k_{th} and k_{ep} values for three different irradiation sites in a SLOWPOKE reactor, which suggests that these parameters may be constant to within 10% in the irradiation sites of all research reactors. Now, a 10% error in k_{th} or k_{ep} will result in only about a 3% error in the calculated effective self-shielding factor G_{eff} (for G_{eff} greater than 0.5). Thus, combining Eqs. 5.2 to 5.6, we can now write a practical expression that can be used to correct both thermal and epithermal self-shielding in the irradiation sites of any research reactor and which will likely be sufficiently accurate for the purpose of routine neutron activation analysis. For a given element, the expression is:

$$G_{eff} = \frac{f}{f+Q_0}\left[\frac{1.00}{1+\left(m\ N_{Av}k_{th}\,\sigma_{abs}/\left(r\,(r+h)\,M_{at}\right)\right)^{0.964}}\right] + \frac{Q_0}{f+Q_0}\left[\frac{0.94}{1+\left(m\ N_{Av}\,k_{ep}\,\sigma_{abs,ep}/\left(r\,(r+h)\,M_{at}\right)\right)^{0.82}}+0.06\right] \tag{5.7}$$

This expression can be used with the mean values of Table 5.1: $k_{th} = 0.91$ and $k_{ep} = 0.95$. The values of the elemental thermal neutron absorption cross-sections σ_{abs} are commonly available in the nuclear libraries such as "Table of Nuclides" [http://atom.kaeri.re.kr/]. The expression also requires values of the epithermal neutron absorption cross-sections, $\sigma_{abs,ep}$, which we plan to experimentally measure or estimate with sufficient accuracy with an expression like the one proposed by Gonçalves et al. [2004]. So far we have measured $\sigma_{abs,ep}$ for 5 nuclides, see experimental data of Ref. [Chilian[a] et al.2006]; the values are given in Table 5.2.

Table 5.2 Experimental values of $\sigma_{abs,ep}$

Reaction	$\sigma_{abs,ep}$ (b)
$^{127}I(n,\gamma)^{128}I$	387 ± 24
$^{79}Br(n,\gamma)^{80}Br$	233 ± 19
$^{81}Br(n,\gamma)^{82}Br$	253 ± 17
$^{96}Zr(n,\gamma)^{97}Zr$	10.3 ± 0.8
$^{114}Cd(n,\gamma)^{115}Cd$	78 ± 5

5.5. Conclusions

A previous study [Chilian[a] et al. 2006] proposed a method to correct neutron self-shielding in cylindrical samples, using the measured concentrations of the activated neutron absorbing elements to determine iteratively G_{th} and G_{ep}. To correct thermal neutron self-shielding for cylindrical samples, the necessary parameter, m_{th}, can be calculated for each element from the absorption cross-section, the geometrical characteristics r and h, and the constant k_{th}. Despite the difference between activation mechanisms: thermal and epithermal and, also, the complexity of the resonance patterns, the geometrical dependence, $r(r+h)$, of both self-shielding parameters, m_{th} and m_{ep}, is confirmed for the inner irradiation site of the SLOWPOKE reactor where the flux is slightly anisotropic. In the case of a small research reactor like SLOWPOKE, and likely for most research reactors, the small site dependence of the thermal and epithermal self-shielding parameters can be neglected since the expressions for self-shielding are slowly varying functions of the amounts of the elements and the other parameters and, consequently, the correction factors should be more accurate than the parameters used to calculate them. However, for irradiation sites situated far from the reactor core, where the neutron flux is highly anisotropic, the $r(r+h)$ dependence of the self-shielding parameters for cylindrical samples may not hold.

The first practical expression has been proposed for the calculation of both thermal and epithermal neutron self-shielding in neutron activation analysis with cylindrical samples.

5.6. References

CHILIAN, C.[a], KASSAKOV, M., ST-PIERRE, J., KENNEDY, G., 2006. Extending NAA to Materials with High Concentrations of Neutron Absorbing Elements. *Journal of Radioanalytical and Nuclear Chemistry.* 270: 2, 417-423.

GILAT, J., GURFINKEL, Y., 1963. Self-Shielding in Activation Analysis. *Nucleonics.* 21 :8. 143-144.

GONÇALVES, I.F., MARTINHO, E., SALGADO, J., 2005. Thermal Neutron Self-Shielding in Foils, A Universal Curve. *Proc. IAEA Int. Conf. On Research Reactors,* Santiago, Chile, 2003. IAEA, Vienna 375.

GONÇALVES, I.F., MARTINHO, E., SALGADO, J., 2004. Extension to cylindrical samples of the universal curve of resonance neutron self-shielding factors. *Nuclear Instruments and Methods in Physics Research, Section B.* 213, 186-188.

KENNEDY, G., ST-PIERRE, J. 1997. Parameterization of Detector Efficiency for the Standardization of NAA With Stable Low Flux Reactors. *Journal of Radioanalytical and Nuclear Chemistry.* 215: 2, 235-239.

KENNEDY, G., ST-PIERRE, J., WANG, K., ZHANG, Y., PRESTON, J., GRANT, C., VUTHKOV, M. 2000. Activation Constants for SLOWPOKE and MNS Reactors Calculated from the Neutron Spectrum and k_0 and Q_0 Values. *Journal of Radioanalytical Nuclear and Chemistry.* 245:0, 167-172.

MARTINHO, E., GONÇALVES, I.F., SALGADO, J. 2003. Universal curve of epithermal neutron resonance self-shielding factors in foils, wires and spheres. *Applied Radiation and Isotopes.* 58:3. 371-375.

SALGADO, J., MARTINHO, E., GONÇALVES, I.F., 2004. The calculation of neutron self-shielding factors of a group of isolated resonances. *Journal of Radioanalytical and Nuclear Chemistry.* 260:2, 317-320.

ST-PIERRE, J., KENNEDY, G., 2004. Standardizing NAA of Biological samples of Varying Size, Shape and Composition. *Journal of Radioanalytical and Nuclear Chemistry.* 259: 3, 431-434.

TZIKA, F., STAMATELOS, I.E., 2004. Thermal Neutron Self-Shielding Corrections for Large Sample Instrumental Neutron Activation Analysis Using the MCNP Code. *Nuclear Instruments and Methods in Physics Research B.* 213, 177-181.

Table of Nuclides, http://atom.kaeri.re.kr/

Chapter 6 Third Article: Complete Thermal and Epithermal Neutron Self-Shielding Corrections for NAA using a Spreadsheet*

C. Chilian[1], J. St-Pierre[2] and G. Kennedy[2]

[1]Atomic Energy of Canada Limited, Chalk River, Canada, [2]Ecole Polytechnique, P.O.Box 6079, Downtown, Montreal, H3C 3A7, Canada

Abstract

An analytical expression has been developed to calculate the neutron self-shielding in a cylindrical sample using the elemental thermal neutron absorption cross-sections, σ_{abs}, and the newly-defined epithermal neutron absorption cross-sections, $\sigma_{abs,ep}$. The $\sigma_{abs,ep}$ were measured experimentally for 13 nuclides and calculated from resonance parameters for 76 nuclides. Agreement between the two was good to about 20% in most cases. A spreadsheet program was written to use these nuclear parameters to perform iterative self-shielding corrections of concentrations measured by NAA. In cases with up to 30% self-shielding, the correction factors had uncertainties varying from 2% to 3%.

---

* Journal of Radioanalytical and Nuclear Chemistry (in press, 2008)

6.1. Introduction

Instrumental neutron activation analysis is an excellent technique for the chemical analysis of a wide variety of materials. It can give accurate average bulk concentrations of many elements using large, representative samples. However, many interesting materials contain high concentrations of elements that strongly absorb thermal and epithermal neutrons, and a routine method is needed to correct the self-shielding effect. Fortunately, a few years ago, reactor physicists showed that the amount of epithermal as well as thermal self-shielding could be expressed by the same analytical function, a sigmoid, for all nuclides [Martinho et al. 2003, Gonçalves et al. 2004, Martinho et al. 2004]. Subsequently, this discovery was adapted to neutron activation analysis [Chilian[a,b] et al. 2006], and expressions were developed to calculate thermal and epithermal neutron self-shielding factors in a cylindrical sample irradiated in a nearly isotropic mixed flux. The thermal neutron self-shielding factor is given by [Chilian[b] et al. 2006]:

$$G_{th} = \frac{1}{1 + \left(\frac{N_{Av} k_{th}}{r(r+h)} \sum_i \frac{m_i \sigma_{abs,i}}{M_{at,i}} \right)^{0.964}} \qquad (6.1)$$

N_{Av} - Avogadro's number

k_{th} - thermal self-shielding constant

r - radius of cylinder

h - height of cylinder

m_i - amount of element i (grammes)

$\sigma_{abs,i}$ - thermal neutron absorption cross-section for element i

$M_{at,i}$ - atomic mass of element i

The thermal neutron self-shielding is the same for any nuclide in a given sample, and in Eq. 6.1 it can be seen that it is the sum of the contributions of all the elements. The thermal self-shielding constant, k_{th}, was found to vary only slightly for the three different irradiation sites of the SLOWPOKE reactor[5], and the mean measured value was 0.91 at an approximate moderator temperature of 30°C near the irradiation sites. Since most neutron absorption cross-sections decrease as the square-root of the neutron energy, it is expected that k_{th} would be about 5% lower in reactors with much higher moderator temperature, 60°C.

The epithermal neutron self-shielding factor is given by [Chilian[b] et al. 2006]:

$$G_{ep} = \frac{0.94}{1 + \left(\frac{m N_{Av} k_{ep} \sigma_{abs,ep}}{r(r+h) M_{at}} \right)^{0.82}} + 0.06 \qquad (6.2)$$

m - amount of the element (grammes)

k_{ep} - epithermal self-shielding constant

$\sigma_{abs,ep}$ - epithermal neutron absorption cross-section

M_{at} - atomic mass of the element

The epithermal self-shielding constant, k_{ep}, was defined as unity for the inner irradiation sites of the SLOWPOKE reactor [Chilian[b] et al. 2006], where the first measurements of $\sigma_{abs,ep}$ were performed. It is expected that k_{ep} will be independent of moderator temperature and the nature of the reflector surrounding the irradiation site. The epithermal neutron absorption cross-section, $\sigma_{abs,ep}$, by definition, includes the absorption of neutrons by the resonances of all isotopes of the element which may overlap with the

resonances of the nuclide being activated. However, Eq. 6.2 ignores the possible shielding by other elements in the sample; this should usually be negligible because the sharp resonances will not usually overlap, but it may be significant if the sample contains very high concentrations of certain other elements.

For a sample irradiated in a typical reactor neutron spectrum with both thermal and epithermal neutrons, the effective neutron self-shielding factor, G_{eff}, is given by the appropriately weighted mean of the thermal and epithermal factors:

$$G_{eff} = \frac{f}{f + Q_0(\alpha)} G_{th} + \frac{Q_0(\alpha)}{f + Q_0(\alpha)} G_{ep} \qquad (6.3)$$

f - ratio of thermal to epithermal neutron flux

α - slope parameter of the epithermal neutron spectrum

Q_0 - ratio of resonance integral to thermal activation cross-section

Combining the above three equations gives the general expression for the effective neutron self-shielding factor:

$$G_{eff} = \frac{f}{f+Q_0(\alpha)}\left[\frac{1.00}{1+\left(\frac{N_{Av}k_{th}}{r(r+h)}\sum_i \frac{m_i\,\sigma_{abs,i}}{M_{at,i}}\right)^{0.964}}\right] + \frac{Q_0(\alpha)}{f+Q_0(\alpha)}\left[\frac{0.94}{1+\left(\frac{m\;N_{Av}\,k_{ep}\,\sigma_{abs,ep}}{r(r+h)M_{at}}\right)^{0.82}}+0.06\right] \quad (6.4)$$

G_{eff} can be thought of as the activity of a nuclide in an absorbing sample relative to that produced in a similar sample irradiated in the same neutron spectrum and with the same fluence, but with no neutron absorption. Thus, in neutron activation analysis, the concentration of an element measured with this nuclide needs to be divided by G_{eff} to correct for self-shielding. For several different reactor irradiation channels and for long cylinders, $h >> r$, and for flat cylinders, $h << r$, it was shown [Chilian[b] et al. 2006] that both G_{th} and G_{ep} were accurately calculated by this expression. Wires can also be calculated, since they are long cylinders, as can thin foils, square or round, since they have the same self-shielding as flat cylinders of the same thickness.

The values of $\sigma_{abs,i}$ and $\sigma_{abs,ep}$, with the $\sigma_{abs,ep}$ calculated as described below or estimated from the resonance integrals, were compared for 86 nuclides used in neutron activation analysis. This revealed that $\sigma_{abs,ep}$ was greater than $\sigma_{abs,i}$ in 76 of 86 cases, and in 52 cases by more than a factor of 10. Thus, epithermal self-shielding is usually more severe than thermal self-shielding, $G_{ep} < G_{th}$. However, many reactors have well-thermalized neutron

spectra, $f >> 20$, and for many nuclides, especially those of light elements, Q_0 is small, meaning that the second term of Eq. 6.4 is often negligible.

The use of Eq. 6.4 for any nuclide requires the knowledge of the thermal and epithermal neutron absorption cross-sections. The well-known elemental thermal neutron absorption cross-sections, $\sigma_{abs,i}$, can be found in many compilations. The newly-defined [Chilian[b] et al. 2006] epithermal neutron absorption cross-sections, $\sigma_{abs,ep}$, need to be measured or estimated with sufficient accuracy for each nuclide. In this work, we measure $\sigma_{abs,ep}$ for several nuclides activated by *(n,γ)* reactions with high Q_0 values, we calculate $\sigma_{abs,ep}$ from resonance parameters for all the other nuclides and we develop a spreadsheet for routine self-shielding corrections in neutron activation analysis work.

6.2. Experimental

In a previous work [Chilian[b] et al. 2006], $\sigma_{abs,ep}$ was defined and then measured for the $^{79}Br(n,\gamma)^{80}Br$, $^{81}Br(n,\gamma)^{82}Br$, $^{96}Zr(n,\gamma)^{97}Zr$, $^{114}Cd(n,\gamma)^{115}Cd$ and $^{127}I(n,\gamma)^{128}I$ reactions; details of the measurements are given there. In this work, $\sigma_{abs,ep}$ was measured for eight reactions: $^{115}In(n,\gamma)^{116m}In$, $^{121}Sb(n,\gamma)^{122}Sb$, $^{123}Sb(n,\gamma)^{124}Sb$, $^{133}Cs(n,\gamma)^{134}Cs$, $^{152}Sm(n,\gamma)^{153}Sm$, $^{186}W(n,\gamma)^{187}W$, $^{197}Au(n,\gamma)^{198}Au$ and $^{238}U(n,\gamma)^{239}U$. For each reaction studied, several 1 mL cylindrical samples, with r = 5.0 mm and h = 12.7 mm, were prepared with accurately known masses of the element. For the more dilute samples, the compounds were dissolved in water, or in HCl for Sm_2O_3, and 1 mL aliquots were sealed in 10 mm diameter, 1.4 mL polyethylene vials. For some of the more concentrated

samples, a weighed amount of the compound, a fine powder, was mixed with epoxy resin, in the vial, which then hardened to form the 1 mL cylinder. The type of sample and range of masses used is given in Table 6.1 for each element. For Sb, both powders and solutions were used. For Zr, metal discs were used as described previously [Chilian[b] et al. 2006].

All the samples were irradiated at a thermal neutron flux of 5.59 x 10^{11} $cm^{-2}s^{-1}$ in the inner irradiation site in the beryllium reflector of the Ecole Polytechnique SLOWPOKE reactor. This irradiation site was previously characterized [St-Pierre and Kennedy 2006], having f = 18.0 and α = -0.051. It was previously shown [St-Pierre and Kennedy 2004] that 1 mL of water or organic resin moderates the neutrons and increases the thermal flux by 5%. Thus, the value of f was adjusted, between 18.0 and 18.9, for each measurement. To measure the activities, the samples were counted 10 cm from a germanium detector. The gamma-ray peak count rates, corrected for decay time, were converted to activities using detector efficiencies calculated taking into account sample-detector distance, sample geometry and gamma-ray attenuation in the sample [Kennedy and St-Pierre 1997]. In general, no relative efficiency correction was needed for sample-detector distance or geometry because these were the same for all samples of a given element, except the Zr discs; the main correction was for the variation of gamma-ray attenuation as the amount of element increased. To determine the specific activity, proportional to G_{eff}, the measured activity was divided by the known amount of the element in the sample. Specific activities were converted to G_{eff} using the most dilute samples, which are known to have G_{eff} = 1. To obtain the experimental G_{ep}, the thermal part was subtracted from G_{eff}

using Eq. 6.3, with G_{th} calculated by Eq. 6.1. The resulting experimental G_{ep} values were plotted as a function of the mass of the element and a least-squares fit of the data with Eq. 6.2, with $k_{ep} = 1$, yielded $\sigma_{abs,ep}$ for each nuclide.

Values of $\sigma_{abs,ep}$ were also calculated by a formula derived from Eqs 2 and 5 of Salgado et al. [Salgado et al. 2004] for capture reactions with several resonances:

$$\sigma_{abs,ep,Salgado} = 0.195\ \theta\ \frac{\sum_{i=1}^{n} w_i \left(\sigma_{tot,i}(E_{res,i}) \sqrt{\frac{\Gamma_\gamma}{\Gamma}} \right)}{\sum_{i=1}^{n} w_i} \tag{6.5}$$

with

$$w_i = \left(\frac{\Gamma_\gamma}{E_{res}^2} \frac{(2J+1)\Gamma_n}{(2I+1)\Gamma} \right)_i \tag{6.6}$$

θ - isotopic abundance

$\sigma_{tot,i}(E_{res,i})$ - total cross section at the peak of resonance i

w_i - weighting factor

Γ_γ - radiative resonance width

Γ - total resonance width

Γ_n - neutron resonance width

J - spin of the resonance state

I - spin of the target nucleus

The weighting factor of resonance i is proportional to the radiative resonance width, Γ_γ, and inversely proportional to the square of the resonance energy, E_{res}. The data for the

resonance cross-sections were taken from the JANIS software obtained from the nea.fr website [Janis 3.0, http://www.nea.fr/janis/].

A computer spreadsheet was written to calculate neutron self-shielding using Eqs. 6.1, 6.2 and 6.4 (Appendix B). It contains the thermal neutron absorption cross-sections for 71 elements and the epithermal neutron absorption cross-sections for 76 nuclides. It has two pages. The first page is used to correct neutron activation analysis measurements: the measured concentrations are entered and an iterative calculation is performed to calculate G_{eff} for each nuclide, correcting the measured concentrations with each iteration. The calculation of G_{eff} requires the parameters f and α of the neutron spectrum of the irradiation channel used. The dimensions of the cylindrical sample, r and h, are also entered, as well as the sample mass. The second page is used to estimate the self-shielding in materials of approximately known composition; the equations are applied directly to calculate G_{th}, G_{ep} and G_{eff}.

6.3. Results and Discussion

The measured values of G_{ep}, as a function of the amount of the element in 1 mL cylindrical samples, are shown in Figs. 6.1 and 6.2 for two of the elements studied, W and Au. The error bars in the figures are the estimated standard uncertainties of the measurements. The measurements for the other elements are similar. The expression of Eq. 6.2 was fitted to these data to determine $\sigma_{abs,ep}$.

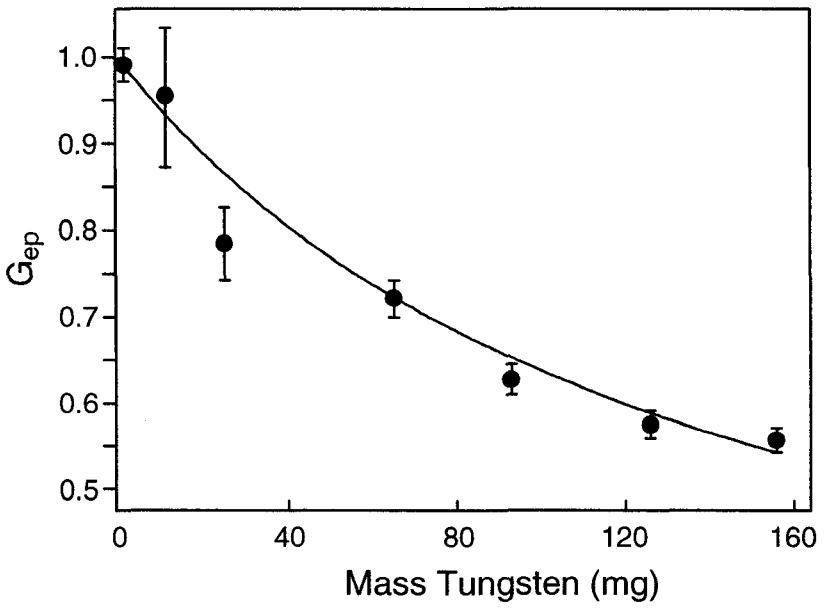

Figure 6.1 The measured G_{ep} of $^{186}W(n,\gamma)^{187}W$ and the fitted expression

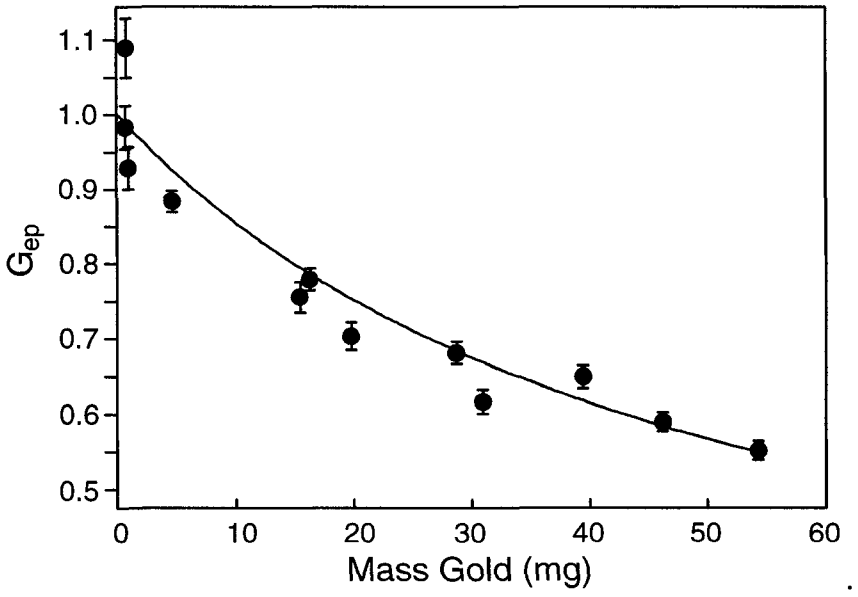

Figure 6.2 The measured G_{ep} of $^{197}Au(n,\gamma)^{198}Au$ and the fitted expression

The measured values of $\sigma_{abs,ep}$ are shown in Table 6.1 along with some of the details of the measurements. Also shown in Table 6.1 are the values calculated with Eq. 6.5.

The measured values of $\sigma_{abs,ep}$ agree fairly well with the calculated values, $\sigma_{abs,ep,Salgado}$, except for ^{116m}In, for which the discrepancy is more than a factor of two. It is suspected that the reason for this discrepancy may be that Eq. 6.5 is not accurate for resonances at very low energies; the main resonance of the ^{115}In(n,γ) ^{116m}In reaction is at 1.46 eV, the lowest of the 13 cases studied.

For the 12 other cases, the differences are mostly of the order of 20%. Since the measured $\sigma_{abs,ep}$ have experimental uncertainties of less than 10% in most cases, we attribute the 20% differences to inaccuracy in the calculated $\sigma_{abs,ep,Salgado}$. It is not surprising that the $\sigma_{abs,ep,Salgado}$ would often be in error by 20% or more, because Eq. 6.5 assumes a simple pattern of neutron resonances, all with the same Breit-Wigner shape [Salgado et al. 2004], and 20% is the order of magnitude of the uncertainty estimated by Salgado et al.[2004] for these calculations. For ^{122}Sb, the calculated value is 40% below the experimental value. In this case there is a large experimental uncertainty, 86 b at the 68% confidence level; so it is possible that much of the difference could be due to experimental error. For ^{128}I, the calculated value is 47% higher than the experimental value. The ^{127}I(n,γ)^{128}I reaction is exceptional in that it has a large number of significant, closely-spaced resonances, and Salgado et al. [2004] admitted that their formula would not be accurate in such cases. For the 13 cases studied here, the contribution of the very small resonances not included in the calculation of Eq. 6.5, as well as the possible overlap

of resonances of other isotopes of the same element, were investigated in detail. These two contributions were found to be less than 5% in all 13 cases.

Table 6.1 Measured and calculated values of epithermal neutron absorption cross-sections, $\sigma_{abs,ep}$, for 13 nuclides. The values in parentheses are the experimental standard uncertainties, corresponding to the 68% confidence interval

Reaction	Material, Range of masses	Measured $\sigma_{abs,ep}$ (uncertainty) (b)	Calculated $\sigma_{abs,ep,Salgado}$ (b)
$^{79}Br(n,\gamma)^{80}Br$	KBr soln. 1 - 400 mg	233 (19)	290
$^{81}Br(n,\gamma)^{82}Br$	KBr soln. 1 - 400 mg	253 (17)	239
$^{96}Zr(n,\gamma)^{97}Zr$	Zr metal discs 65 mg - 8.4 g	10.3 (0.8)	8.0
$^{114}Cd(n,\gamma)^{115}Cd$	$Cd(NO_3)_2{:}4H_2O$ soln. 1 - 200 mg	78 (5)	80
$^{115}In(n,\gamma)^{116m}In$	$InCl_3$ soln. 0.2 - 40.7 mg	2582 (243)	5922
$^{121}Sb(n,\gamma)^{122}Sb$	$K(SbO)C_4H_4O_6$ soln. 14 - 557 mg	500 (86)	297
$^{123}Sb(n,\gamma)^{124}Sb$	$K(SbO)C_4H_4O_6$ powd. 14 - 557 mg	442 (75)	535
$^{127}I(n,\gamma)^{128}I$	KI soln. 1 - 300 mg	387 (24)	567
$^{133}Cs(n,\gamma)^{134}Cs$	$CsNO_3$ soln. 9 – 161 mg	1033 (140)	1289
$^{152}Sm(n,\gamma)^{153}Sm$	Sm_2O_3 soln. in HCl 0.3 - 70.6 mg	5930 (262)	5729
$^{186}W(n,\gamma)^{187}W$	WO_2 powder 11 - 156 mg	1790 (181)	2270
$^{197}Au(n,\gamma)^{198}Au$	$NaAuCl_4{:}2H_2O$ 0.13 - 5.40 mg	4648 (290)	5774
$^{238}U(n,\gamma)^{239}U$	$UO_2(C_2H_3O_2){:}2H_2O$ 0.4 - 55.2 mg	1148 (129)	1330

The spreadsheet developed calculates G_{th}, G_{ep} and G_{eff} for 76 nuclides. It uses elemental thermal neutron absorption cross-sections, $\sigma_{abs,i}$, taken from the Table of Nuclides [http://atom.kaeri.re.kr/]. For the 13 nuclides studied here, the measured $\sigma_{abs,ep}$ are used, and for the other 63 nuclides, calculated $\sigma_{abs,ep,Salgado}$ are used; it is assumed the latter have 20% uncertainty. The spreadsheet was found to be very convenient for correcting neutron activation analysis measurements for self-shielding. Since an analytical expression is used, the uncertainties of the corrected concentrations can be calculated from the uncertainties of all the parameters used, and error propagation. Assuming accurate measurements of the concentrations, the uncertainties of the corrected concentrations will depend on the uncertainty of the calculation of the values of G_{eff}. We tested the importance of various parameters towards the final uncertainties. For nuclides with high Q_0 values, say $Q_0 > 10$, and in poorly thermalized irradiation channels, say $f <$ 20, it was found that the largest contribution to the uncertainty in G_{eff} was from the uncertainty in $\sigma_{abs,ep}$. In a typical difficult case, a 7 mL sample weighing 7 g, with 97,000 *ppm* Cl (thermal neutron absorber) and 74,000 *ppm* As, irradiated in a neutron spectrum with $f = 18$, the result for ^{76}As ($Q_0 = 15$) was $G_{th} = 0.900$, $G_{ep} = 0.700$ and $G_{eff} = 0.797$, with an uncertainty in G_{eff} of 2.8%. The contributions to the uncertainty in G_{eff} due to the uncertainties in f, α, Q_0 and $\sigma_{abs,i}$ were less than 0.5%. The 5% uncertainties in r and h caused 1% uncertainty in G_{eff}. The main contribution, 2.3%, was from the 20% uncertainty in $\sigma_{abs,ep}$.

With this spreadsheet, neutron activation analysis measurements are now routinely corrected for neutron self-shielding in our laboratory, with typical uncertainty of about 2% when the self-shielding effect is of the order of 20%. Page two of the spreadsheet is used to screen materials of approximately known composition, before irradiation; the estimates of G_{th}, G_{ep} and G_{eff} help to determine the parameters of NAA measurements, such as sample size and the appropriate irradiation channel.

It should be noted that all the measurements of this work and previous work [Chilian[a,b] et al. 2006] were done with $G_{th} > 0.6$ and $G_{ep} > 0.6$. Thus, they give no assurance that the method developed here will be accurate for samples with more than 40% thermal or epithermal self-shielding. However, there are data [Martinho et al. 2003, Goncalves et al. 2004, Martinho et al. 2004, Salgado et al. 2004] to suggest that Eqs. 6.1 and 6.2 may still be accurate to about 10% for values of G_{th} and G_{ep} as low as 0.1.

6.4. Conclusion

A spreadsheet has been developed which calculates the thermal and epithermal neutron self-shielding for any nuclide in a cylindrical sample irradiated in a reactor neutron spectrum. In our SLOWPOKE reactor laboratory, element concentrations measured by neutron activation analysis are routinely corrected for self-shielding with typical accuracy of 2%; similar accuracy should be achievable with other reactors as long as the appropriate parameters f, α, k_{th} and k_{ep} are used. The spreadsheet is available from the authors on request. Future work will include the measurement of several more epithermal

neutron absorption cross-sections, which will improve the accuracy of the self-shielding corrections for these nuclides.

6.5. References

CHILIAN, C.[a], KASSAKOV, M., ST-PIERRE, J., KENNEDY, G., 2006. Extending NAA to Materials with High Concentrations of Neutron Absorbing Elements. *Journal of Radioanalytical and Nuclear Chemistry*. 270: 2, 417-423.

CHILIAN, C.[b], ST-PIERRE, J., KENNEDY, G., 2006. Dependence of thermal and epithermal neutron self-shielding on sample size and irradiation site. *Nuclear Instruments and Methods in Physics Research, Section A*. 564:2, 629-635.

GONÇALVES, I.F., MARTINHO, E., SALGADO, J., 2004. Extension to cylindrical samples of the universal curve of resonance neutron self-shielding factors. *Nuclear Instruments and Methods in Physics Research, Section B*. 213, 186-188.

Janis 3.0, http://www.nea.fr/janis/

KENNEDY, G., ST-PIERRE, J. 1997. Parameterization of Detector Efficiency for the Standardization of NAA With Stable Low Flux Reactors. *Journal of Radioanalytical and Nuclear Chemistry*. 215: 2, 235-239.

MARTINHO, E., GONÇALVES, I.F., SALGADO, J. 2003. Universal curve of epithermal neutron resonance self-shielding factors in foils, wires and spheres. *Applied Radiation and Isotopes*. 58:3. 371-375.

MARTINHO, E., SALGADO, J., GONÇALVES, I.F., 2004. Universal curve of the thermal neutron self-shielding factor in foil, wires, spheres and cylinders. *Journal of Radioanalytical and Nuclear Chemistry*. 261:3, 637-643.

SALGADO, J., MARTINHO, E., GONÇALVES, I.F., 2004. The calculation of neutron self-shielding factors of a group of isolated resonances. *Journal of Radioanalytical and Nuclear Chemistry*. 260:2, 317-320.

ST-PIERRE, J., KENNEDY, G., 2004. Standardizing NAA of Biological samples of Varying Size, Shape and Composition. *Journal of Radioanalytical and Nuclear Chemistry*. 259: 3, 431-434.

ST-PIERRE, J., KENNEDY, G., 2006. Re-Measurement of Q_0 and k_0 Values for 14 Nuclides. *Nuclear Instruments and Methods in Physics Research, Section A*. 564: 2, 669-774.

Table of Nuclides, http://atom.kaeri.re.kr/

General Discussions, Conclusions and Future Perspectives

The main objective of this work was to investigate the epithermal self-shielding in neutron activation analysis and to develop a general method to correct both thermal and epithermal neutron self-shielding. This would extend instrumental neutron activation analysis to a new class of materials with high concentrations of thermal and epithermal neutron absorbers. Due to the complexity of the resonance pattern of the neutron absorption cross section in the epithermal region, combined with the particularities of the irradiation conditions, we conducted our research in three distinct stages: a preliminary evaluation of the method and its applicability in activation analysis, a verification of the dependency of the thermal and epithermal self-shielding factors on the sample dimensions and on the irradiation site, and finally, the complete development of the neutron self-shielding correction method and its implementation in routine activation analysis.

We started by formulating the theoretical expressions of the thermal and epithermal self-shielding factors and we verified their validity for some pure and well-characterized substances containing strong thermal and epithermal neutron absorbers, such as chlorine, iodine and bromine. For these particular cases, and for constant geometry samples, we investigated changes in the self-shielding factor with the amount of element present in the sample. Once the theoretical expressions were validated and their characteristic parameters identified, we developed an iterative method for correcting neutron self-shielding in activation analysis, and we tested this method for two extreme cases: first for

shielding in activation analysis, and we tested this method for two extreme cases: first for a very concentrated sample containing a mixture of a thermal neutron absorber, chlorine, and an epithermal neutron absorber, iodine; and secondly for a very concentrated sample containing two strong epithermal neutron absorbers, iodine and bromine, with their isotopes ^{79}Br, ^{81}Br and ^{127}I. The correction for thermal neutron self-shielding was accurate because the effects of several elements are combined in a straightforward manner, and the error in determining the real concentrations was less than 1.5%. However, for mixture of several epithermal absorbers, the error in determining the iodine and bromine concentrations was as high as 6.5%, which was explained by the mutual self-shielding between the resonances of the nuclides present in the sample. Thus, the method is limited for a concentrated mixture of strong epithermal neutron absorbers. If we wish to determine several elements activated by epithermal neutrons, in a sample containing one element that strongly absorbs epithermal neutrons, we would need to know the shielding of the strongly absorbing element on the resonances of the nuclides of the other elements. This would require a large number of calibration measurements, one measurement per element-nuclide pair, or Monte Carlo calculations. Since an extreme case like the one described above is encountered rarely in activation analysis, a sample dilution could be the best approach in analysing this type of sample. When we wish to conserve the integrity of the sample, an alternative to sample dilution would be INAA followed by a Monte Carlo calculation, which may need to be iterative.

In the second phase of the project, we have investigated the dependence of thermal and epithermal self-shielding factors on sample size and irradiation site. This was done by

way of a carefully-designed set of experiments, in which materials were judiciously chosen in such a manner that samples of different geometries but identical composition were prepared and alternatively activated in three different irradiation sites with different neutron flux composition and anisotropy, different distance from the reactor core, and different surrounding moderator. The outcome clearly showed that the thermal and epithermal self-shielding have only a small dependency on the irradiation site characteristics. From conversations at international conferences, we have learned that this is contrary to what was commonly believed in the neutron activation analysis community. In the case of the SLOWPOKE reactor, the impact of the site dependency of the thermal and epithermal self-shielding correction factor is usually less than 1%. Of equal importance, the predicted dependence of the thermal and epithermal self-shielding factors holds for various sample geometries. However, for irradiation sites where the neutron flux is highly anisotropic, the proposed sample geometry dependency of the self-shielding parameters for cylindrical samples may not hold, and it will be investigated in future studies.

In the above distinct steps of the study regarding the variation of thermal and epithermal neutron self-shielding with sample composition, geometry of the sample, and practical irradiation conditions, we have been able to validate the study's hypothesis that, in activation analysis, epithermal neutron self-shielding is described by a unique sigmoid function of the mass of the element present in the sample. The next step was to extend the method to correcting epithermal and thermal self-shielding for all 76 important nuclides in activation analysis, and generalize the method for any cylindrical sample geometry.

For 13 relevant nuclides in activation analysis, we have experimentally evaluated the dependency of the epithermal self-shielding factor on the element mass present in the sample. In each case, we correlated the epithermal neutron self-shielding with the mass and sample dimensions, and hence we were able to identify and define an empirical nuclear parameter, epithermal absorption cross section, which characterizes the activation by epithermal neutrons. For the other 63 nuclides commonly used in activation analysis we calculated the neutron self-shielding nuclear parameters with a theoretical formula based on the resonances. Also, for these 63 nuclides we investigated and discussed the limitations in using the theoretical approach. In addition, for each of the 13 nuclides for which we compared measurement and theory, we systematically investigated the potential mutual self-shielding of the resonances of all the isotopes of the element, and we concluded that it is negligible in all 13 cases. Finally, the experimental values of epithermal absorption cross-section, together with the theoretically estimated values, allow us to create a complete thermal and epithermal neutron self-shielding correction method by using a spreadsheet for all 76 commonly used nuclides in activation analysis.

For the first time in the field of INAA, a systematic method for correcting neutron self-shielding, for cylindrical samples of any composition, and for any reactor irradiation site, was implemented in routine activation analysis, representing an important step forward in activation analysis.

We predict that about one hundred neutron activation analysis laboratories will use our method within the next few years. Feedback from these users will be important for future improvements to the method.

Bibliography

ABRASHKIN, S., 1984. Epithermal Neutron Self-Shielding in the Reactor Production of ^{99}Mo. *Applied Radiation and Isotopes*. 36: 5. 385-388.

AXTON, E.J., RYVES, T.B., 1967. Scattering Resonance Self-Shielding Correction for use with Manganese Sulphate Solutions. *Journal of Nuclear Energy*. 21: 7, 543-546.

BLAAUW, M., 1995. Confusing Issue of the Neutron Capture Cross Section to use in Thermal Neutron Self-Shielding Computations. *Nuclear Instruments & Methods in Physics Research, Section A*. 356: 2-3, 403.

BLAAUW, M., 1996. Derivation and proper use of Stewart's formula for thermal neutron self-shielding in scattering media. *Nuclear Science and Engineering*, 124: 3, 431-435.

BLAAUW, M., MACKEY, E.A.M., 1997. Neutron self-shielding in hydrogenous samples. *Journal of Radioanalytical and Nuclear Chemistry*, 216: 1, 65.

BLAAUW, M.[a], POSTMA, H., MUTTI, P., 2003. Quantitative neutron capture resonance analysis verified with instrumental neutron activation analysis. *Nuclear Instruments and Methods in Physics Research, Section A*. 505: 1-2, 508-511.

BLAAUW, M.[b], BAAS, H.W., DONZE, M., 2003. Height-resolved large-sample NAA of a 1 m long, 13 cm diameter ditch-bottom sample. *Nuclear Instruments and Methods in Physics Research, Section A*. 505: 1-2, 512-516.

BLOCK, R.C., HARRIS, D.R., KIM, S.H., KOBAYASHI, K., 1981. Uranium-238 Resonance Self-Indication Capture Measurements. *Nuclear Science and Engineering*. 80: 2, 263-281.

CHIBA, G., 2003. Combined method to evaluate the resonance self shielding effect in power fast reactor fuel assembly calculation. *Journal of Nuclear Science and Technology*. 40: 7, 537-543.

CHILIAN, C.[a], KASSAKOV, M., ST-PIERRE, J., KENNEDY, G., 2006. Extending NAA to Materials with High Concentrations of Neutron Absorbing Elements. *Journal of Radioanalytical and Nuclear Chemistry*. 270: 2, 417-423.

CHILIAN, C.[b], ST-PIERRE, J., KENNEDY, G., 2006. Dependence of thermal and epithermal neutron self-shielding on sample size and irradiation site. *Nuclear Instruments and Methods in Physics Research, Section A*. 564: 2, 629-635.

COPLEY, J.R.D., STONE, C.A., 1989. Neutron scattering and its effect on reaction rates in neutron absorption experiments. *Nuclear Instruments & Methods in Physics Research, Section A*. 281: 3, 593-604.

CRANE, J.L., DOERNER, R.C., 1963. Thermal self-shielding and edge effects in absorbing foils. *Nuclear Science and Engineering*, 16: 3, 259-262.

DALTON, G.R., OSBORN, R.K., 1964. Effect of flux anisotropy on neutron-detector foils. *Nuclear Science and Engineering*. 20: 4, 481-492.

DE CORTE, F., 1987. The k_0-Standardization Method, A Move to the Optimization of Neutron Activation Analysis. *Ph. D. Thesis, University of Gent, Netherlands.*

DE CORTE, F., SIMONITS, A., DE WISPELAERE, A., 1989. Comparative Study of Measured and Critically Evaluated Resonance Integral to Thermal Cross Section Ratios, III. . *Journal of Radioanalytical and Nuclear Chemistry*. 133: 1, 131-151.

DE CORTE, F., SIMONITS, A., 2003. Reccommended Nuclear Data for Use in the k_0 Standardization of Neutron Activation Analysis. *Atomic Data and Nuclear Data Tables*.85: 47-48.

DE SOETE, GIJBELS, R., D., HOSTE, J., 1973. Neutron Activation Analysis. *Wiley Interscience.*

DO CARMO LOPES, M., AVILA, J.M., 1989. Multiple-Scattering resonance self-shielding factors in foils. *Nuclear Instruments & Methods in Physics Research, Section A.* 280: 2-3, 304-309.

DO CARMO LOPES, M., MOLINA AVILA, J., 1990. Energy dependence of neutron self-shielding factors in an isolated resonance. *Nuclear Science and Engineering*. 104: 1, 40-45.

EL HAJJAJI, O., 1999. La physique du reacteur SLOWPOKE-2 de l'Ecole Polytechnique de Montreal. Ph. D. Thesis, Ecole Polytechnique, Montreal, Canada.

EPAA 2.2. User's Manual.

FASTWOOD, T.A., WERNER, R.D., 1962. Resonance and thermal neutron self-shielding in cobalt foils and wires. *Nuclear Science and Engineering.* 13: 4, 385-390.

FLEMING, R.F., 1982. Neutron Self-Shielding Factors for Simple Geometries. *International Journal of Applied Radiation and Isotopes*. 33. 1263-1268.

FUJINO, M., TAKAHASHI, F., YAMAMOTO, H., 1976. Measurements Of Resonance Neutron Self Shielding Factors For Gold And Silver Using Slowing-Down Time Spectrometer. *Journal of Nuclear Science and* Technology. 13: 10, 566-573.

GILAT, J., GURFINKEL, Y., 1963. Self-Shielding in Activation Analysis. *Nucleonics.* 21 :8. 143-144.

GONÇALVES, I.F.[a], MARTINHO, E., SALGADO, J., 2001. Measurement of thermal neutron cross-sections and resonance integrals for ^{71}Ga(n,γ) Monte Carlo calculation of resonance self-shielding factors for epithermal neutron spectra. *Radiation Physics and Chemistry.* 61: 3-6, 461-462.

GONÇALVES, I.F.[b], MARTINHO, E., SALGADO, J., 2001. Monte Carlo calculation of epithermal neutron resonance self-shielding factors in wires of different materials. *Applied Radiation and Isotopes.* 55: 4, 447-451.

GONÇALVES, I.F., MARTINHO, E., SALGADO, J., 2002. Monte Carlo calculation of epithermal neutron resonance self-shielding factors in foils of different materials. *Applied Radiation and Isotopes.* 56: 6, 945-951.

GONÇALVES, I.F., MARTINHO, E., SALGADO, J., 2005. Thermal Neutron Self-Shielding in Foils, A Universal Curve. *Proc. IAEA Int. Conf. On Research Reactors,* Santiago, Chile, 2003. IAEA, Vienna 375.

GONÇALVES, I.F., MARTINHO, E., SALGADO, J., 2004. Extension to cylindrical samples of the universal curve of resonance neutron self-shielding factors. *Nuclear Instruments and Methods in Physics Research, Section B.* 213, 186-188.

GOPALAKRISHNAN, V., GANESAN, S., 1998. Self-shielding and energy dependence of dilution cross-section in the resolved resonance region. *Annals of Nuclear Energy,* 25: 11, 839-857.

GRIFFIN, P.J., KELLY, J.G., 1995. A Rigorous Treatment of Self-Shielding and Covers in Neutron Spectra Determinations. *IEEE Transactions on Nuclear Science.* 42: 6, 1878-1885.

HÉBERT, A., MARLEAU, G., 1990. Generalization of the Stamm'ler Method for the Self-Shielding of Resonant Isotopes in Arbitrary Geometries. Nuclear Science and Engineering. 1081, 230-239.

HÉBERT, A., 2005. The Ribon Extended Self-Shielding Model. Nuclear Science and Engineering. 151: 1, 1-24.

JANIS 3.0, http://www.nea.fr/janis/

KAMEMOTO, V., 1964. On the Self-Shielding Effect in Thermal Activation of Metals. *International Journal of Applied radiation and Isotopes.* 15, 447-448.

KASSAKOV, M., 2007. Analyse par activation neutronique des substances ayant des sections efficaces macroscopiques élevées pour l'absorption de neutrons thermiques. *Master Thesis.* École Polytechnique Montréal, Canada.

KENNA, B.T., VAN DOMELEN, B.H., 1966. Neutron Activation: Relationship of Sample Mass to Self-Shielding Factor. *International Journal of Applied Radiation and Isotopes.* 17. 47-50.

KENNEDY, G., ST-PIERRE, J. 1997. Parameterization of Detector Efficiency for the Standardization of NAA With Stable Low Flux Reactors. *Journal of Radioanalytical and Nuclear Chemistry.* 215: 2, 235-239.

KENNEDY, G., ST-PIERRE, J., WANG, K., ZHANG, Y., PRESTON, J., GRANT, C., VUTHKOV, M. 2000. Activation Constants for SLOWPOKE and MNS Reactors Calculated from the Neutron Spectrum and k_0 and Q_0 Values. *Journal of Radioanalytical Nuclear and Chemistry* . 245: 0, 167-172.

KENNEDY, G., ST-PIERRE, J. 2003. Is the k_0 Method Accurate for Elements with High Q_0 Values?. *Journal of Radioanalytical and Nuclear Chemistry.* 257: 3, 475-480.

KENNEDY, G., 2004. Posibilities of a Commercial Neutron Activation Analysis Service with a Small Reactor. *IAEA, Technical Meeting on Commercial Applications of Nuclear Analytical Techniques.*

KIRÁLY, B., SANAMI, T., CSIKAI, J., 2003. Advantages and Limitations of Thermal and Epithermal Analysis of Bulk Samples. *Applied Radiation and Isotopes.* 58, 691-695.

KRINNINGER, H., RUPPERT, E., HINTZE, L., 1974. Neutron Self-Shielding Factors for Tantalum in the Energy Range of 45eV to 50keV. *Nuclear Instruments and Methods.* 117: 1, 45-60.

KUČERA, J., ZEISLER, R., 2004. Do we need radiochemical separation in activation analysis?. *Journal of Radioanalytical and Nuclear Chemistry.* 262: 1, 255-260.

LINDSTROM, R.M., 2006. Neutron Self-Shielding Factors For Simple Geometries – Revisited. *Transactions of the American Nuclear Society*, v 95, 395-396.

LYNCH, J.H., PETERS, JR., L.E., 1969. Measured thermal-neutron-flux perturbations in cylinders in test reactor. *Nuclear Applications and Technology.* 7: 2, 128-138.

MACKU, K., JATUFF, F., MURPHY, M.F., JONEJA, O.P., BISCHOFBERGER, R., CHAWLA, R., 2006. Advanced foil activation techniques for the measurement of within-pin distributions of the $^{63}Cu(n,\gamma)^{64}Cu$ reaction rate in nuclear fuel. *Nuclear Instruments and Methods in Physics Research, Section A*. 562: 1, 393-400.

MARTINHO, E., GONÇALVES, I.F., SALGADO, J. 2003. Universal curve of epithermal neutron resonance self-shielding factors in foils, wires and spheres. *Applied Radiation and Isotopes*. 58: 3. 371-375.

MARTINHO, E., SALGADO, J., GONÇALVES, I.F., 2004. Universal curve of the thermal neutron self-shielding factor in foil, wires, spheres and cylindres. *Journal of Radioanalytical and Nuclear Chemistry*. 261: 3, 637-643.

MO, S.C., OTT, K.O., 1987. Resonance Self-Shielding Near Zone Interfaces. *Nuclear Science and Engineering*. 96: 2, 112-121.

NASRABADI, M.N., JALALI, M., MOHAMMADI, A., 2007. Calculation of thermal neutron self-shielding correction factors for aqueous bulk sample prompt gamma neutron activation analysis using the MCNP code. *Nuclear Instruments and Methods in Physics Research, Section B*. 263: 2, 473-476.

POSTMA, H., BLAAUW, M., BODE, P., MUTTI, P., CORVI, F., SIEGLER, P., 2001. Neutron-Resonance Capture Analysis of Materials. *Journal of Radioanalytical and Nuclear Chemistry*. 248: 1, 115-120.

REYNOLDS, S.A., MULLINS, W.T., 1963. Neutron Flux Perturbation in Activation Analysis. *International Journal of Applied radiation and Isotopes*. 14, 421-425.

SALGADO, J.[a], GONÇALVES, I.F., MARTINHO, E., 2004. Development of a unique curve for thermal neutron self-shielding factor in spherical scattering materials. *Nuclear Science and Engineering*. 148: 3, 426-428.

SALGADO, J.[b], GONÇALVES, I.F., MARTINHO, E., 2004. Epithermal neutron self-shielding factors in foils for collimated beams. *Applied Radiation and Isotopes*. 60: 5, 677-681.

SALGADO, J.[c], MARTINHO, E., GONÇALVES, I.F., 2004. The calculation of neutron self-shielding factors of a group of isolated resonances. *Journal of Radioanalytical and Nuclear Chemistry*. 260:2, 317-320.

SCHERBAKOV, O., HARADA, H., 2002. Resonance Self-Shielding Corrections for Activation Cross Sections Measurements. *Journal of Nuclear Science and Technologies*. 39: 5. 548-553.

SHAKIR, N.S., JERVIS, R.E., 2001. Correction Factors Required for Quantitative Large Volume NAA. *Journal of Radioanalytical Nuclear and Chemistry.* 248:1, 61-68.

SMODIŠ, B., BUČAR, T., 2006. Overall Measurement Uncertainty of k_0-Based Neutron Activation Analysis. *Journal of Radioanalytical and Nuclear Chemistry.* 269: 2, 311-316.

ST-PIERRE, J., KENNEDY, G., 1999. Effects of Reactor Temperature and Sample Mass on the Activation of Biological and Geological Materials With a SLOWPOKE Reactor. *Biological Trace Elements Research.* 71-72, 481-487.

ST-PIERRE, J., KENNEDY, G., 2004. Standardizing NAA of Biological samples of Varying Size, Shape and Composition. *Journal of Radioanalytical and Nuclear Chemistry.* 259: 3, 431-434.

ST-PIERRE, J., KENNEDY, G., 2006. Re-Measurement of Q_0 and k_0 Values for 14 Nuclides. *Nuclear Instruments and Methods in Physics Research, Section A.* 564: 2, 669-774.

SUDARSHAN, K. TRIPATHI, R.; NAIR, A.G.C.; ACHARYA, R.; REDDY, A.V.R.; GOSWAMI, A., 2005. A Simple Method for Correcting the Neutron Self-Shielding Effect of Matrix and Improving the Analytical Response In Prompt Gamma-Ray Neutron Activation Analysis. *Analytica Chimica Acta.* 549: 1-2, 205-211.

Table of Nuclides, http://atom.kaeri.re.kr/

TIAN, W., NI, B., WANG, P., PENG, L., 1994. Parametric Normalization for Full-Energy Peak Count Rates Obtained at Different Geometries. . *Journal of Radioanalytical and Nuclear Chemistry.* 170 : 1, 27-42.

TIAN, W., NI, B., 1994. Further Study on Parametric Standardization in Reactor NAA. *Journal of Radioanalytical and Nuclear Chemistry.* 179: 1, 119-129.

TOMURO, H., TOMURA, K., 2002. Neutron Activation Analysis of Manganese in Japanese Iron Reference Standard Materials with Large Amounts of Manganese. *Journal of Radioanalytical and Nuclear Chemistry.* 254: 2, 241-248.

TOWNES, B.M., HILBORN, J.W., 1985. The SLOWPOKE-2 Reactor with Low Enrichment Uranium Oxide Fuel. *AECL* (Atomic Energy Canada Limited).

TZIKA, F., STAMATELOS, I.E., 2004. Thermal Neutron Self-Shielding Corrections for Large Sample Instrumental Neutron Activation Analysis Using the MCNP Code. *Nuclear Instruments and Methods in Physics Research B.* 213, 177-181.

VAN LIERDE, S., DE CORTE, F., BOSSUS, D., VAN SLUIJS, R., POMME, S., 1999. Determination of k0 and Related Nuclear Data to be Used in KAYZERO-NAA at DSM research. *Nuclear and Instruments and Methods in Physics Research, Section A.* 422, 874-879.

Appendices

Appendix A Epithermal Absorption Cross Section Calculation

Appendix A presents the calculation of the epithermal absorption cross section, and gives an example of $\sigma_{abs,ep,Salgado}$ calculation for ^{186}W.

A.1 Epithermal Absorption Cross Section Calculation

For 76 nuclides currently used in NAA, epithermal absorption cross section, $\sigma_{abs,ep}$ values were calculated by a formula derived from Eq. 2.10 for capture reactions with several resonances in the epithermal energy region.

$$\sigma_{abs,ep,Salgado} = 0.195\ \theta\ \frac{\sum_{i=1}^{n} w_i \left(\sigma_{tot,i}(E_{res,i}) \sqrt{\frac{\Gamma_{\gamma,i}}{\Gamma_i}} \right)}{\sum_{i=1}^{n} w_i} \qquad \text{(A.1)}$$

where w_i is the weighting factor defined by the following formula:

$$w_i = \frac{\Gamma_{\gamma,i}}{E_{res,i}^2} \frac{g \cdot \Gamma_{n,i}}{\Gamma_i} \qquad \text{(A.2)}$$

with g being statistical weighting factor: g = $(2J+1)/2(2I+1)$, where J is the resonance state spin and I is the target nucleus spin.

In this work, for calculating $\sigma_{abs,ep,Salgado}$, we used the values of nuclear parameters $\sigma_{tot,i}(E_{res})$, $E_{res,i}$, Γ_i, $\Gamma_{\gamma,i}$, $\Gamma_{n,i}$, I, J, provided by JANIS 3.0 software (ENDFB 6.8, JEF 2.2

or JEFF 3.0) [http://www.nea.fr/janis/] and isotopic abundances, θ, from Table of Nuclides [http://atom.kaeri.re.kr/].

The following table gives an example of the calculation of $\sigma_{abs,ep,Salgado}$ for ^{186}W, with an isotopic abundance of 0.28426, resulting in a value of $\sigma_{abs,ep,Salgado}$ (^{186}W) = 2270 b.

Epithermal Absorption Cross Section Calculation for ^{186}W									
$\sigma_{abs,ep,Salgado}$ = **2270 b**									
θ = **0.2843**									
E_{res}(eV)	l	J	Γ(eV)	Γ_n(eV)	Γ_γ(eV)	$\sigma_{tot}(E_{res})$ (b)	g	w	$w\sigma_{tot}(E_{res})(\Gamma_\gamma/\Gamma)^{1/2}$
18.81	0	0.5	0.329	0.280	0.049	109363.821	1	1.18E-04	4.97E+00
170.40	0	0.5	0.089	0.025	0.064	885.917	1	6.19E-07	4.65E-04
204.00	0	0.5	0.073	0.008	0.065	204.808	1	1.62E-07	3.13E-05
219.00	0	0.5	0.582	0.520	0.062	8257.962	1	1.16E-06	3.11E-03
286.50	0	0.5	0.094	0.029	0.065	474.719	1	2.44E-07	9.64E-05
405.50	0	0.5	0.138	0.082	0.056	791.392	1	2.02E-07	1.02E-04
509.50	0	0.5	0.122	0.078	0.044	538.797	1	1.08E-07	3.51E-05
540.50	0	0.5	0.560	0.495	0.065	2553.463	1	1.97E-07	1.71E-04
662.50	0	0.5	0.765	0.680	0.085	2375.714	1	1.72E-07	1.36E-04
714.00	0	0.5	0.090	0.025	0.065	104.955	1	3.54E-08	3.16E-06
723.50	0	0.5	2.172	2.080	0.092	3229.220	1	1.68E-07	1.12E-04
769.00	0	0.5	0.071	0.006	0.065	22.586	1	9.29E-09	2.01E-07
830.00	0	0.5	0.091	0.026	0.065	87.145	1	2.70E-08	1.99E-06
962.50	0	0.5	1.132	1.060	0.072	1907.217	1	7.28E-08	3.50E-05
1070.00	0	0.5	0.631	0.570	0.061	1129.316	1	4.81E-08	1.69E-05
1120.00	0	0.5	0.482	0.420	0.062	825.656	1	4.31E-08	1.28E-05
1185.50	0	0.5	0.880	0.825	0.055	1282.060	1	3.67E-08	1.18E-05
1417.00	0	0.5	0.260	0.170	0.090	251.081	1	2.93E-08	4.33E-06
1470.00	0	0.5	0.074	0.009	0.065	12.123	1	3.48E-09	3.97E-08
1498.00	0	0.5	1.298	1.230	0.068	1192.300	1	2.87E-08	7.84E-06
1593.00	0	0.5	0.070	0.005	0.065	6.829	1	1.96E-09	1.29E-08
1682.00	0	0.5	0.071	0.006	0.065	6.528	1	1.82E-09	1.14E-08
1793.00	0	0.5	0.128	0.063	0.065	66.531	1	9.95E-09	4.72E-07
1817.00	0	0.5	0.080	0.015	0.065	15.569	1	3.69E-09	5.18E-08
1930.50	0	0.5	0.725	0.665	0.060	563.546	1	1.48E-08	2.39E-06
2023.00	0	0.5	0.547	0.480	0.067	398.107	1	1.44E-08	2.00E-06
2069.00	0	0.5	0.077	0.012	0.065	10.253	1	2.37E-09	2.23E-08
2103.50	0	0.5	0.207	0.140	0.067	115.749	1	1.02E-08	6.74E-07
2346.50	0	0.5	0.250	0.180	0.070	125.951	1	9.15E-09	6.10E-07
2386.00	0	0.5	0.138	0.083	0.055	57.130	1	5.81E-09	2.10E-07
2510.00	0	0.5	0.320	0.250	0.070	157.108	1	8.68E-09	6.38E-07
								$\sum_{i=1}^{n} w_i$	$\sum_{i=1}^{n} w_i \left(\sigma_{tot,i}(E_{res,i}) \sqrt{\frac{\Gamma_{\gamma,i}}{\Gamma_i}} \right)$
								1.21E-04	4.98E+00
								$\sigma_{abs,ep,Salgado}$	2272

Appendix B Spreadsheet for Correcting Thermal and Epithermal Self-Shielding for NAA Measurements with Cylindrical Samples

Appendix B presents the iterative algorithm for correcting the self-shielding and its implementation in the spreadsheet "Self-Shielding Corrections for NAA Measurements with Cylindrical Samples".

B.1 Algorithm for Correcting Self-Shielding in NAA

As a first step, the neutron self-shielding correction is initialized by judiciously choosing the irradiation channel characteristics and by inputting sample dimensions and sample mass. The second step is to enter the measured concentrations of elements present in the sample. This action will automatically generate the calculation of the thermal and epithermal self-shielding factors and the corrected concentrations. At each iteration, the algorithm calculates G_{th}, G_{ep} and G_{eff} for 76 nuclides by using: elemental thermal neutron absorption cross-sections, $\sigma_{abs,i}$, taken from the Table of Nuclides [http://atom.kaeri.re.kr/]; measured and calculated values of epithermal neutron absorption cross-sections, $\sigma_{abs,ep,i}$ for the activated isotope of the element i. The self-shielding corrected element concentration is obtained by dividing the original concentration by G_{eff}.

For the case of a sample containing n elements, the algorithm steps are:

1. choose irradiation channel characteristics;

2. input the sample dimensions, volume and weight;

3. measure by NAA the element concentrations, and input these values in the spreadsheet;

4. calculate $m_{0,i}$ of each element i, from element concentration and sample weight;

5. for each element i, calculate the following term:

$$\frac{N_{Av} k_{th}}{r(r+h)} \frac{m_{o,i}\, \sigma_{abs,i}}{M_{at,i}} \tag{B.1}$$

6. sum the values obtained at step 5 and calculate z_{th} given by the following formula:

$$z_{th} = \frac{N_{Av} k_{th}}{r(r+h)} \sum_{i=1}^{n} \frac{m_{0,i}\, \sigma_{abs,i}}{M_{at,i}} \tag{B.2}$$

7. calculate the thermal self-shielding factor, G_{th}, with the formula:

$$G_{th,0} = \frac{1.00}{1 + z_{th}^{0.964}} \tag{B.3}$$

8. for each element i, calculate z_{ep} with the following formula:

$$z_{ep,i} = \frac{m_{0,i}\, N_{Av}\, k_{ep}\, \sigma_{abs,ep,i}}{r(r+h) M_{at}} \tag{B.4}$$

9. calculate the epithermal self-shielding factor, $G_{ep,i}$, for the element i:

$$G_{ep,0,i} = \frac{0.94}{1 + z_{ep,i}^{0.82}} + 0.06 \tag{B.5}$$

10. calculate the effective self-shielding factor for each element *i* with the formula:

$$G_{eff,0,i} = \frac{f}{f + Q_0(\alpha)} G_{th,0} + \frac{Q_0(\alpha)}{f + Q_0(\alpha)} G_{ep,0,i} \qquad \text{(B.6)}$$

11. correct the element mass from the step 4, $m_{0,i}$, by dividing with $G_{eff,0,i}$, and obtain the mass corrected for self-shielding, $m_{1,i}$:

$$m_{1,i} = \frac{m_{0,i}}{G_{eff,0,i}} \qquad \text{(B.7)}$$

12. stop after the fourth iteration; calculate corrected concentrations using the corrected masses;

13. go back to step 5 and perform the next iteration using corrected element masses in the formulas of the steps 5 to 8.

The algorithm presented in the section B.1 was implemented in page one of the spreadsheet "Self-Shielding Corrections for NAA Measurements with Cylindrical Samples". Section B.2 presents this page and an example of correcting the self-shielding for a concentrated sample containing high concentrations of chlorine and arsenic.

Page two of the spreadsheet, "Neutron Self-Shielding Calculation for Cylindrical Samples", presented in the section B.3, calculates the self-shielding in materials of known or estimated composition and uses the steps 1 to 10 of the above algorithm. The known or estimated concentrations of the elements are entered and the calculation of the self-shielding factors is non-iterative. It can be used to screen materials of approximately

known composition, before irradiation; the estimates of G_{th}, G_{ep} and G_{eff} help to determine the parameters of NAA measurements, such as sample size and the appropriate irradiation channel.

B.2 Page 1 of the spreadsheet: Self-Shielding Corrections for NAA Measurements with Cylindrical Samples

Self-shielding corrections for NAA measurements with cylindrical samples											
Enter sample dimensions and mass in B14, B15 and B17											
Enter measured concentrations in D23 to D124											
See corrected concentrations in E25 to E124											
				Irradiation Channel		site 1			site 1	site 6	site 8
						Unc.					
				f =	18.0	0.2			18.0	48.6	52.7
				alpha =	-0.051	0.005			-0.051	0.016	0.018
				kth =	0.94	0.08			0.94	0.86	0.94
				kep =	1.00	0			1.00	1.00	1.00
	Sample										
		r (mm)	small vial	large vial	jumbo						
d (mm)	14	7.0	5	7	12.7						
h (mm)	46		20	46	44						
volume (cm³	7.00		1.571	7.081	22.295						
mass (g)	7.000										
		Gamma	Measured	Corrected							
Element	Nuclide	Energy	Conc.(ppm)	Conc.(ppm)	Gth	Gep	Geff				
Li	Li		0	0.0							
B	B		0	0.0							
N	N		0	0.0							
F	F-20	1633	0	0.0	0.900	1.000	0.916	F-20			
Na	Na-24	1368	0	0.0	0.900	1.000	0.904	Na-24			
Mg	Mg-27	1014	0	0.0	0.900	1.000	0.905	Mg-27			
Al	Al-28	1779	0	0.0	0.900	1.000	0.905	Al-28			
Si	Si-31	1266	0	0.0	0.900	1.000	0.908	Si-31			
	Si-Al-29	1273	0	0.0	1	1	1	Si-Al-29			
P	P-32	beta	0	0.0	0.900	1.000	0.903	P-32			
S	S-37	3102	0	0.0	0.900	1.000	0.908	S-37			
Cl	Cl-38	1642	87600	96828.6	0.900	0.996	0.905	Cl-38			
K	K-42	1525	0	0.0	0.900	1.000	0.907	K-42			
Ca	Ca-49	3084	0	0.0	0.900	1.000	0.903	Ca-49			
Sc	Sc-46	889	0	0.0	0.900	1.000	0.903	Sc-46			
	Sc-46m	142	0	0.0	0.900	1.000	0.904	Sc-46m			
Ti	Ti-51	320	0	0.0	0.900	1.000	0.905	Ti-51			
V	V-52	1434	0	0.0	0.900	1.000	0.904	V-52			
Cr	Cr-51	320	0	0.0	0.900	1.000	0.904	Cr-51			
Mn	Mn-56	1811	0	0.0	0.900	1.000	0.907	Mn-56			
Fe	Fe-59	1099	0	0.0	0.900	1.000	0.907	Fe-59			
Co	Co-60	1173	0	0.0	0.900	1.000	0.912	Co-60			
Ni	Ni-65	1482	0	0.0	0.900	1.000	0.905	Ni-65			
	Ni-Co-58	811	0	0.0	1	1	1	Ni-Co-58			
Cu	Cu-64	511	0	0.0	0.900	1.000	0.908	Cu-64			
	Cu-66	1039	0	0.0	0.900	1.000	0.907	Cu-66			
Zn	Zn-65	1115	0	0.0	0.900	1.000	0.913	Zn-65			
	Zn-69m	439	0	0.0	0.900	1.000	0.919	Zn-69m			
Ga	Ga-71	834	0	0.0	0.900	1.000	0.932	Ga-71			
Ge	Ge-75	264	0	0.0	0.900	1.000	0.911	Ge-75			
	Ge-75m	139	0	0.0	0.900	1.000	0.916	Ge-75m			
	Ge-77	264	0	0.0	0.900	1.000	0.950	Ge-77			
As	As-76	559	59000	73986.5	0.900	0.700	0.797	As-76			
Se	Se-75	265	0	0.0	0.900	1.000	0.942	Se-75			
	Se-77m	162	0	0.0	0.900	1.000	0.905	Se-77m			
Br	Br-80	616	0	0.0	0.900	1.000	0.945	Br-80			
	Br-82	554	0	0.0	0.900	1.000	0.958	Br-82			

		Gamma	Measured	Corrected				
Element	Nuclide	Energy	onc.(ppm)	onc.(ppm)	Gth	Gep	Geff	
Rb	Rb-86	1077	0	0.0	0.900	1.000	0.954	Rb-86
	Rb-86m	556	0	0.0	0.900	1.000	0.947	Rb-86m
	Rb-88	1836	0	0.0	0.900	1.000	0.964	Rb-88
Sr	Sr-85	514	0	0.0	0.900	1.000	0.950	Sr-85
	Sr-87m	388	0	0.0	0.900	1.000	0.924	Sr-87m
Y	Y-90m	479	0	0.0	0.900	1.000	0.933	Y-90m
Zr	Zr-95	724	0	0.0	0.900	1.000	0.931	Zr-95
	Zr-97	743	0	0.0	0.900	1.000	0.995	Zr-97
Nb	Nb-94m	871	0	0.0	0.900	1.000	0.936	Nb-94m
Mo	Mo-99	141	0	0.0	0.900	1.000	0.980	Mo-99
	Mo-101	307	0	0.0	0.900	1.000	0.959	Mo-101
Ru	Ru-103	497	0	0.0	0.900	1.000	0.921	Ru-103
	Ru-105	724	0	0.0	0.900	1.000	0.949	Ru-105
Rh	Rh-104m	51	0	0.0	0.900	1.000	0.928	Rh-104m
	Rh-104m	558	0	0.0	0.900	1.000	0.928	Rh-104m
Pd	Pd-109	88	0	0.0	0.900	1.000	0.964	Pd-109
Ag	Ag-108	633	0	0.0	0.900	1.000	0.916	Ag-108
	Ag-110	658	0	0.0	0.900	1.000	0.953	Ag-110
	Ag-110m	884	0	0.0	0.900	1.000	0.950	Ag-110m
Cd	Cd-115	336	0	0.0	0.900	1.000	0.974	Cd-115
In	In-116m	1097	0	0.0	0.900	1.000	0.949	In-116m
Sn	Sn-125m	332	0	0.0	0.900	1.000	0.981	Sn-125m
Sb	Sb-122	564	0	0.0	0.900	1.000	0.968	Sb-122
	Sb-124	1691	0	0.0	0.900	1.000	0.966	Sb-124
Te	Te-I-131	364	0	0.0	0.900	1.000	0.912	Te-I-131
I	I-128	443	0	0.0	0.900	1.000	0.963	I-128
Cs	Cs-134	796	0	0.0	0.900	1.000	0.949	Cs-134
	Cs-134m	127	0	0.0	0.900	1.000	0.943	Cs-134m
Ba	Ba-131	496	0	0.0	0.900	1.000	0.960	Ba-131
	Ba-139	166	0	0.0	0.900	1.000	0.906	Ba-139
La	La-140	1596	0	0.0	0.900	1.000	0.908	La-140
Ce	Ce-141	145	0	0.0	0.900	1.000	0.906	Ce-141
Pr	Pr-142	1576	0	0.0	0.900	1.000	0.910	Pr-142
Nd	Nd-147	91	0	0.0	0.900	1.000	0.913	Nd-147
Sm	Sm-153	103	0	0.0	0.900	1.000	0.947	Sm-153
	Sm-155	246	0	0.0	0.900	1.000	0.923	Sm-155
Eu	Eu-152	1408	0	0.0	0.900	1.000	0.907	Eu-152
	Eu-152m	842	0	0.0	0.900	1.000	0.906	Eu-152m
Gd	Gd-153	103	0	0.0	0.900	1.000	0.905	Gd-153
	Gd-159	363	0	0.0	0.900	1.000	0.967	Gd-159
Tb	Tb-160	299	0	0.0	0.900	1.000	0.954	Tb-160
Dy	Dy-165	95	0	0.0	0.900	1.000	0.901	Dy-165
	Dy-165m	108	0	0.0	0.900	1.000	0.901	Dy-165m
Ho	Ho-166	81	0	0.0	0.900	1.000	0.941	Ho-166
Er	Er-171	308	0	0.0	0.900	1.000	0.924	Er-171
Tm	Tm-170	84	0	0.0	0.900	1.000	0.946	Tm-170
Yb	Yb-169	177	0	0.0	0.900	1.000	0.922	Yb-169
	Yb-175	396	0	0.0	0.900	1.000	0.903	Yb-175
Lu	Lu-177	208	0	0.0	0.900	1.000	0.908	Lu-177
Hf	Hf-179m	214	0	0.0	0.900	1.000	0.951	Hf-179m
	Hf-181	482	0	0.0	0.900	1.000	0.915	Hf-181
Ta	Ta-182	1221	0	0.0	0.900	1.000	0.970	Ta-182
W	W-187	686	0	0.0	0.900	1.000	0.947	W-187
Re	Re-186	137	0	0.0	0.900	1.000	0.948	Re-186
	Re-188	155	0	0.0	0.900	1.000	0.923	Re-188
Os	Os-191	129	0	0.0	0.900	1.000	0.912	Os-191
	Os-193	460	0	0.0	0.900	1.000	0.914	Os-193
Ir	Ir-192	316	0	0.0	0.900	1.000	0.925	Ir-192
Pt	Pt-Au-199	158	0	0.0	0.900	1.000	0.955	Pt-Au-199

Elem	Mat	SigmaTh				Mass(g)	Sth/Mat	Mass(g)	/Sth/Mat	Mass(g)	/Sth/Mat	Mass(g)	/Sth/Mat	Mass(g)		Conc.(pp	Geff
Li	6.94	71.00	Li		0	0.000	0.00	0.000	0.00	0.000	0.00	0.000	0.00	0.000	Li	0.0	
B	10.81	760.00	B		0	0.000	0.00	0.000	0.00	0.000	0.00	0.000	0.00	0.000	B	0.0	
N	14.01	1.89	N		0	0.000	0.00	0.000	0.00	0.000	0.00	0.000	0.00	0.000	N	0.0	
F	19.00	0.01	F-20	1633	0	0.000	0.00	0.000	0.00	0.000	0.00	0.000	0.00	0.000	F-20	0.0	0.916
Na	22.99	0.53	Na-24	1368	0	0.000	0.00	0.000	0.00	0.000	0.00	0.000	0.00	0.000	Na-24	0.0	0.904
Mg	24.31	0.07	Mg-27	1014	0	0.000	0.00	0.000	0.00	0.000	0.00	0.000	0.00	0.000	Mg-27	0.0	0.905
Al	26.98	0.23	Al-28	1779	0	0.000	0.00	0.000	0.00	0.000	0.00	0.000	0.00	0.000	Al-28	0.0	0.905
Si	28.09	0.17	Si-31	1266	0	0.000	0.00	0.000	0.00	0.000	0.00	0.000	0.00	0.000	Si-31	0.0	0.908
			Si-Al-29	1273	0	0.000		0.000		0.000		0.000		0.000	Si-Al-29	0.0	1
P	30.97	0.17	P-32	bêta	0	0.000	0.00	0.000	0.00	0.000	0.00	0.000	0.00	0.000	P-32	0.0	0.903
S	32.07	0.52	S-37	3102	0	0.000	0.00	0.000	0.00	0.000	0.00	0.000	0.00	0.000	S-37	0.0	0.908
Cl	35.45	33.50	Cl-38	1642	87600	0.613	0.58	0.672	0.63	0.677	0.64	0.678	0.64	0.678	Cl-38	98828.6	0.905
K	39.10	2.10	K-42	1525	0	0.000	0.00	0.000	0.00	0.000	0.00	0.000	0.00	0.000	K-42	0.0	0.907
Ca	40.08	0.43	Ca-49	3084	0	0.000	0.00	0.000	0.00	0.000	0.00	0.000	0.00	0.000	Ca-49	0.0	0.903
Sc	44.96	27.20	Sc-46	889	0	0.000	0.00	0.000	0.00	0.000	0.00	0.000	0.00	0.000	Sc-46	0.0	0.903
			Sc-46m	142	0	0.000		0.000		0.000		0.000		0.000	Sc-46m	0.0	0.904
Ti	47.87	6.10	Ti-51	320	0	0.000	0.00	0.000	0.00	0.000	0.00	0.000	0.00	0.000	Ti-51	0.0	0.905
V	50.94	5.00	V-52	1434	0	0.000	0.00	0.000	0.00	0.000	0.00	0.000	0.00	0.000	V-52	0.0	0.904
Cr	52.00	3.10	Cr-51	320	0	0.000	0.00	0.000	0.00	0.000	0.00	0.000	0.00	0.000	Cr-51	0.0	0.904
Mn	54.94	13.30	Mn-56	1811	0	0.000	0.00	0.000	0.00	0.000	0.00	0.000	0.00	0.000	Mn-56	0.0	0.907
Fe	55.85	2.56	Fe-59	1099	0	0.000	0.00	0.000	0.00	0.000	0.00	0.000	0.00	0.000	Fe-59	0.0	0.907
Co	58.93	37.20	Co-60	1173	0	0.000	0.00	0.000	0.00	0.000	0.00	0.000	0.00	0.000	Co-60	0.0	0.912
Ni	58.69	4.50	Ni-65	1482	0	0.000	0.00	0.000	0.00	0.000	0.00	0.000	0.00	0.000	Ni-65	0.0	0.905
			Ni-Co-58	811	0	0.000		0.000		0.000		0.000		0.000	Ni-Co-58	0.0	1
Cu	63.55	3.80	Cu-64	511	0	0.000	0.00	0.000	0.00	0.000	0.00	0.000	0.00	0.000	Cu-64	0.0	0.908
			Cu-66	1039	0	0.000		0.000		0.000		0.000		0.000	Cu-66	0.0	0.907
Zn	65.41	1.10	Zn-65	1115	0	0.000	0.00	0.000	0.00	0.000	0.00	0.000	0.00	0.000	Zn-65	0.0	0.913
			Zn-69m	439	0	0.000		0.000		0.000		0.000		0.000	Zn-69m	0.0	0.919
Ga	69.72	2.90	Ga-71	834	0	0.000	0.00	0.000	0.00	0.000	0.00	0.000	0.00	0.000	Ga-71	0.0	0.932
Ge	72.64	2.20	Ge-75	264	0	0.000	0.00	0.000	0.00	0.000	0.00	0.000	0.00	0.000	Ge-75	0.0	0.911
			Ge-75m	139	0	0.000		0.000		0.000		0.000		0.000	Ge-75m	0.0	0.916
			Ge-77	264	0	0.000		0.000		0.000		0.000		0.000	Ge-77	0.0	0.950
As	74.92	4.20	As-76	559	59000	0.413	0.02	0.503	0.03	0.516	0.03	0.518	0.03	0.518	As-76	73986.5	0.797
Se	78.96	11.70	Se-75	265	0	0.000	0.00	0.000	0.00	0.000	0.00	0.000	0.00	0.000	Se-75	0.0	0.942
			Se-77m	162	0	0.000		0.000		0.000		0.000		0.000	Se-77m	0.0	0.905
Br	79.90	6.80	Br-80	616	0	0.000	0.00	0.000	0.00	0.000	0.00	0.000	0.00	0.000	Br-80	0.0	0.945
			Br-82	554	0	0.000		0.000		0.000		0.000		0.000	Br-82	0.0	0.958
Rb	85.47	0.39	Rb-86	1077	0	0.000	0.00	0.000	0.00	0.000	0.00	0.000	0.00	0.000	Rb-86	0.0	0.954
			Rb-86m	556	0	0.000		0.000		0.000		0.000		0.000	Rb-86m	0.0	0.947
			Rb-88	1836	0	0.000		0.000		0.000		0.000		0.000	Rb-88	0.0	0.964
Sr	87.62	1.20	Sr-85	514	0	0.000	0.00	0.000	0.00	0.000	0.00	0.000	0.00	0.000	Sr-85	0.0	0.950
			Sr-87m	388	0	0.000		0.000		0.000		0.000		0.000	Sr-87m	0.0	0.924
Y	88.91	1.28	Y-90m	479	0	0.000	0.00	0.000	0.00	0.000	0.00	0.000	0.00	0.000	Y-90m	0.0	0.933
Zr	91.22	0.18	Zr-95	724	0	0.000	0.00	0.000	0.00	0.000	0.00	0.000	0.00	0.000	Zr-95	0.0	0.931
			Zr-97	743	0	0.000		0.000		0.000		0.000		0.000	Zr-97	0.0	0.995
Nb	92.91	1.15	Nb-94m	871	0	0.000	0.00	0.000	0.00	0.000	0.00	0.000	0.00	0.000	Nb-94m	0.0	0.936
Mo	95.94	2.50	Mo-99	141	0	0.000	0.00	0.000	0.00	0.000	0.00	0.000	0.00	0.000	Mo-99	0.0	0.980
			Mo-101	307	0	0.000		0.000		0.000		0.000		0.000	Mo-101	0.0	0.959
Ru	101.07	2.60	Ru-103	497	0	0.000	0.00	0.000	0.00	0.000	0.00	0.000	0.00	0.000	Ru-103	0.0	0.921
			Ru-105	724	0	0.000		0.000		0.000		0.000		0.000	Ru-105	0.0	0.949
Rh	102.91	145.00	Rh-104m	51	0	0.000	0.00	0.000	0.00	0.000	0.00	0.000	0.00	0.000	Rh-104r	0.0	0.928
			Rh-104m	558	0	0.000		0.000		0.000		0.000		0.000	Rh-104r	0.0	0.928
Pd	106.42	7.00	Pd-109	88	0	0.000	0.00	0.000	0.00	0.000	0.00	0.000	0.00	0.000	Pd-109	0.0	0.964
Ag	107.87	63.00	Ag-108	633	0	0.000	0.00	0.000	0.00	0.000	0.00	0.000	0.00	0.000	Ag-108	0.0	0.916
			Ag-110	658	0	0.000		0.000		0.000		0.000		0.000	Ag-110	0.0	0.953
			Ag-110m	884	0	0.000		0.000		0.000		0.000		0.000	Ag-110r	0.0	0.950

Elem	Mat	SigmaTh			Mass(g)	Sth/Mat	Mass(g)	Sth/Mat	Mass(g)	Sth/Mat	Mass(g)	Sth/Mat	Mass(g)		Conc.(ppm	Geff
Cd	112.41	2520.00	Cd-115	336	0 0.000	0.00	0.000	0.00	0.000	0.00	0.000	0.00	0.000	Cd-115	0.0	0.974
In	114.82	194.00	In-116m	1097	0 0.000	0.00	0.000	0.00	0.000	0.00	0.000	0.00	0.000	In-116m	0.0	0.949
Sn	118.71	0.61	Sn-125m	332	0 0.000	0.00	0.000	0.00	0.000	0.00	0.000	0.00	0.000	Sn-125m	0.0	0.981
Sb	121.76	5.10	Sb-122	564	0 0.000	0.00	0.000	0.00	0.000	0.00	0.000	0.00	0.000	Sb-122	0.0	0.968
			Sb-124	1691	0 0.000		0.000		0.000		0.000		0.000	Sb-124	0.0	0.966
Te	127.60	4.20	Te-I-131	364	0 0.000	0.00	0.000	0.00	0.000	0.00	0.000	0.00	0.000	Te-I-131	0.0	0.912
I	126.90	6.20	I-128	443	0 0.000	0.00	0.000	0.00	0.000	0.00	0.000	0.00	0.000	I-128	0.0	0.963
Cs	132.91	29.00	Cs-134	796	0 0.000	0.00	0.000	0.00	0.000	0.00	0.000	0.00	0.000	Cs-134	0.0	0.949
			Cs-134m	127	0 0.000		0.000		0.000		0.000		0.000	Cs-134m	0.0	0.943
Ba	137.33	1.30	Ba-131	496	0 0.000	0.00	0.000	0.00	0.000	0.00	0.000	0.00	0.000	Ba-131	0.0	0.960
			Ba-139	166	0 0.000		0.000		0.000		0.000		0.000	Ba-139	0.0	0.906
La	138.91	9.00	La-140	1596	0 0.000	0.00	0.000	0.00	0.000	0.00	0.000	0.00	0.000	La-140	0.0	0.908
Ce	140.12	0.63	Ce-141	145	0 0.000	0.00	0.000	0.00	0.000	0.00	0.000	0.00	0.000	Ce-141	0.0	0.906
Pr	140.91	11.40	Pr-142	1576	0 0.000	0.00	0.000	0.00	0.000	0.00	0.000	0.00	0.000	Pr-142	0.0	0.910
Nd	144.24	50.00	Nd-147	91	0 0.000	0.00	0.000	0.00	0.000	0.00	0.000	0.00	0.000	Nd-147	0.0	0.913
Sm	150.36	5600.00	Sm-153	103	0 0.000	0.00	0.000	0.00	0.000	0.00	0.000	0.00	0.000	Sm-153	0.0	0.947
			Sm-155	246	0 0.000		0.000		0.000		0.000		0.000	Sm-155	0.0	0.923
Eu	151.96	4600.00	Eu-152	1408	0 0.000	0.00	0.000	0.00	0.000	0.00	0.000	0.00	0.000	Eu-152	0.0	0.907
			Eu-152m	842	0 0.000		0.000		0.000		0.000		0.000	Eu-152m	0.0	0.906
Gd	157.25	######	Gd-153	103	0 0.000	0.00	0.000	0.00	0.000	0.00	0.000	0.00	0.000	Gd-153	0.0	0.905
			Gd-159	363	0 0.000		0.000		0.000		0.000		0.000	Gd-159	0.0	0.967
Tb	158.93	23.20	Tb-160	299	0 0.000	0.00	0.000	0.00	0.000	0.00	0.000	0.00	0.000	Tb-160	0.0	0.954
Dy	162.50	950.00	Dy-165	95	0 0.000	0.00	0.000	0.00	0.000	0.00	0.000	0.00	0.000	Dy-165	0.0	0.901
			Dy-165m	108	0 0.000		0.000		0.000		0.000		0.000	Dy-165m	0.0	0.901
Ho	164.93	61.00	Ho-166	81	0 0.000	0.00	0.000	0.00	0.000	0.00	0.000	0.00	0.000	Ho-166	0.0	0.941
Er	167.26	160.00	Er-171	308	0 0.000	0.00	0.000	0.00	0.000	0.00	0.000	0.00	0.000	Er-171	0.0	0.924
Tm	168.93	105.00	Tm-170	84	0 0.000	0.00	0.000	0.00	0.000	0.00	0.000	0.00	0.000	Tm-170	0.0	0.946
Yb	173.04	50.00	Yb-169	177	0 0.000	0.00	0.000	0.00	0.000	0.00	0.000	0.00	0.000	Yb-169	0.0	0.922
			Yb-175	396	0 0.000		0.000		0.000		0.000		0.000	Yb-175	0.0	0.903
Lu	174.97	84.00	Lu-177	208	0 0.000	0.00	0.000	0.00	0.000	0.00	0.000	0.00	0.000	Lu-177	0.0	0.908
Hf	178.49	104.00	Hf-179m	214	0 0.000	0.00	0.000	0.00	0.000	0.00	0.000	0.00	0.000	Hf-179m	0.0	0.951
			Hf-181	482	0 0.000		0.000		0.000		0.000		0.000	Hf-181	0.0	0.915
Ta	180.95	20.00	Ta-182	1221	0 0.000	0.00	0.000	0.00	0.000	0.00	0.000	0.00	0.000	Ta-182	0.0	0.970
W	183.84	18.20	W-187	686	0 0.000	0.00	0.000	0.00	0.000	0.00	0.000	0.00	0.000	W-187	0.0	0.947
Re	186.21	89.00	Re-186	137	0 0.000	0.00	0.000	0.00	0.000	0.00	0.000	0.00	0.000	Re-186	0.0	0.948
			Re-188	155	0 0.000		0.000		0.000		0.000		0.000	Re-188	0.0	0.923
Os	190.23	15.00	Os-191	129	0 0.000	0.00	0.000	0.00	0.000	0.00	0.000	0.00	0.000	Os-191	0.0	0.912
			Os-193	460	0 0.000		0.000		0.000		0.000		0.000	Os-193	0.0	0.914
Ir	192.22	420.00	Ir-192	316	0 0.000	0.00	0.000	0.00	0.000	0.00	0.000	0.00	0.000	Ir-192	0.0	0.925
Pt	195.08	10.00	Pt-Au-19	158	0 0.000	0.00	0.000	0.00	0.000	0.00	0.000	0.00	0.000	Pt-Au-19	0.0	0.955
Au	196.97	98.70	Au-198	412	0 0.000	0.00	0.000	0.00	0.000	0.00	0.000	0.00	0.000	Au-198	0.0	0.949
Hg	200.59	374.00	Hg-197	77	0 0.000	0.00	0.000	0.00	0.000	0.00	0.000	0.00	0.000	Hg-197	0.0	0.901
			Hg-203	279	0 0.000		0.000		0.000		0.000		0.000	Hg-203	0.0	0.906
Th	232.04	7.37	Th-Pa-23	312	0 0.000	0.00	0.000	0.00	0.000	0.00	0.000	0.00	0.000	Th-Pa-23	0.0	0.944
U	238.03	7.57	U-239	75	0 0.000	0.00	0.000	0.00	0.000	0.00	0.000	0.00	0.000	U-239	0.0	0.987
			U-Np-23	278	0 0.000		0.000		0.000		0.000		0.000	U-Np-23	0.0	0.987
					sum	0.60		0.66		0.67		0.67				
					Zth	0.092		0.101		0.102		0.102				
					Gth	0.909		0.901		0.900		0.900				

					0.0109			Geff = Gth*f/(f+Q0) + Gep*Q0/(f+Q0)							
					.0109TE.4				initial	1st iter.		2nd iter.		3rd iter.	
	theta(%	Q0(a)	I(0)(b)	Sabs, ep(b)	m init(g)	Gep		Geff	Gep	Geff	Gep	Geff	Gep	Geff	
F-19 -> F-20 (1	100	3.50	0.02	1.19	0	1.000	F-20	0.924	1.000	0.917	1.000	0.917	1.000	0.916	
Na-23 -> Na-24 (	100	0.71	0.31	1.96	0	1.000	Na-24	0.912	1.000	0.905	1.000	0.904	1.000	0.904	
Mg-26 -> Mg-27	11.01	0.86	0.02	0.03	0	1.000	Mg-27	0.913	1.000	0.906	1.000	0.905	1.000	0.905	
Al-27 -> Al-28 (2	100	0.92	0.16	3.21	0	1.000	Al-28	0.913	1.000	0.906	1.000	0.905	1.000	0.905	
Si-30 -> Si-31 (2	3.087	1.47	0.12	0.1	0	1.000	Si-31	0.916	1.000	0.909	1.000	0.908	1.000	0.908	
P-31 -> P-32 (	100	0.53	0.08	5.8	0	1.000	P-32	0.912	1.000	0.904	1.000	0.903	1.000	0.903	
S-36 -> S-37 (	0.02	1.45	0.22	0.0	0	1.000	S-37	0.916	1.000	0.908	1.000	0.908	1.000	0.908	
Cl-37 -> Cl-38 (3	24.22	0.89	0.30	0.48	0.6132	0.996	Cl-38	0.913	0.996	0.906	0.996	0.905	0.996	0.905	
K-41 -> K-42 (1	6.73	1.28	1.42	2.64	0	1.000	K-42	0.915	1.000	0.908	1.000	0.907	1.000	0.907	
Ca-48 -> Ca-49 (	0.187	0.51	0.44	0.00	0	1.000	Ca-49	0.911	1.000	0.904	1.000	0.903	1.000	0.903	
Sc-45 -> Sc-46 (	100	0.46	11.61	4.16	0	1.000	Sc-46	0.911	1.000	0.904	1.000	0.903	1.000	0.903	
Sc-45 -> Sc-46m	100	0.68	15.39	4.16	0	1.000	Sc-46m	0.912	1.000	0.905	1.000	0.904	1.000	0.904	
Ti-50 -> Ti-51 (5	5.18	0.89	0.12	0.06	0	1.000	Ti-51	0.913	1.000	0.906	1.000	0.905	1.000	0.905	
V-51 -> V-52 (	99.75	0.65	2.70	2.28	0	1.000	V-52	0.912	1.000	0.905	1.000	0.904	1.000	0.904	
Cr-50 -> Cr-51 (2	4.345	0.62	8.22	0.18	0	1.000	Cr-51	0.912	1.000	0.904	1.000	0.904	1.000	0.904	
Mn-55 -> Mn-56	100	1.32	14.00	66.73	0	1.000	Mn-56	0.915	1.000	0.908	1.000	0.907	1.000	0.907	
Fe-58 -> Fe-59 (	0.282	1.22	1.26	0.05	0	1.000	Fe-59	0.915	1.000	0.907	1.000	0.907	1.000	0.907	
Co-59 -> Co-60 (	100	2.47	71.75	580.02	0	1.000	Co-60	0.920	1.000	0.913	1.000	0.912	1.000	0.912	
Ni-64 -> Ni-65 (2	0.926	0.86	1.07	0.15	0	1.000	Ni-65	0.913	1.000	0.906	1.000	0.905	1.000	0.905	
Cu-63 -> Cu-64 (	69.17	1.48	5.13	965.53	0	1.000	Cu-64	0.916	1.000	0.909	1.000	0.908	1.000	0.908	
Cu-65 -> Cu-66 (	30.83	1.35	2.30	6.88	0	1.000	Cu-66	0.915	1.000	0.908	1.000	0.907	1.000	0.907	
Zn-64 -> Zn-65 (2	48.63	2.67	1.45	6.65	0	1.000	Zn-65	0.921	1.000	0.914	1.000	0.913	1.000	0.913	
Zn-68 -> Zn-69m (	18.75	4.29	2.78	42.32	0	1.000	Zn-69m	0.926	1.000	0.920	1.000	0.919	1.000	0.919	
Ga-71 -> Ga-72 (	39.89	8.56	32.11	149.31	0	1.000	Ga-71	0.938	1.000	0.933	1.000	0.932	1.000	0.932	
Ge-74 -> Ge-75 (	36.28	2.19	0.69	7.07	0	1.000	Ge-75	0.919	1.000	0.912	1.000	0.911	1.000	0.911	
Ge-74 -> Ge-75m	36.28	3.42	1.05	7.07	0	1.000	Ge-75m	0.924	1.000	0.917	1.000	0.916	1.000	0.916	
Ge-76 -> Ge-77 (	7.61	17.72	1.94	9.34	0	1.000	Ge-77	0.954	1.000	0.950	1.000	0.950	1.000	0.950	
As-75 -> As-76 (	100	18.95	63.00	354.41	0.413	0.736	As-76	0.820	0.704	0.800	0.700	0.798	0.700	0.797	
Se-74 -> Se-75 (	0.89	12.79	561.60	44.95	0	1.000	Se-75	0.947	1.000	0.942	1.000	0.942	1.000	0.942	
Se-76 -> Se-77m	9.37	0.99	68.85	17.67	0	1.000	Se-77m	0.914	1.000	0.906	1.000	0.905	1.000	0.905	
Br-79 -> Br-80 (1	50.69	14.95	130.68	233	0	1.000	Br-80	0.950	1.000	0.946	1.000	0.946	1.000	0.945	
Br-81 -> Br-82 (1	49.31	24.85	51.15	253	0	1.000	Br-82	0.962	1.000	0.958	1.000	0.958	1.000	0.958	
Rb-85 -> Rb-86 (	72.17	20.72	7.40	36.12	0	1.000	Rb-86	0.958	1.000	0.954	1.000	0.954	1.000	0.954	
Rb-85 -> Rb-86m (	72.17	15.93	5.70	36.12	0	1.000	Rb-86m	0.952	1.000	0.948	1.000	0.947	1.000	0.947	
Rb-87 -> Rb-88 (	27.83	31.63	2.35	39.27	0	1.000	Rb-88	0.967	1.000	0.964	1.000	0.964	1.000	0.964	
Sr-84 -> Sr-85 (6	0.56	18.08	10.64	1.66	0	1.000	Sr-85	0.955	1.000	0.951	1.000	0.950	1.000	0.950	
Sr-86 -> Sr-87m (	9.86	5.64	3.37	15.32	0	1.000	Sr-87m	0.931	1.000	0.925	1.000	0.924	1.000	0.924	
Y-89 -> Y-90m (	100	8.89	7.60	23.35	0	1.000	Y-90m	0.939	1.000	0.934	1.000	0.933	1.000	0.933	
Zr-94 -> Zr-95 (6	17.38	8.08	0.27	3.08	0	1.000	Zr-95	0.937	1.000	0.932	1.000	0.931	1.000	0.931	
Zr-96 -> Zr-97 (1	2.8	338.48	5.54	10.3	0	1.000	Zr-97	0.995	1.000	0.995	1.000	0.995	1.000	0.995	
Nb-93 -> Nb-94m	100	10.03	8.09	42.20	0	1.000	Nb-94m	0.942	1.000	0.936	1.000	0.936	1.000	0.936	
Mo-98 -> Mo-99	24.13	70.13	6.90	21.08	0	1.000	Mo-99	0.981	1.000	0.980	1.000	0.980	1.000	0.980	
Mo-100 -> Mo-101	9.63	26.12	3.58	15.37	0	1.000	Mo-101	0.963	1.000	0.960	1.000	0.959	1.000	0.959	
Ru-102 -> Ru-103	31.55	4.64	4.72	15.03	0	1.000	Ru-103	0.928	1.000	0.921	1.000	0.921	1.000	0.921	
Ru-104 -> Ru-105	18.62	17.44	6.02	20.73	0	1.000	Ru-105	0.954	1.000	0.950	1.000	0.949	1.000	0.949	
Rh-103 -> Rh-104m	100	6.97	987.45	203.17	0	1.000	Rh-104	0.934	1.000	0.929	1.000	0.928	1.000	0.928	
Rh-103 -> Rh-104 (	100	6.97	987.45	203.17	0	1.000	Rh-104	0.934	1.000	0.929	1.000	0.928	1.000	0.928	
Pd-108 -> Pd-109	26.46	31.68	215.40	875.38	0	1.000	Pd-109	0.967	1.000	0.964	1.000	0.964	1.000	0.964	
Ag-107 -> Ag-108	51.84	3.44	2.06	179.56	0	1.000	Ag-108	0.924	1.000	0.917	1.000	0.916	1.000	0.916	
Ag-109 -> Ag-110	48.16	20.17	1681.76	2313.88	0	1.000	Ag-110	0.957	1.000	0.953	1.000	0.953	1.000	0.953	
Ag-109 -> Ag-110m	48.16	17.86	1489.82	2313.88	0	1.000	Ag-110	0.954	1.000	0.950	1.000	0.950	1.000	0.950	
Cd-114 -> Cd-115	28.73	51.88	13.46	78	0	1.000	Cd-115	0.977	1.000	0.975	1.000	0.974	1.000	0.974	
In-115 -> In-116m (	95.71	17.21	3410.40	2582	0	1.000	In-116m	0.953	1.000	0.949	1.000	0.949	1.000	0.949	
Sn-124 -> Sn-125m	5.79	74.79	8.05	7.27	0	1.000	Sn-125	0.982	1.000	0.981	1.000	0.981	1.000	0.981	
Sb-121 -> Sb-122	57.21	37.60	198.00	500	0	1.000	Sb-122	0.971	1.000	0.968	1.000	0.968	1.000	0.968	
Sb-123 -> Sb-124	42.79	34.10	116.93	442	0	1.000	Sb-124	0.969	1.000	0.966	1.000	0.966	1.000	0.966	

					0.0109				Geff = Gth*f/(f+Q0) + Gep*Q0/(f+Q0)							
					.0109TE.4l				initial	1st iter.		2nd iter.		3rd iter.		
		theta(%	Q0(a)	I(0)(b)	Sabs, ep(b)	m init(g)	Gep		Geff	Gep	Geff	Gep	Geff	Gep	Geff	
I-127 -> I-128 (24		100	29.94	151.28	387	0	1.000	I-128	0.966	1.000	0.963	1.000	0.963	1.000	0.963	
Cs-133 -> Cs-134		100	16.90	446.96	1033	0	1.000	Cs-134	0.953	1.000	0.949	1.000	0.949	1.000	0.949	
Cs-133 -> Cs-134m		100	13.76	364.08	1033	0	1.000	Cs-134	0.948	1.000	0.944	1.000	0.943	1.000	0.943	
Ba-130 -> Ba-131		0.106	26.75	194.40	1.64	0	1.000	Ba-131	0.963	1.000	0.960	1.000	0.960	1.000	0.960	
Ba-138 -> Ba-139		71.7	1.20	0.38	3.97	0	1.000	Ba-139	0.915	1.000	0.907	1.000	0.907	1.000	0.906	
La-139 -> La-140	(	99.91	1.47	11.16	240.23	0	1.000	La-140	0.916	1.000	0.909	1.000	0.908	1.000	0.908	
Ce-140 -> Ce-141		88.45	1.09	0.48	8.44	0	1.000	Ce-141	0.914	1.000	0.907	1.000	0.906	1.000	0.906	
Pr-141 -> Pr-142	(	100	1.91	17.21	196.06	0	1.000	Pr-142	0.918	1.000	0.911	1.000	0.910	1.000	0.910	
Nd-146 -> Nd-147		17.2	2.68	2.80	9.44	0	1.000	Nd-147	0.921	1.000	0.914	1.000	0.913	1.000	0.913	
Sm-152 -> Sm-153		26.75	16.05	3024.00	5930	0	1.000	Sm-153	0.952	1.000	0.948	1.000	0.947	1.000	0.947	
Sm-154 -> Sm-155		22.75	5.45	30.10	54.2	0	1.000	Sm-155	0.930	1.000	0.924	1.000	0.923	1.000	0.923	
Eu-151 -> Eu-152		47.81	1.25	11505.00	1708.28	0	1.000	Eu-152	0.915	1.000	0.907	1.000	0.907	1.000	0.907	
Eu-151 -> Eu-152m		47.81	1.20	11044.80	1708.28	0	1.000	Eu-152	0.915	1.000	0.907	1.000	0.907	1.000	0.906	
Gd-152 -> Gd-153		0.2	0.86	539.00	4.03	0	1.000	Gd-153	0.913	1.000	0.906	1.000	0.905	1.000	0.905	
Gd-158 -> Gd-159		24.84	36.37	71.76	139.82	0	1.000	Gd-159	0.970	1.000	0.967	1.000	0.967	1.000	0.967	
Tb-159 -> Tb-160	(	100	20.71	415.28	798.74	0	1.000	Tb-160	0.958	1.000	0.954	1.000	0.954	1.000	0.954	
Dy-164 -> Dy-165		28.18	0.15	513.00	279.17	0	1.000	Dy-165	0.910	1.000	0.902	1.000	0.901	1.000	0.901	
Dy-164 -> Dy-165m		28.18	0.23	675.00	279.17	0	1.000	Dy-165	0.910	1.000	0.902	1.000	0.902	1.000	0.901	
Ho-165 -> Ho-166		100	12.36	665.99	1110.52	0	1.000	Ho-166	0.946	1.000	0.941	1.000	0.941	1.000	0.941	
Er-170 -> Er-171	(	14.93	5.58	26.52	202.58	0	1.000	Er-171	0.930	1.000	0.924	1.000	0.924	1.000	0.924	
Tm-169 -> Tm-170		100	15.49	1501.50	3065.1	0	1.000	Tm-170	0.951	1.000	0.947	1.000	0.946	1.000	0.946	
Yb-168 -> Yb-169		0.13	4.89	11431.00	13.3	0	1.000	Yb-169	0.928	1.000	0.922	1.000	0.922	1.000	0.922	
Yb-174 -> Yb-175		31.83	0.51	55.20	247.8	0	1.000	Yb-175	0.911	1.000	0.904	1.000	0.903	1.000	0.903	
Lu-176 -> Lu-177	(	2.59	1.59	3844.34	60.55	0	1.000	Lu-177	0.916	1.000	0.909	1.000	0.908	1.000	0.908	
Hf-178 -> Hf-179m		27.28	18.43	1328.00	902.7	0	1.000	Hf-179m	0.955	1.000	0.951	1.000	0.951	1.000	0.951	
Hf-180 -> Hf-181	(	35.08	3.13	32.76	244.49	0	1.000	Hf-181	0.922	1.000	0.916	1.000	0.915	1.000	0.915	
Ta-181 -> Ta-182	(	100	41.56	738.44	2134.05	0	1.000	Ta-182	0.972	1.000	0.970	1.000	0.970	1.000	0.970	
W-186 -> W-187		28.43	15.94	520.60	1790	0	1.000	W-187	0.952	1.000	0.948	1.000	0.947	1.000	0.947	
Re-185 -> Re-186		37.4	16.40	1729.42	1657.39	0	1.000	Re-186	0.952	1.000	0.948	1.000	0.948	1.000	0.948	
Re-187 -> Re-188		62.6	5.20	329.73	170.19	0	1.000	Re-188	0.929	1.000	0.923	1.000	0.923	1.000	0.923	
Os-190 -> Os-191		26.26	2.50	26.39	65.2	0	1.000	Os-191	0.920	1.000	0.913	1.000	0.912	1.000	0.912	
Os-192 -> Os-193		40.78	2.87	4.68	12.9	0	1.000	Os-193	0.921	1.000	0.915	1.000	0.914	1.000	0.914	
Ir-191 -> Ir-192	(73	37.3	5.86	5336.81	932.38	0	1.000	Ir-192	0.931	1.000	0.925	1.000	0.925	1.000	0.925	
Pt-198 -> Au-199	(	7.163	21.48	64.60	32.5	0	1.000	Au-199	0.958	1.000	0.955	1.000	0.955	1.000	0.955	
Au-197 -> Au-198		100	17.16	1550.58	4648	0	1.000	Au-198	0.953	1.000	0.949	1.000	0.949	1.000	0.949	
Hg-196 -> Hg-197		0.15	0.13	418.60	1.7	0	1.000	Hg-197	0.910	1.000	0.902	1.000	0.901	1.000	0.901	
Hg-202 -> Hg-203		29.86	1.17	4.46	20.44	0	1.000	Hg-203	0.915	1.000	0.907	1.000	0.906	1.000	0.906	
Th-232 -> Pa-233		100	14.07	84.98	409.76	0	1.000	Pa-233	0.949	1.000	0.944	1.000	0.944	1.000	0.944	
U-238 -> U-239	(	99.27	119.41	277.11	1148	0	1.000	U-239	0.988	1.000	0.987	1.000	0.987	1.000	0.987	
U-238 -> Np-239		99.27	119.41	277.11	1148	0	1.000	Np-239	0.988	1.000	0.987	1.000	0.987	1.000	0.987	
					bold +- 10%											
					not bold +-20%											
					grey +-100%											

B.3 Page 2 of the spreadsheet: Neutron Self-Shielding Calculation for Cylindrical Samples

Neutron self-shielding calculations for cylindrical samples										
Enter sample dimensions and mass in B10, B11 and B13										
Enter element concentrations in B18 to B118										
See self-shielding factors in G21 to I119										
				Irradiation Channel		site 1		site 1	site 6	site 8
						Unc.				
				f =	18	0.2		18	48.6	52.7
	Sample			alpha =	-0.051	0.005		-0.051	0.016	0.018
		r (mm)		kth =	0.94	0.08		0.94	0.86	0.94
d (mm)	10	5		kep =	1	0		1	1	1
h (mm)	12.7									
volume (cm3	0.997458									
mass (g)	1									
				Gamma						
Element	Conc.(ppm)		Nuclide	Energy	Conc.(ppm)	Gth	Gep	Geff		
Li	0		Li		0				Li	
B	1000		B		1000				B	
N	0		N		0				N	
F	0		F-20	1633	0	0.9521413	1	0.9599392	F-20	
Na	0		Na-24	1368	0	0.9521413	1	0.9539502	Na-24	
Mg	0		Mg-27	1014	0	0.9521413	1	0.9543276	Mg-27	
Al	0		Al-28	1779	0	0.9521413	1	0.9544604	Al-28	
Si	0		Si-31	1266	0	0.9521413	1	0.9557628	Si-31	
			Si-Al-29	1273	0	1	1	1	Si-Al-29	
P	0		P-32	beta	0	0.9521413	1	0.9535193	P-32	
S	0		S-37	3102	0	0.9521413	1	0.9557005	S-37	
Cl	0		Cl-38	1642	0	0.9521413	1	0.9543904	Cl-38	
K	0		K-42	1525	0	0.9521413	1	0.9553109	K-42	
Ca	0		Ca-49	3084	0	0.9521413	1	0.9534511	Ca-49	
Sc	0		Sc-46	889	0	0.9521413	1	0.9533463	Sc-46	
			Sc-46m	142	0	0.9521413	1	0.9538868	Sc-46m	
Ti	0		Ti-51	320	0	0.9521413	1	0.9543886	Ti-51	
V	0		V-52	1434	0	0.9521413	1	0.9538186	V-52	
Cr	0		Cr-51	320	0	0.9521413	1	0.9537414	Cr-51	
Mn	0		Mn-56	1811	0	0.9521413	1	0.9554047	Mn-56	
Fe	0		Fe-59	1099	0	0.9521413	1	0.9551683	Fe-59	
Co	0		Co-60	1173	0	0.9521413	1	0.9579217	Co-60	
Ni	0		Ni-65	1482	0	0.9521413	1	0.9543135	Ni-65	
			Ni-Co-58	811	0	1	1	1	Ni-Co-58	
Cu	0		Cu-64	511	0	0.9521413	1	0.9557698	Cu-64	
			Cu-66	1039	0	0.9521413	1	0.9554774	Cu-66	
Zn	0		Zn-65	1115	0	0.9521413	1	0.958324	Zn-65	
			Zn-69m	439	0	0.9521413	1	0.9613457	Zn-69m	
Ga	0		Ga-71	834	0	0.9521413	1	0.9675634	Ga-71	
Ge	0		Ge-75	264	0	0.9521413	1	0.9573417	Ge-75	
			Ge-75m	139	0	0.9521413	1	0.9597885	Ge-75m	
			Ge-77	264	0	0.9521413	1	0.9758829	Ge-77	
As	0		As-76	559	0	0.9521413	1	0.9766838	As-76	
Se	0		Se-75	265	0	0.9521413	1	0.972018	Se-75	
			Se-77m	162	0	0.9521413	1	0.954637	Se-77m	
Br	0		Br-80	616	0	0.9521413	1	0.9738561	Br-80	
			Br-82	554	0	0.9521413	1	0.9798938	Br-82	
Rb	0		Rb-86	1077	0	0.9521413	1	0.9777525	Rb-86	
			Rb-86m	556	0	0.9521413	1	0.9746098	Rb-86m	
			Rb-88	1836	0	0.9521413	1	0.9826422	Rb-88	

Element	Conc.(ppm)	Nuclide	Energy	Conc.(ppm)	Gth	Gep	Geff	
Sr	0	Sr-85	514	0	0.95214128	1	0.97612154	Sr-85
		Sr-87m	388	0	0.95214128	1	0.96355638	Sr-87m
Y	0	Y-90m	479	0	0.95214128	1	0.96796587	Y-90m
Zr	0	Zr-95	724	0	0.95214128	1	0.96696903	Zr-95
		Zr-97	743	0	0.95214128	1	0.99758347	Zr-97
Nb	0	Nb-94m	871	0	0.95214128	1	0.96926939	Nb-94m
Mo	0	Mo-99	141	0	0.95214128	1	0.99022569	Mo-99
		Mo-101	307	0	0.95214128	1	0.98047661	Mo-101
Ru	0	Ru-103	497	0	0.95214128	1	0.96194336	Ru-103
		Ru-105	724	0	0.95214128	1	0.97569195	Ru-105
Rh	0	Rh-104m	51	0	0.95214128	1	0.96549542	Rh-104m
		Rh-104m	558	0	0.95214128	1	0.96549542	Rh-104m
Pd	0	Pd-109	88	0	0.95214128	1	0.98265902	Pd-109
Ag	0	Ag-108	633	0	0.95214128	1	0.95982021	Ag-108
		Ag-110	658	0	0.95214128	1	0.97742942	Ag-110
		Ag-110m	884	0	0.95214128	1	0.9759804	Ag-110m
Cd	0	Cd-115	336	0	0.95214128	1	0.98767183	Cd-115
In	0	In-116m	1097	0	0.95214128	1	0.97553367	In-116m
Sn	0	Sn-125m	332	0	0.95214128	1	0.99071622	Sn-125m
Sb	0	Sb-122	564	0	0.95214128	1	0.9845064	Sb-122
		Sb-124	1691	0	0.95214128	1	0.98346593	Sb-124
Te	0	Te-I-131	364	0	0.95214128	1	0.95802686	Te-I-131
I	100	I-128	443	100	0.95214128	0.99910348	0.98147036	I-128
Cs	0	Cs-134	796	0	0.95214128	1	0.97531557	Cs-134
		Cs-134m	127	0	0.95214128	1	0.9728778	Cs-134m
Ba	0	Ba-131	496	0	0.95214128	1	0.98075152	Ba-131
		Ba-139	166	0	0.95214128	1	0.95513612	Ba-139
La	0	La-140	1596	0	0.95214128	1	0.95576562	La-140
Ce	0	Ce-141	145	0	0.95214128	1	0.95488372	Ce-141
Pr	0	Pr-142	1576	0	0.95214128	1	0.95672889	Pr-142
Nd	0	Nd-147	91	0	0.95214128	1	0.95834864	Nd-147
Sm	0	Sm-153	103	0	0.95214128	1	0.97469901	Sm-153
		Sm-155	246	0	0.95214128	1	0.96326021	Sm-155
Eu	0	Eu-152	1408	0	0.95214128	1	0.95525234	Eu-152
		Eu-152m	842	0	0.95214128	1	0.95514051	Eu-152m
Gd	0	Gd-153	103	0	0.95214128	1	0.95431642	Gd-153
		Gd-159	363	0	0.95214128	1	0.984157	Gd-159
Tb	0	Tb-160	299	0	0.95214128	1	0.97774875	Tb-160
Dy	0	Dy-165	95	0	0.95214128	1	0.95253267	Dy-165
		Dy-165m	108	0	0.95214128	1	0.95273859	Dy-165m
Ho	0	Ho-166	81	0	0.95214128	1	0.9716291	Ho-166
Er	0	Er-171	308	0	0.95214128	1	0.96346186	Er-171
Tm	0	Tm-170	84	0	0.95214128	1	0.97427692	Tm-170
Yb	0	Yb-169	177	0	0.95214128	1	0.96236756	Yb-169
		Yb-175	396	0	0.95214128	1	0.95345073	Yb-175
Lu	0	Lu-177	208	0	0.95214128	1	0.95603225	Lu-177
Hf	0	Hf-179m	214	0	0.95214128	1	0.97635442	Hf-179m
		Hf-181	482	0	0.95214128	1	0.95922457	Hf-181
Ta	0	Ta-182	1221	0	0.95214128	1	0.98553655	Ta-182
W	0	W-187	686	0	0.95214128	1	0.97462163	W-187
Re	0	Re-186	137	0	0.95214128	1	0.97495658	Re-186
		Re-188	155	0	0.95214128	1	0.96287233	Re-188
Os	0	Os-191	129	0	0.95214128	1	0.9579814	Os-191
		Os-193	460	0	0.95214128	1	0.95871665	Os-193
Ir	0	Ir-192	316	0	0.95214128	1	0.96389619	Ir-192

Element	Mat	SigmaTh				Mass (g)	M Sth / Mat	
Li	6.941	71	Li			0	0	0
B	10.811	760	B			1000	0.001	0.0702988
N	14.007	1.89	N			0	0	0
F	18.998	0.009	F-20		1633	0	0	0 F-20
Na	22.99	0.53	Na-24		1368	0	0	0 Na-24
Mg	24.305	0.066	Mg-27		1014	0	0	0 Mg-27
Al	26.982	0.23	Al-28		1779	0	0	0 Al-28
Si	28.085	0.168	Si-31		1266	0	0	0 Si-31
			Si-Al-29		1273	0	0	Si-Al-29
P	30.974	0.17	P-32	bêta		0	0	0 P-32
S	32.065	0.52	S-37		3102	0	0	0 S-37
Cl	35.453	33.5	Cl-38		1642	0	0	0 Cl-38
K	39.098	2.1	K-42		1525	0	0	0 K-42
Ca	40.078	0.43	Ca-49		3084	0	0	0 Ca-49
Sc	44.956	27.2	Sc-46		889	0	0	0 Sc-46
			Sc-46m		142	0	0	Sc-46m
Ti	47.867	6.1	Ti-51		320	0	0	0 Ti-51
V	50.941	5	V-52		1434	0	0	0 V-52
Cr	51.996	3.1	Cr-51		320	0	0	0 Cr-51
Mn	54.938	13.3	Mn-56		1811	0	0	0 Mn-56
Fe	55.845	2.56	Fe-59		1099	0	0	0 Fe-59
Co	58.933	37.2	Co-60		1173	0	0	0 Co-60
Ni	58.693	4.5	Ni-65		1482	0	0	0 Ni-65
			Ni-Co-58		811	0	0	Ni-Co-58
Cu	63.546	3.8	Cu-64		511	0	0	0 Cu-64
			Cu-66		1039	0	0	Cu-66
Zn	65.409	1.1	Zn-65		1115	0	0	0 Zn-65
			Zn-69m		439	0	0	Zn-69m
Ga	69.723	2.9	Ga-71		834	0	0	0 Ga-71
Ge	72.64	2.2	Ge-75		264	0	0	0 Ge-75
			Ge-75m		139	0	0	Ge-75m
			Ge-77		264	0	0	Ge-77
As	74.922	4.2	As-76		559	0	0	0 As-76
Se	78.96	11.7	Se-75		265	0	0	0 Se-75
			Se-77m		162	0	0	Se-77m
Br	79.904	6.8	Br-80		616	0	0	0 Br-80
			Br-82		554	0	0	Br-82
Rb	85.468	0.39	Rb-86		1077	0	0	0 Rb-86
			Rb-86m		556	0	0	Rb-86m
			Rb-88		1836	0	0	Rb-88
Sr	87.62	1.2	Sr-85		514	0	0	0 Sr-85
			Sr-87m		388	0	0	Sr-87m
Y	88.906	1.28	Y-90m		479	0	0	0 Y-90m
Zr	91.224	0.184	Zr-95		724	0	0	0 Zr-95
			Zr-97		743	0	0	Zr-97
Nb	92.906	1.15	Nb-94m		871	0	0	0 Nb-94m
Mo	95.94	2.5	Mo-99		141	0	0	0 Mo-99
			Mo-101		307	0	0	Mo-101
Ru	101.07	2.6	Ru-103		497	0	0	0 Ru-103
			Ru-105		724	0	0	Ru-105
Rh	102.905	145	Rh-104m		51	0	0	0 Rh-104m
			Rh-104m		558	0	0	Rh-104m
Pd	106.42	7	Pd-109		88	0	0	0 Pd-109
Ag	107.868	63	Ag-108		633	0	0	0 Ag-108
			Ag-110		658	0	0	Ag-110
			Ag-110m		884	0	0	Ag-110m
Cd	112.411	2520	Cd-115		336	0	0	0 Cd-115
In	114.818	194	In-116m		1097	0	0	0 In-116m

Element	Mat	SigmaTh			Mass (g)	M Sth / Mat	
Sn	118.71	0.61	Sn-125m	332	0	0	0 Sn-125m
Sb	121.76	5.1	Sb-122	564	0	0	0 Sb-122
			Sb-124	1691	0	0	Sb-124
Te	127.6	4.2	Te-I-131	364	0	0	0 Te-I-131
I	126.904	6.2	I-128	443	100	0.0001	4.886E-06 I-128
Cs	132.905	29	Cs-134	796	0	0	0 Cs-134
			Cs-134m	127	0	0	Cs-134m
Ba	137.327	1.3	Ba-131	496	0	0	0 Ba-131
			Ba-139	166	0	0	Ba-139
La	138.905	9	La-140	1596	0	0	0 La-140
Ce	140.116	0.63	Ce-141	145	0	0	0 Ce-141
Pr	140.908	11.4	Pr-142	1576	0	0	0 Pr-142
Nd	144.24	50	Nd-147	91	0	0	0 Nd-147
Sm	150.36	5600	Sm-153	103	0	0	0 Sm-153
			Sm-155	246	0	0	Sm-155
Eu	151.964	4600	Eu-152	1408	0	0	0 Eu-152
			Eu-152m	842	0	0	Eu-152m
Gd	157.25	49000	Gd-153	103	0	0	0 Gd-153
			Gd-159	363	0	0	Gd-159
Tb	158.925	23.2	Tb-160	299	0	0	0 Tb-160
Dy	162.5	950	Dy-165	95	0	0	0 Dy-165
			Dy-165m	108	0	0	Dy-165m
Ho	164.93	61	Ho-166	81	0	0	0 Ho-166
Er	167.259	160	Er-171	308	0	0	0 Er-171
Tm	168.934	105	Tm-170	84	0	0	0 Tm-170
Yb	173.04	50	Yb-169	177	0	0	0 Yb-169
			Yb-175	396	0	0	Yb-175
Lu	174.967	84	Lu-177	208	0	0	0 Lu-177
Hf	178.49	104	Hf-179m	214	0	0	0 Hf-179m
			Hf-181	482	0	0	Hf-181
Ta	180.948	20	Ta-182	1221	0	0	0 Ta-182
W	183.84	18.2	W-187	686	0	0	0 W-187
Re	186.207	89	Re-186	137	0	0	0 Re-186
			Re-188	155	0	0	Re-188
Os	190.23	15	Os-191	129	0	0	0 Os-191
			Os-193	460	0	0	Os-193
Ir	192.217	420	Ir-192	316	0	0	0 Ir-192
Pt	195.078	10	Pt-Au-199	158	0	0	0 Pt-Au-199
Au	196.967	98.7	Au-198	412	0	0	0 Au-198
Hg	200.59	374	Hg-197	77	0	0	0 Hg-197
			Hg-203	279	0	0	Hg-203
Th	232.038	7.37	Th-Pa-233	312	0	0	0 Th-Pa-233
U	238.029	7.57	U-239	75	0	0	0 U-239
			U-Np-239	278	0	0	U-Np-239

sum	0.0703037
Zth	0.044953
Gth	0.9521413

		Mat	theta(%)	sigma0(b)	Q0	Er	Q0(a)	I(0)(b)	ThEr.4I	Sabs,ep(b)	m init (g	Gep		Egamm	Geff
F-19 -> F-20 (11.03 s)	F	18.998	100	0.0094	2.19	44700	3.50374252	0.020586	149.174633	1.1941487	0	1	F-20	1633	0.95994
Na-23 -> Na-24 (14.9 h)	Na	22.99	100	0.53	0.59	3380	0.70705151	0.3127	806.667503	1.96407706	0	1	Na-24	1368	0.95395
Mg-26 -> Mg-27 (9.462 m)	Mg	24.305	11.01	0.039	0.64	257000	0.86166281	0.02496	40.0871471	0.03152	0	1	Mg-27	1014	0.95433
Al-27 -> Al-28 (2.2406 m)	Al	26.982	100	0.23	0.71	11800	0.91666831	0.1633	694.606731	3.21440355	0	1	Al-28	1779	0.95446
Si-30 -> Si-31 (2.622 h)	Si	28.085	3.087	0.107	1.11	2280	1.47356934	0.11877	8.08011096	0.08807321	0	1	Si-31	1266	0.95576
P-31 -> P-32 (14.28 d)	P	30.974	100	0.17	0.47	38500	0.53363167	0.0799	545.420015	5.94507817	0	1	P-32	bēta	0.95352
S-36 -> S-37 (5.05 m)	S	32.065	0.02	0.2	1.12	1000	1.4462115	0.224	0.07100322	0.00077394	0	1	S-37	3102	0.9557
Cl-37 -> Cl-38 (37.24 m)	Cl	35.453	24.22	0.43	0.69	13700	0.88762392	0.2967	324.474007	0.48009531	0	1	Cl-38	1642	0.95439
K-41 -> K-42 (12.36 h)	K	39.098	6.73	1.46	0.97	2960	1.2766493	1.4162	233.161231	2.6416665	0	1	K-42	1525	0.95531
Ca-48 -> Ca-49 (8.716 m)	Ca	40.078	0.187	0.98	0.45	1330000	0.50648811	0.441	23.2177886	8.3059E-05	0	1	Ca-49	3084	0.95345
Sc-45 -> Sc-46 (83.83 d)	Sc	44.956	100	27	0.43	5130	0.46492834	11.61	35389.8862	4.15842689	0	1	Sc-46	889	0.95335
Sc-45 -> Sc-46m (18.7 s)	Sc	44.956	100	27	0.57	5130	0.68137157	15.39	46912.1747	4.15842689	0	1	Sc-46m	142	0.95389
Ti-50 -> Ti-51 (5.76 m)	Ti	47.867	5.18	0.177	0.67	63200	0.88688251	0.11859	51.1286894	0.05614021	0	1	Ti-51	320	0.95439
V-51 -> V-52 (3.75 m)	V	50.941	99.75	4.9	0.55	7230	0.65375359	2.695	9399.98137	2.277766	0	1	V-52	1434	0.95382
Cr-50 -> Cr-51 (27.704 d)	Cr	51.996	4.345	15.5	0.53	7530	0.62261709	8.215	1268.57264	0.17821521	0	1	Cr-51	320	0.95374
Mn-55 -> Mn-56 (2.5785 h)	Mn	54.938	100	13.3	1.053	468	1.31720389	14.0049	16382.4312	66.7338143	0	1	Mn-56	1811	0.9554
Fe-58 -> Fe-59 (44.496 d)	Fe	55.845	0.282	1.3	0.97	637	1.21536592	1.261	4.70565375	0.04813078	0	1	Fe-59	1099	0.95517
Co-59 -> Co-60 (5.271 y)	Co	58.933	100	36	1.993	136	2.47269364	71.748	51194.7425	580.015793	0	1	Co-60	1173	0.95792
Ni-64 -> Ni-65 (2.52 h)	Ni	58.693	0.9256	1.6	0.67	14200	0.85583178	1.072	45.4499562	0.15091567	0	1	Ni-65	1482	0.95431
Cu-63 -> Cu-64 (12.701 h)	Cu	63.546	69.17	4.5	1.14	1040	1.47668292	5.13	5712.79285	965.526098	0	1	Cu-64	511	0.95577
Cu-65 -> Cu-66 (5.1 m)	Cu	63.546	30.83	2.17	1.06	766	1.34875277	2.3002	1010.25412	6.88071969	0	1	Cu-66	1039	0.95548
Zn-64 -> Zn-65 (244.1 d)	Zn	65.409	48.63	0.76	1.908	2560	2.67031157	1.45008	1627.76692	6.6483084	0	1	Zn-65	1115	0.95832
Zn-68 -> Zn-69m (13.76 h)	Zn	65.409	18.75	0.872	3.19	590	4.28616719	2.78168	669.3438	42.323465	0	1	Zn-69m	439	0.96135
Ga-71 -> Ga-72 (14.1 h)	Ga	69.723	39.892	4.8	6.69	154	8.55820352	32.112	9606.41742	149.314245	0	1	Ga-71	834	0.96756
Ge-74 -> Ge-75 (1.3797 h)	Ge	72.64	36.28	0.44	1.57	3540	2.19433346	0.6908	658.598765	7.06928663	0	1	Ge-75	264	0.95734
Ge-74 -> Ge-75m (48 s)	Ge	72.64	36.28	0.44	2.38	3540	3.4231419	1.0472	998.385389	7.06928663	0	1	Ge-75m	139	0.95979
Ge-76 -> Ge-77 (11.30 h)	Ge	72.64	7.61	0.15	12.9	583	17.7197893	1.935	188.075856	9.33677287	0	1	Ge-77	264	0.97588
As-75 -> As-76 (1.097 d)	As	74.922	100	4.2	15	106	18.9467012	63	40687.677	354.413574	0	1	As-76	559	0.97668
Se-74 -> Se-75 (119.77 d)	Se	78.96	0.89	52	10.8	29.4	12.7860957	561.6	1932.66258	44.9491167	0	1	Se-75	265	0.97202
Se-76 -> Se-77m (17.45 s)	Se	78.96	9.37	85	0.81	577	0.99030263	68.85	8205.66647	17.6703275	0	1	Se-77m	162	0.95464
Br-79 -> Br-80 (17.68 m)	Br	79.904	50.69	10.8	12.1	69.3	14.9506159	130.68	36093.1437	233	0	1	Br-80	616	0.97386
Br-81 -> Br-82 (1.4708 d)	Br	79.904	49.31	2.65	19.3	152	24.8453605	51.145	18813.7609	253	0	1	Br-82	554	0.97989
Rb-85 -> Rb-86 (18.66 d)	Rb	85.468	72.17	0.5	14.8	839	20.7214888	7.4	7890.29443	36.123031	0	1	Rb-86	1077	0.97775
Rb-85 -> Rb-86m (1.017 m)Roth	Rb	85.468	72.17	0.5	11.4	839	15.9286726	5.7	6077.65922	36.123031	0	1	Rb-86m	556	0.97461
Rb-87 -> Rb-88 (17.8 m)	Rb	85.468	27.83	0.1	23.5	364	31.6294916	2.35	691.865416	39.2671531	0	1	Rb-88	1836	0.98264
Sr-84 -> Sr-85 (64.84 d)	Sr	87.62	0.56	0.8	13.3	469	18.076738	10.64	69.7587664	1.65852667	0	1	Sr-85	514	0.97612
Sr-86 -> Sr-87m (2.795 h)	Sr	87.62	9.86	0.82	4.11	795	5.63807474	3.3702	480.484565	15.3232504	0	1	Sr-87m	388	0.96356
Y-89 -> Y-90m (3.19 h)	Y	88.906	100	1.281	5.93	4300	8.89184825	7.59633	21577.0071	23.3495555	0	1	Y-90m	479	0.96797
Zr-94 -> Zr-95 (64.02 d)	Zr	91.224	17.38	0.05	5.306	6260	8.08027868	0.2653	152.200737	3.08394718	0	1	Zr-95	724	0.96697
Zr-96 -> Zr-97 (16.74 h)	Zr	91.224	2.8	0.022	251.6	338	338.484821	5.5352	159.168832	10.3	0	1	Zr-97	743	0.99758
Nb-93 -> Nb-94m (6.26 m)	Nb	92.906	100	1.1	7.35	574	10.0325322	8.085	10262.3018	42.1983606	0	1	Nb-94m	871	0.96927
Mo-98 -> Mo-99 (2.7477 d)	Mo	95.94	24.13	0.13	53.1	241	70.1347656	6.903	1494.17688	21.0806035	0	1	Mo-99	141	0.99023
Mo-100 -> Mo-101 (14.6 m)	Mo	95.94	9.63	0.19	18.84	672	26.1243607	3.5796	466.024228	15.3709217	0	1	Mo-101	307	0.98048
Ru-102 -> Ru-103 (39.254 d)	Ru	101.07	31.55	1.3	3.63	181	4.63617954	4.719	1191.02471	15.0319245	0	1	Ru-103	497	0.96194
Ru-104 -> Ru-105 (4.44 h)	Ru	101.07	18.62	0.47	12.8	495	17.4391597	6.016	1340.07648	20.7265685	0	1	Ru-105	724	0.97569
Rh-103 -> Rh-104m (4.34 m)	Rh	102.905	100	145	6.81	1.45	6.96645357	987.45	114567.732	203.168793	0	1	Rh-104n	51	0.9655
Rh-103 -> Rh-104 (4.34m, 42.3s)	Rh	102.905	100	145	6.81	1.45	6.96645357	987.45	114567.732	203.168793	0	1	Rh-104n	558	0.9655

		Mat	theta(%)	sigma0(b)	Q0	Er	Q0(a)	I(0)(b)	ThEr.4I	Sabs,ep(b)	m init (g	Gep		Egamm	Geff
Pd-108 -> Pd-109 (13.7 h)	Pd	106.42	26.46	8.19	26.3	39.7	31.6775337	215.397	24851.1043	875.376021	0	1	Pd-109	88	0.98266
Ag-107 -> Ag-108 (2.37 m)	Ag	107.868	51.839	0.71	2.9	38.5	3.4400561	2.059	459.724081	179.558846	0	1	Ag-108	633	0.95982
Ag-109 -> Ag-110 (24.6 s)	Ag	107.868	48.161	91.4	18.4	6.08	20.1672429	1681.76	166732.763	2313.88283	0	1	Ag-110	658	0.97743
Ag-109 -> Ag-110m (249.76 d)	Ag	107.868	48.161	91.4	16.3	6.08	17.8647496	1489.82	147703.48	2313.88283	0	1	Ag-110n	884	0.97598
Cd-114 -> Cd-115 (2.228 d)	Cd	112.411	28.73	0.34	39.6	207	51.8771163	13.464	3265.11038	78	0	1	Cd-115	336	0.98767
In-115 -> In-116m (54.15 m)	In	114.818	95.71	203	16.8	1.56	17.2099019	3410.4	389953.188	2582	0	1	In-116m	1097	0.97553
Sn-124 -> Sn-125m (9.52 m)	Sn	118.71	5.79	0.134	60.1	74.2	74.7916336	8.0534	261.10753	7.26577834	0	1	Sn-125n	332	0.99072
Sb-121 -> Sb-122 (2.7 d)	Sb	121.76	57.21	6	33	13.1	37.6008194	198	31699.0069	500	0	1	Sb-122	564	0.98451
Sb-123 -> Sb-124 (60.2 d)	Sb	121.76	42.79	4.06	28.8	28.2	34.1019386	116.928	19026.5677	442	0	1	Sb-124	1691	0.98347
Te-130 -> I-131 (8.04 d)	Te	127.6	34.08	0.2	1.8	2950	2.52400453	0.36	299.730469	1.99576128	0	1	I-131	364	0.95803
I-127 -> I-128 (24.99 m)	I	126.904	100	6.2	24.4	57.6	29.9393247	151.28	76550.9367	387	0.0001	1	I-128	443	0.98147
Cs-133 -> Cs-134 (2.062 y)	Cs	132.905	100	29.6	15.1	9.27	16.8988014	446.96	108918.224	1033	0	1	Cs-134	796	0.97532
Cs-133 -> Cs-134m (2.91 h)	Cs	132.905	100	29.6	12.3	9.27	13.7620573	364.08	88721.4674	1033	0	1	Cs-134n	127	0.97288
Ba-130 -> Ba-131 (11.5 d)	Ba	137.327	0.106	9	21.6	69.9	26.7545399	194.4	112.666031	1.64293972	0	1	Ba-131	496	0.98075
Ba-138 -> Ba-139 (1.3798 h)	Ba	137.327	71.698	0.43	0.88	15700	1.20157107	0.3784	1293.65369	3.97079693	0	1	Ba-139	166	0.95514
La-139 -> La-140 (1.678 d)	La	138.905	99.91	9	1.24	76	1.47482749	11.16	6303.74433	240.231314	0	1	La-140	1596	0.95577
Ce-140 -> Ce-141 (32.5 d)	Ce	140.116	88.45	0.58	0.83	7200	1.09414839	0.4814	1486.40419	8.44320586	0	1	Ce-141	145	0.95488
Pr-141 -> Pr-142 (19.13 h)	Pr	140.908	100	11.4	1.51	296	1.90836143	17.214	16764.8041	196.063023	0	1	Pr-142	1576	0.95673
Nd-146 -> Nd-147 (10.98 d)	Nd	144.24	17.2	1.4	2	874	2.68256609	2.8	723.254345	9.44095654	0	1	Nd-147	91	0.95835
Sm-152 -> Sm-153 (1.946 d)	Sm	150.36	26.75	210	14.4	8.53	16.0483495	3024	190671.238	5930	0	1	Sm-153	103	0.9747
Sm-154 -> Sm-155 (22.1 m)	Sm	150.36	22.75	7	4.3	142	5.44751823	30.1	4971.22288	54.1863293	0	1	Sm-155	246	0.96326
Eu-151 -> Eu-152 (13.5 y)	Eu	151.964	47.81	9204	1.25	0.448	1.25144059	11505	398948.257	1708.28237	0	1	Eu-152	1408	0.95525
Eu-151 -> Eu-152m1 (9.32 h)	Eu	151.964	47.81	9204	1.2	0.448	1.20344679	11044.8	382990.327	1708.28237	0	1	Eu-152n	842	0.95514
Gd-152 -> Gd-153 (241.6 d)	Gd	157.25	0.2	700	0.77	16.7	0.85703473	539	332.433934	4.03313612	0	1	Gd-153	103	0.95432
Gd-158 -> Gd-159 (18.56 h)	Gd	157.25	24.84	2.4	29.9	48.2	36.3746116	71.76	8399.48844	139.815979	0	1	Gd-159	363	0.98416
Tb-159 -> Tb-160 (72.3 d)	Tb	158.925	100	23.2	17.9	18.1	20.7149837	415.28	132255.105	798.738578	0	1	Tb-160	299	0.97775
Dy-164 -> Dy-165 (2.334 h)	Dy	162.5	28.18	2700	0.19	224	0.14841858	513	125938.223	279.166399	0	1	Dy-165	95	0.95253
Dy-164 -> Dy-165m (1.258 m)	Dy	162.5	28.18	2700	0.25	224	0.22748897	675	165708.188	279.166399	0	1	Dy-165n	108	0.95274
Ho-165 -> Ho-166 (1.117 d)	Ho	164.93	100	61.1	10.9	12.3	12.3641046	665.99	181731.308	1110.51779	0	1	Ho-166	81	0.97163
Er-170 -> Er-171 (7.52 h)	Er	167.259	14.93	6	4.42	129	5.57692403	26.52	2766.1085	202.581302	0	1	Er-171	308	0.96346
Tm-169 -> Tm-170 (128.6 d)	Tm	168.934	100	105	14.3	4.8	15.4896484	1501.5	281204.218	3065.12598	0	1	Tm-170	84	0.97428
Yb-168 -> Yb-169 (32.022 d)	Yb	173.04	0.13	2300	4.97	0.61	4.89133859	11431	1219.4374	13.2918677	0	1	Yb-169	177	0.96237
Yb-174 -> Yb-175 (4.19 d)	Yb	173.04	31.83	120	0.46	602	0.50634794	55.2	22730.7786	247.765487	0	1	Yb-175	396	0.95345
Lu-176 -> Lu-177 (6.71 d)	Lu	174.967	2.59	2302	1.67	0.158	1.59292668	3844.34	4759.7527	60.5544303	0	1	Lu-177	208	0.95603
Hf-178 -> Hf-179m (18.7 s)	Hf	178.49	27.28	80	16.6	7.9	18.4320492	1328	82812.0008	902.650808	0	1	Hf-179n	214	0.97635
Hf-180 -> Hf-181 (42.39 d)	Hf	178.49	35.08	13	2.52	115	3.12686343	32.76	7668.009	244.490792	0	1	Hf-181	482	0.95922
Ta-181 -> Ta-182 (115 d)	Ta	180.948	99.998	20.012	36.9	10.4	41.5609739	738.4428	188417.618	2134.04827	0	1	Ta-182	1221	0.98554
W-186 -> W-187 (23.9 h)	W	183.84	28.43	38	13.7	20.5	15.9445279	520.6	49543.0304	1790	0	1	W-187	686	0.97462
Re-185 -> Re-186 (3.777 d)	Re	186.207	37.4	112.3	15.4	3.4	16.3985352	1729.42	105527.013	1657.38638	0	1	Re-186	137	0.97496
Re-187 -> Re-188 (16.98 h)	Re	186.207	62.6	75.8	4.35	41.1	5.20255763	329.73	91257.7012	170.185127	0	1	Re-188	155	0.96287
Os-190 -> Os-191 (15.4 d)	Os	190.23	26.26	13	2.03	114	2.50180141	26.39	4607.8258	50.2253013	0	1	Os-191	129	0.95798
Os-192 -> Os-193 (1.271 d)	Os	190.23	40.78	2	2.34	89.7	2.86693198	4.68	1152.94888	12.5671428	0	1	Os-193	460	0.95872
Ir-191 -> Ir-192 (73.831 d)	Ir	192.217	37.3	920.14	5.8	1.1	5.86055333	5336.812	206798.703	932.377702	0	1	Ir-192	316	0.9639
Pt-198 -> Au-199 (3.14 d)	Pt	195.078	7.163	3.8	17	106	21.483702	64.6	2988.47629	32.5743916	0	1	Au-199	158	0.97818
Au-197 -> Au-198 (2.6935 d)	Au	196.967	100	98.7	15.71	5.65	17.1553005	1550.577	309965.042	4648	0	1	Au-198	412	0.9755
Hg-196 -> Hg-197 (2.672 d)	Hg	200.59	0.15	3220	0.13	10	0.12712543	418.6	157.721349	1.7191627	0	1	Hg-197	279	0.95248
Hg-202 -> Hg-203 (46.6 d)	Hg	200.59	29.86	4.9	0.91	1960	1.17140983	4.459	2762.03835	20.4408006	0	1	Hg-203	279	0.95507

		Mat	theta(%)	sigma0(b)	Q0	Er	Q0(a)	I(0)(b)	ThEr.4I	Sabs,ep(b)	m init (g	Gep		Egamm	Geff
Th-232 -> Pa-233 (27 d)	Th	232.038	100	7.37	11.53	54.4	14.0739941	84.9761	42027.7708	409.762512	0	1	Pa-233	312	0.97314
U-238 -> U-239 (23.5 m)	U	238.029	99.27	2.68	103.4	16.9	119.405907	277.112	85236.9766	1148	0	1	U-239	75	0.99373
U-238 -> Np-239 (2.355 d)	U	238.029	99.27	2.68	103.4	16.9	119.405907	277.112	85236.9766	1148	0	1	Np-239	278	0.99373